This draft document is currently under revision by the European Commission (EC) and has not yet been validated or approved by the EC. The content provided herein is subject to change, and the information presented may not represent the final position or official stance of the EC.

GO-VIKING

Research and Innovation Action (RIA)

This project has received funding from the Euratom research and innovation programme 2021-2025 under Grant Agreement No 101059603

Start date : 2022-06-01 Duration : 48 Months

FIV phenomena in NPPs

Authors : Dr. Daniele VIVALDI (IRSN)

GO-VIKING - Contract Number: 101059603

Project officer: Panagiotis MANOLATOS

Document title	FIV phenomena in NPPs
Author(s)	Dr. Daniele VIVALDI
Number of pages	112
Document type	Deliverable
Work Package	WP1
Document number	D1.2
Issued by	IRSN
Date of completion	2023-10-26 13:56:36
Dissemination level	Public

Summary

Report on FIV phenomena, known examples in NPPs, available experimental data and numerical methods.

Approval

Date	By
2023-10-26 13:57:31	Dr. Daniele VIVALDI (IRSN)
2023-10-26 14:05:55	Dr. Papukchiev ANGEL (GRS)

Flow-induced vibrations in nuclear power plants

Deliverable D1.2 of the GO-VIKING project (101060826)

Version N°1.0
July 2023

Daniele Vivaldi (IRSN), Angel Papukchiev (GRS), Kevin Zwijsen (NRG), Mohammed Muaaz Hussain (NRG), William Benguigui (EDF), Sofiane Benhamadouche (EDF)

Funded by
the European Union

Disclaimer

The content of this report reflects only the author's view. The European Commission is not responsible for any use that may be made of the information it contains.

Document information

Grant Agreement / Proposal ID	101060826
Project Title	Gathering expertise On Vibration ImpaKt In Nuclear power Generation
Project Acronym	GO-VIKING
Scientific Coordinator	Angel Papukchiev, Angel.Papukchiev@grs.de, GRS
Project starting date (duration)	1st June 2022 – 31st May 2026 (48 Months)
Related Work Package	WP 1
Related Task(s)	-
Lead Organisation	IRSN
Contributing Partner(s)	IRSN, NRG, EDF, GRS
Due Date	31.07.2023
Submission Date	31.07.2023
Dissemination level	PUB

History

Date	Version	Submitted by	Reviewed by	Comments
31/07/2023	1	Daniele Vivaldi	Angel Papukchiev	

Table of contents

Summary

This report is composed by three chapters: the first chapter presents the most important Flow-Induced Vibration (FIV) phenomena in nuclear power plants, the second chapter presents available experimental data and numerical methods for FIV in fuel assemblies, the third chapter deals with available experimental data and numerical methods for FIV in steam generators.

Keywords

Fluid-induced vibrations, Fuel assemblies, Steam generators, Experimental data, numerical methods, CFD.

1. Documentation of the most important FIV phenomena, relevant for the operational safety of nuclear reactors.

D. Vivaldi, A. Papukchiev

Mechanical wear is a structure degradation type broadly characterized as a mechanically induced or aided degradation mechanism. Degradation from small amplitude, oscillatory motion, between continuously rubbing surfaces, is generally termed fretting. Vibration of relatively large amplitude, resulting in intermittent sliding contact between two parts, is termed sliding wear, or wear. Wear generally results from concurrent effects of vibration and corrosion. The major stressor in fretting and wear is the FIV. Initiation, stability, and damage growth characteristics resulting from these mechanisms may be functions of a large number of variables, including the local geometry, the stiffness of the component, the gap size between the parts, flow velocities and directions, surface roughness, and oxide layer characteristics. Wear is defined as the removal of material surface layers due to the relative motion between two surfaces [1].

Fretting and wear are phenomena that must be avoided in nuclear power plants (NPP). Fuel designers continue developing fuel assemblies with improved materials to accommodate the current fuel operation conditions aiming at higher burnup, higher power density, power management, etc. The fuel assembly mechanical design should preclude debris and grid-to-rod fretting, by providing filtering mechanisms to trap debris (debris catchers) before it enters the core, and by reducing the cladding wear by improving grid-to-rod contact, using wear resistant cladding, and avoiding fuel bundle vibration caused by the coolant flow by adequate hydraulic design and stiffening of the fuel structure by inserting additional spacer grids and thickening guide tubes [2]. All this is being done primarily to improve the vibration behavior of the fuel assemblies, which is one the main triggers of the grid-to-rod-fretting wear.

1.1 Grid-to-rod fretting wear in fuel assemblies

1.1.1 Grid-to-rod fretting wear in NPPs

NPP fuel assemblies (FAs) have historically been concerned by fuel leakage. Grid-to-rod fretting wear (GTRFW) is one of the most common cause of fuel failure. GTRFW is generally caused by the turbulent coolant flow, that exerts fluid forces on the fuel rod surface over a broad frequency; these forces, in turn, result in the rod vibrations and consequent impacts between the rod surface and the spacer grid contact points (springs and dimples). Specific FIV mechanisms such as self-excited vibrations can occur: in this case, the vibrations are caused by hydraulically unbalanced (asymmetric) mixing vane pattern across the spacer grid, which generates rotational flow forces on the FA. This mechanism is triggered within a certain flow range.

Examples of fuel rod failure due GTRFW in the USA date back to the 80's, with events reported at Yankee Rowe NPP (PWR), Salem NPP Unit 2 (PWR, most failures occurred on the core periphery)

[3], Millstone NPP Unit 2 (PWR, mainly in the area of the first grid or at the upper end of the fuel rods) [4].

In 1993, shutdown inspections at Beaver Valley NPP Unit 1 (PWR) and Salem NPP Unit 2 (PWR) discovered numerous fuel rods that had developed fretting wear and perforation, occurred at the mid-grid spacer grids [5]. In the same year, 44 failed fuel rods were discovered at Wolf Creek NPP (PWR) in FAs that had completed two cycles of operation (burnups of 24,000 MWd/MTU), with failures located at the lower spacer grids; the most severely degraded fuel rod fragmented into three segments during fuel handling operations while offloading the core [5]. GTRFW was the cause of leaking fuel rods at the Ft. Calhoun NPP (PWR) during the 90's [6].

In the 90's, GTRFW caused fuel failure in a PWR in Korea on the twice-burned FA at about 90 days after startup (22,000 MWd/MTU) [7]: almost one hundred rods were found to be leaking, generally located around the periphery of the FA. The wear of these fuel rods are shown in Figure 1 and present the typical spring and dimple marks on the rod surface.

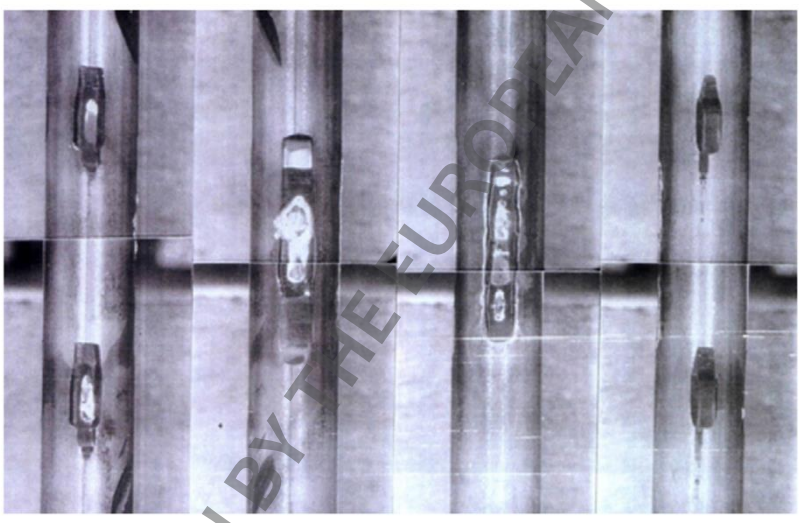

Figure 1: Perforated grid-to-rod fretting wear configurations of failed KOFA fuel rods [7].

In France, several fuel rod failures due to GTRFW were reported in the 2000s in the 1300MWe PWRs, with the most severe event consisting in 92 failed rods (mainly at the third cycle and to a lesser extent at the second cycle) at the Cattenom NPP Unit 3, in 2000 [8].

The IAEA [9] collected information on fuel rod experience from worldwide countries and issued a document describing the results. Figure 2 presents PWR FA failure rates for the USA, France and worldwide average between 1994 and 2006: depending on the country and on the specific year considered, the number of leaking FAs observed ranged from about 5 to about 25, per 1000 discharged FAs; a number of leaking FAs higher than 35 per 1000 discharged FAs was observed in USA in 2001.

The identified causes of PWR fuel leaks in the USA and France are presented in Figs. 2 and 3, respectively: even if the cause of a certain number of FA failure is unknown (this number is rather significant for France, see Figure 4), rod-to-grid fretting wear (GTRFW) can be considered the dominant fuel rod leaker mechanism in PWRs worldwide (for the considered period going from

1994 to 2006), reaching up to 65% in the United States of America, 39% in France and 37% in Europe (excluding France).

The most recent data collected by IAEA [10] refer to the period from 2006 to 2015: the GTRFW represented about 58% of PWR fuel failure mechanisms worldwide. However, it must be noted that the fuel rod failure rates have always decreased during the years, reducing from about 225 ppm (ppm corresponds to 1 in 1 000 000) in the period 1987-1990 to about 20 ppm in the period 2011-2015 [10].

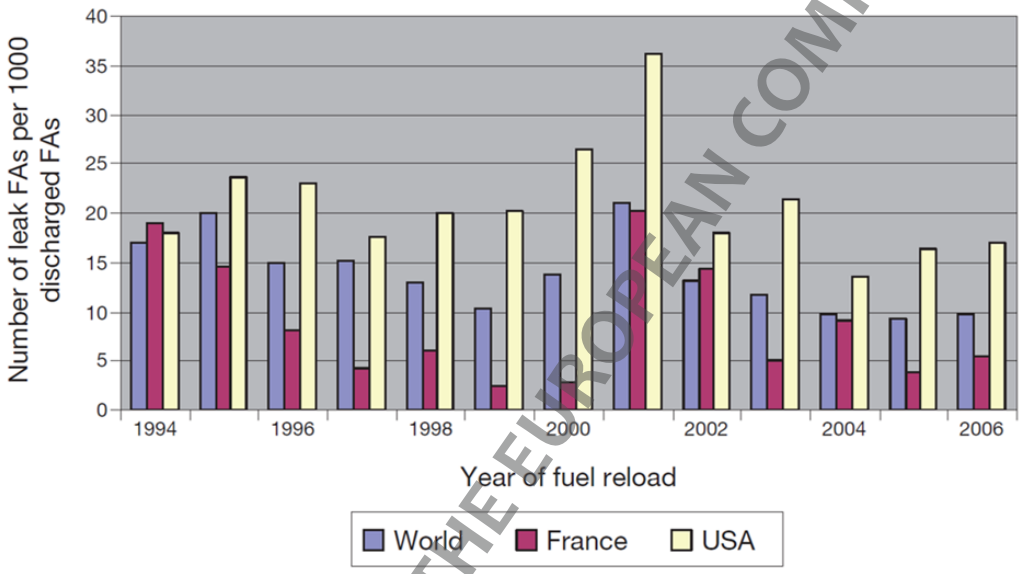

Figure 2: PWR FA leak rate for France, the United States of America and worldwide (the world curve shows the average result for countries and region (Europe minus France), including Brazil and one PWR from China, thus summarizing fuel performance for 95% of PWR units worldwide) [9].

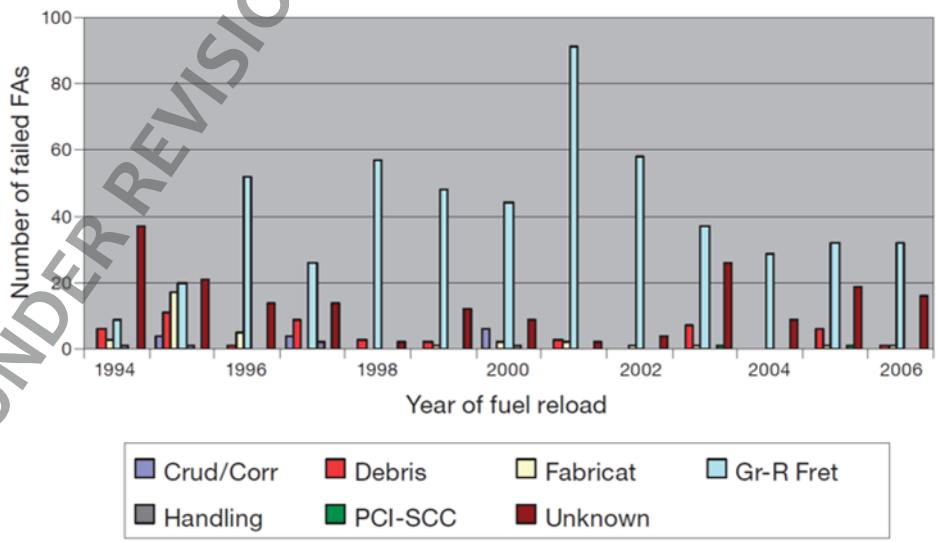

Figure 3: PWR fuel leak causes in the United States of America [7] (Crud/Corr stands for crud/corrosion related failures, Fabricat stands for fabrication related failures, Gr-R fret stands for

grid-to-rod fretting wear related failures, PCI-SCC stands for pellet-cladding interaction/stress corrosion cracking related failures).

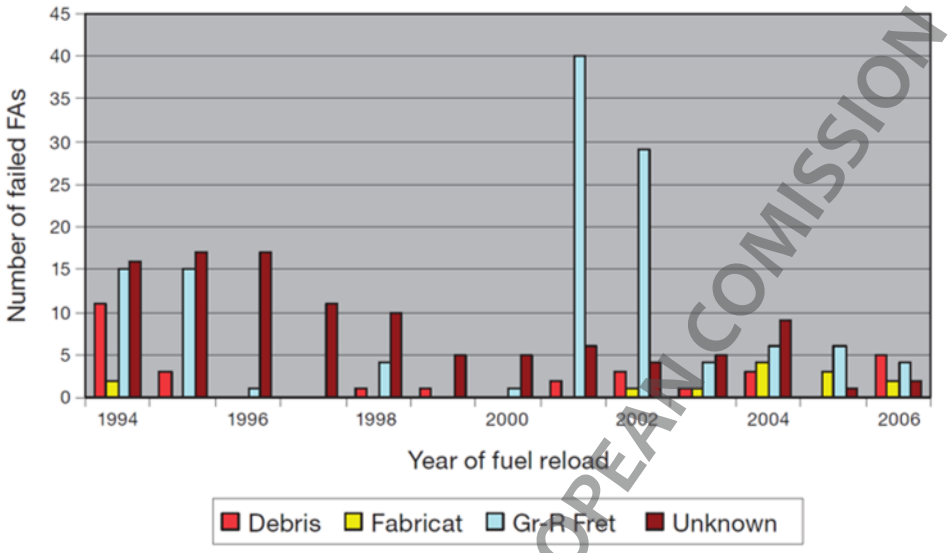

Figure 4: PWR fuel leak causes in France [9].

GTRFW induced fuel failures over the world have occurred with various PWR fuel designs that include Areva (current Framatome) 17x17 AFA 2G [11], 16x16 Korean Optimized Fuel Assemblies (KOFAs) [7], 17x17 Vantage5H of Westinghouse Electric Company, 18x18 FA for Konvoi of the former Siemens and 16x16 Guardian of the former Combustion Engineering, etc [12]. GTRFW would occur mainly at the bottom grid level [11] [13] and at the mid-grid positions; the first leak signals appear in a wide range of operating time/fuel cycles [12].

Such GTRFW events have pushed the fuel designers to search for optimized grid configurations. Improved grid design consisting in adding a second spacer grid at the lowermost position, in order to increase largely the clamping factor of the fuel rods in this part, was adopted by Areva (current Framatome) in order to reduce GTRFW [14]. Efforts for the improvement of the grid design in order to minimize fuel leaks due to GTRFW were made by EDF at the beginning of the years 2000 [15].

It has also to be recalled that the material property evolution with burnup play an important role on the GTRFW mechanism. The creep of springs and dimples under irradiation, for example, result in a relaxation of the support force provided to the rod: this, in turn, results in a more severe vibratory regime, compared to nominal conditions of a fresh FA [14].

Another aggravating factor in terms of GTRFW is the presence of local cross-flow inside the core, which is unavoidable. A non-zero cross-flow velocity increases the FIV, compared to pure axial flow, and a correlation between the regions of highest cross-flows and the position of leaking rods due to GTRFW is observed [15].

According to the IAEA report [9], GTRFW does not seem to represent a main cause of failure in BWRs.

1.2 Flow-induced vibrations resulting from baffle jetting

1.2.1 The baffle jetting phenomenon

According to IAEA [1], at the beginning of the 1980s, jets of water through the core baffles created damage to fuel elements in various NPP. It must be mentioned that baffle jetting is relevant only for reactors with specific reactor pressure vessel (RPV) design, in which counter-flow configuration in the core bypass region exists. In such RPV designs baffle plates are installed between the core barrel and reactor core itself, with the aim to provide the core's lateral restraint and to allow a core bypass flow (see Figure 5) [16] [17]. High pressure (p1) coolant coming from the cold leg enters the reactor downcomer and then part of it penetrates through the core barrel. Since the pressure in the core (p2) is significantly lower than the one in the downcomer, a portion of the bypass water flows through the baffle gaps and then impinges on the fuel assemblies located in the core periphery. In case of significant pressure differences between core and baffle regions and enlarged baffle gaps, the high velocity impinging jets might induce vibrations of the peripheral fuel assemblies' rods and even lead to fuel failure. Such fuel degradation may result in relatively high primary coolant activity and thereby impede periodic maintenance-related functions and/or pose radiological hazards to personnel.

As PWR plants age, more issues with baffle jetting have been observed in the NPPs. Increased baffle gaps that lead to baffle jetting may arise from baffle bolt breakage. Inspection programs of bolts have resulted in significant bolt replacements in impacted plants. Baffle jetting, either due to baffle bolt deterioration or general plant aging occurs in PWR plants with a downflow baffle barrel configuration. In those plants that have experienced baffle jetting, converting to an upflow barrel-baffle configuration has resolved the jetting issue, while also providing more grid-to-rod-fretting margin for third cycle fuel on core peripheries [18].

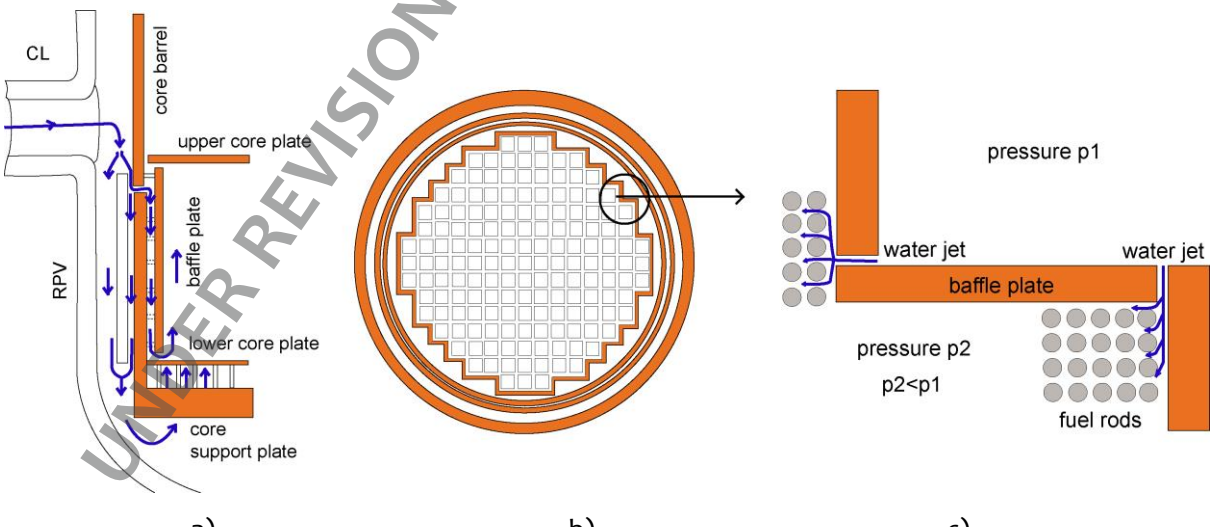

Figure 5 after [3]: Baffle jetting formation: a) downward baffle flow, b) location of peripheral fuel assemblies, c) schematics of water jets impinging through the baffle gaps on the fuel rods.

1.2.2 Baffle jetting in US NPP

Baffle jetting problem has been experienced in a limited number of Westinghouse PWRs. On May 6, 1982, Portland General Electric submitted a Licensee Event Report (LER) 344/82-06 to US NRC, describing abnormal fuel clad degradation identified during a pre-planned fuel inspection to locate suspected leaking fuel assemblies. Fuel rod damage involved 17 fuel assemblies examined at the end of Cycle 4 operation in Trojan NPP. Portions of fuel rods were found missing and loose fuel pellets were discovered and retrieved from reactor vessel internals and the refuelling cavity. Visual inspections revealed severe perimeter fuel rod failures in 8 fuel assemblies. Failures in the remaining 9 assemblies were detected by sipping operations, but did not exhibit visual damage [19].

For the Trojan reactor design, holes in the core barrel provide pathways for bypass flow which is diverted from the annulus between the vessel and the core barrel walls, to a downward direction through holes in the horizontal "former" plate segments (see Figure 6). This small portion of the coolant flow between the baffle plates and the core barrel, provides additional cooling for the barrel. However, most of the coolant flow coming from the vessel cold leg inlet nozzles flows downward through the annulus between the core barrel and the vessel walls, then into a plenum at the bottom of the vessel. It then reverses its direction and flows upward through the core of the reactor. A pressure differential is thereby established between the downward coolant flow in the vessel-barrel annulus and through the "former" plates, and the reversed upward flow through the core inside the barrel [19].

The aforementioned fuel rod damage in the Trojan NPP was attributed a water-jetting-induced motion of fuel rods in fuel assemblies that are close to baffle plate joint locations with enlarged gaps. Two mechanisms for baffle gap-related rod failures have been identified:

1. The first of these is the outside corner or center-injection jetting failure that is similar to clad degradation in the Trojan reactor. In this case, the water jet impacts on the third rod from the corner and causes its failure in the lower axial regions from direct water impingement, combined with induced rod whirling and vibration.

2. The second type of baffle gap-related failure is the inside corner or corner-injection jetting failure, whereby a jet of water flows parallel to the fuel bundle perimeter face between the fuel and the adjacent baffle plate. This flow also causes fuel rod whirling and vibration to occur at the first few rod locations. Such water-jetting parallel to these fuel rods leads to failure of the rods and to increased likelihood of failure propagation to adjacent rods. In general, the water-jetting-induced rod motion causes fuel rod fretting because of abnormal clad wear against the Inconel grid assemblies [20].

Similar fuel rod damage has been encountered previously. In April 1980, fuel rod failures were found in two fuel assemblies at the end of Cycle 2 for the Trojan reactor (LER 344/80-06). Similar events were also reported for the Point Beach 1 reactor during the years 1975 and 1977. These occurrences are delineated in LER 266/75-18 and 76-12, respectively. Further, three damaged fuel pins were found in 1971-1972 at a power plant outside USA, one failed pin was found in 1973 and 1975. In 1975, one fuel pin failed at Point Beach. These six fuel pin failures involved bypass flow through gaps in the inside corner of the baffle. The baffle joints in these plants had not been

peened prior to initial core loading. Joints were peened following discovery of the failures, and no subsequent damaged has been observed near the joints where the above failures were discovered [21].

Two nuclear fuel rods were found damaged during North Anna NPP refuelling in 2014 (LER 50-339/2014-002-00) [22]. On September 15, 2014, with Unit 2 defueled, 10 pieces of debris that had the potential to be fuel fragments was located on the core plate. The material was near the edge of the outer flow hole and partially under the gap between the baffle plate and the core plate. Video inspection of a particular fuel assembly identified that the top springs of two fuel pins were dislodged. This event was reported as any event or condition that results in seriously degraded safety barriers. Detailed video inspections estimated that fifteen fuel pellets were dislodged from the affected fuel assembly (the whole reactor core contains approx. 15 million fuel pellets). During efforts to identify and recover the fuel pellets, debris fragments estimated to represent five fuel pellets were found in the damaged fuel assembly that was then moved in the spent fuel pool. In addition, material from three pellets was retrieved by the foreign object search and retrieval efforts in the reactor. The remaining seven fuel pellets were expected to granulate into fine particles that will dissolve in low flow areas of the primary plant systems or to be removed by normal purification processes [22].

The investigations showed that the direct cause of the event was baffle jetting phenomenon. It caused the rods of the affected fuel assembly to start rotating and vibrating. This movement resulted in fuel rod wear and eventual mechanical failure and rod separation. The root cause of the failed fuel assembly was found to be the change in material properties of the baffle plates and bolting due to aging mechanisms resulting in the gap widening at the baffle joint. Stress, temperature, and irradiation since initial plant start-up have resulted in relaxation, creep, and loss of pre-load in the bolting and baffle plates. The changes in material properties allowed the gap in the corner baffle joint to widen when subjected to the relatively high differential pressure, approximately 1.7 bar, associated with the baffle-barrel downflow configuration in North Anna Unit 2. Unit 2 has operated without indications of baffle jetting for 34 years and Unit 1 has operated without baffle jetting since 1996 when the upflow conversion was performed. While Unit 1 did have baffle jetting issues prior to 1996, the baffle jetting issues were from the center joints. Whereas the Unit 2 baffle jetting was from a corner joint. Additionally, Unit 2 has a different bolting configuration that made it less susceptible to the baffle jetting experienced on Unit 1.

1.2.3 Baffle jetting in other NPP

The IAEA-TECDOC-1119 [1] states that baffle jetting damaged fuel assemblies in six French plants including Bugey 2 and Fessenheim 2. This effect was related to the pressure difference between the baffles with water down-flow in this location. Modifications in the baffle formers assuring water up-flow have reduced the pressure and suppressed baffle jetting. This modification was later implemented practically in all reactors of relevant design. For instance, Framatome converted the reactor lower internals of the Tihange 1 PWR in Belgium from a down-flow to an up-flow configuration in September 1986 [23].

In July 1979 fuel pin damage was detected in ten fuel assemblies at the Swedish Plant, Ringhals Unit 2. In November 1979, fuel pin damage was reported at the Kori Unit 1 in Korea on two fuel assemblies. In all these cases, the failures were encountered in assemblies which had been

associated with center injection points. In addition, the core support structures utilized a baffle plate design with a reduced number of edge-to-edge bolts on adjoining baffles [21].

Six leaking fuel assemblies at the Slovenian Krško NPP were identified by telescope sipping following Cycle 26 [24]. During subsequent core offload activities, it was determined that an object seen in the transfer canal at Krško was a fuel rod part (~50 cm long). Subsequent investigation determined that the fuel rod section separated from one of the leaking assemblies during transport through the canal. The root cause analysis team investigated the use of the six leaking assemblies and determined that the damage observed on fuel assemblies is similar to observations of baffle jetting. It was also pointed out that baffle jetting can cause fluid elastic instability (FEI). This causes large amplitude rod vibration and structural damage. Baffle plates may distort/move under the pressure differential in the baffle-barrel region during operation, due to irradiation-induced effects or some other aging/mechanical phenomenon, such that small gaps can form. There is no clear, identified cause to the onset of baffle jetting seen at Krško. In order for baffle jetting associated fuel damage to occur, there must be [24]:

1. a sufficient pressure difference across the baffle plate and
2. a large enough baffle joint gap to result in sufficient momentum flux to excite the fuel rod into whirling motions resulting in wear between the rod and the grid. Historically, sufficiently strong jets can cause FEI on one to four fuel rods adjacent to the baffle gap.

1.2.4 Measures against baffle jetting

Different solutions were implemented against the baffle-jetting phenomenon in the NPP. One fix of the baffle joint is to peen the entire joint to reduce the gaps between baffle plates. However, as noted in the Trojan Event Report (82-06) relating to the problem, the gaps in the corner-injection baffle joints were apparently enlarged during the peening of the center-injection baffle joints at the end of Cycle 3 operation in 1981. In addition, peening did not entirely dispose of the problem with the center-injection assemblies, since damage was found in three fuel assemblies of this type.

A more successful interim solution includes the use of modified fuel assemblies to replace those damaged assemblies adjacent to baffle plate joints. Such modified fuel assemblies which utilize stainless steel fuel rods have been licensed and used previously. Two fuel assemblies were modified for Cycle 3 operation at Trojan, as a result of the baffle jet problem described in LER 344/80-06. Three Zircaloy-clad rods in each of two assemblies were replaced with solid stainless steel rods of the same diameter and length as the fuel rods. Damage was not observed in the modified assemblies at the end of Cycle 3 or at the end of Cycle 4. These assemblies were located adjacent to baffle corners where water-jetting-induced fuel rod degradation had occurred [20]. LER 344/82-06 cites the continued use of modified fuel assemblies with stainless steel rods, in addition to inserting partial grids that provide midspan support to fuel rods adjacent to corner-injection baffle joints. The partial grids serve to increase the frequencies and decrease the amplitudes of the fundamental modes of vibration for fuel rods, and thus raise the threshold for rod vibration, which causes clad damage. With regard to the center-injection assemblies, the most vulnerable fuel rod (the one nearly aligned with the baffle plate gap) and the two adjacent fuel rods in the first row are to be replaced with stainless steel rods to minimize the possibility of additional baffle-jet-induced

failures. Assemblies with solid stainless steel rods near the baffle plate joints were loaded in the core of Krško NPP.

Further, Westinghouse invented a nuclear fuel assembly design especially suitable for use at a peripheral core location where coolant-jetting through core baffle structure may occur. In addition to ordinary fuel-rod support grids, the fuel assembly includes anti-vibration grids that lend vibration-damping support to the fuel rods near the outer periphery of the fuel assembly. This improved design was patented by the European Patent Office with European Patent Application EP 0 290 865 A3 [25].

1.3 Fuel assembly bow

FA bow can be the result of different mechanisms. On the one hand, non-uniform coolant temperature, non-uniform heat transfer between the coolant and the rods and radial gradients of neutron fluxes cause temperature gradients, which result in differential thermal expansions. The fuel element, therefore, bows in order to accommodate such expansions. On the other hand, the observation of the encountered bow patterns underlines that FA bow is (co)determined to a high degree by fluid-structure interaction (FSI) effects [26].

Numerical studies have demonstrated that the actual flow distribution at the inlet of the core, i.e., with higher velocities at the center of the core, is more likely to cause a deformation of certain FAs, compared to assuming a uniform velocity profile [27]. These results suggest that the cross-flows resulting from the actual flow profile in the lower part of the core has a significant impact on the FA bow.

Hovard and Dressel [27] investigated the impact of a coupled versus an uncoupled approach for the FSI problem. They concluded that taking into account the coupled FSI mechanism had a primary impact on the FA bow, in terms of predicted deformation amplitude. Therefore, the FSI and FIV linked to cross-flow seem to represent a non-negligible contribution to FA bowing phenomena.
Generally speaking, one may also note that FA bow is likely to induce additional local cross-flows, since: first, larger and smaller bypasses resulting from the bow deformation lead to modified pressure loss distributions potentially resulting in locally increased cross-flow inside the core and secondly, the deformation of FAs will result in deviations between the coolant mean axial/vertical flow direction and the fuel rods axis (which, in nominal no-bow conditions, is parallel to the coolant mean axial flow). Moreover, these mechanisms would increase cross-flow bowing forces as a function of the bowing amplitude, in a sort of in chain mechanism. Stating that cross-flows can result in additional excitation sources (turbulent excitation and gap-limited fluid-elastic instability) for fretting wear, King et al. [28] investigated (numerically and experimentally) the impact of bowed FAs on local cross-flows inside the core. They found that bowed FAs have a significant impact on flow distribution because of the modified axial and lateral flow areas and pressure losses, compared to nominal (no bow) conditions: bow-induced cross-flow was found to be much stronger compared to no-bow cross flow in certain core regions.

The bow patterns (or shapes) most commonly observed in discharged FAs are the so-called C-shape and S-shape: they correspond to the first and second FA bending mode, respectively.

The bowing of FAs can result in shorter than nominal or incomplete control rod insertion, because of the increased friction between the control rod and the guide tube. Such issues were observed in several PWRs [29]. One of the first documented Incomplete Rod Cluster Assembly Insert (IRI) event due to FA bow occurred in Ringhals Nuclear Power Plant, Sweden [30]. During a reactor trip in Ringhals unit 4, in August 1994, one Rod Cluster Control Assembly (RCCA) stuck at 18 steps, i.e. in the dashpot region of the guide thimble tubes. At a subsequent hot rod drop test, four RCCAs stuck at the elevations 6, 12, 12, and 24 steps. Measurements of the axial shape of the FAs experiencing sticking showed that they were bent in S-shape and with significant bending amplitudes. The location of the maximum amplitude of the upper hump of the S was coincident with the point where the drop velocity started to decrease and the step increase of the drag force was found during drop time testing.

In 1996, the Belgian units Tihange 3 and Doel 4 experienced IRI [30] [31] after a SCRAM. The position of the control rods was verified after the SCRAM and five control rods were found to have a different position compared to the requested position and the deviation varied between 9 and 19 steps. FA deformation measurements showed C-shaped deformation with a maximum amplitude of 19 mm and S-shaped deformation with a maximum amplitude of 21 mm.

In 2010, irregularities in terms of control rod drop time were detected at unit 2 of the French Chooz B NPP [32]: during a control rod drop test, two rod clusters featured IRI and six did not respect the drop time criteria. EDF attributed these incidents to FA lateral deformations of much higher amplitude than the ones detected before in French NPPs [32].

1.4 Flow-induced vibrations in other NPP components

FIV were observed not only in the reactor core or steam generators – two of the key components of the nuclear steam supply system (NSSS). Vibration phenomena were found also in other NPP components. The following subchapters briefly describe such occurrences in some plants.

1.4.1 FIV as a result of cavitation in orifices

During outage of a Nordic NPP, a small diameter piping started to leak at a weld [33]. It was found that the cause of the leak was high cycle fatigue. The performed root cause analysis showed that this fatigue resulted from:

- Design with a large eccentric mass
- High vibration levels
- The vibration level was above the acceptance criterion.

The cause of the high vibrations was determined to be due to cavitation in orifices in the NPP piping. An orifice plate is a device used for measuring flow rate, for reducing pressure or for restricting flow. Cavitation is the creation of gas bubbles in a liquid when the local, static pressure, p_s, somewhere in the fluid (which is fluctuating in a turbulent flow) becomes below the saturation pressure for a given temperature, $P_s < P_{sat}(T)$. If the liquid with a flowrate Q is flowing in a pipe at high speed, the dynamic pressure and the pressure drop over the orifice plate can become high so

that the local static pressure becomes low and cavitation occurs at a relatively low temperature. Such cavitation phenomenon in an orifice is accompanied by a characteristic sound that reminds of a grovel through the pipe. Increasing cavitation in a flowing liquid in a pipe system is associated with increasing levels of sound or noise and vibrations. It may cause large loads if steam bubbles implode close to the pipe wall, which can be harmful to the pipe system. Such phenomena may result in fatigue due to vibrations and even worse, erosion of the pipe wall. In the worst case, it can lead to a pipe break. Therefore, cavitation is essential to be predicted and prevented in system design [34] in order to eliminate harmful cavitation induced vibrations.

To increase the robustness with respect to high cycle fatigue, some measures were taken at the NPP. First, the heavy flange was replaced with a plug. In a next step, a new orifice design was introduced, in which single stage orifices were replaced with multihole-multistage device. After testing, the new orifice design was installed in the plant and this resulted in acceptable vibration levels.

1.4.2 FIV resulting from power uprate programs in NPP

Many NPP operators strive to uprate the thermal, and eventually the generated electric power of their plants, in order to improve their economics and generate more income from the sold electricity. Power uprates are often related to increased power generation in the core, as well as increased temperatures, pressures, mass flow rates. A thermal power increase of 10% in a boiling water reactor (BWR) would yield a flow velocity increase of the maximum main circulation flow to 18% [35]. The high flow rate results in higher velocities that may induce structural vibrations. Therefore, FIV investigations for different plant components precedes each power uprate program. The preliminary investigation provides only an order of magnitude for the calculated displacements. The results are then used to develop a risk informed measurement, analyses, and inspection program.

First, the velocities in the Recator Pressure Vessel (RPV) have to be analyzed. The RPV is divided into volumes where FIV related issues may occur. Mass flow, local average flow velocities, fluid densities, temperature and pressure are calculated in predefined local areas with system codes. These are calculated for the original design and the uprated one. Not all velocities can be calculated by the codes. In such cases estimations and calculations by hand are performed. In a typical BWR, the highest flow velocities occur in the main steam nozzle (~160 m/s) and in the main steam lines (~60 m/s). Then, the flow excitation mechanism, relevant for each component, is identified. Within a risk assessment, the risk for the structures and the potential consequences are evaluated. The analyses show that BWR head cooling spray piping, especially the long nozzle pipes, have highest increased risk for FIV. Moderate increased risk for FIV is relevant for the in-core neutron flux detectors' guide tubes, the control rods, the control rod guide tubes, and the feedwater lines [35].

1.4.3 FIV in feedwater lines and valves

FIV occurred also in feedwater lines, such occurrence is reported [33]. The feedwater pumps provide secondary water in the PWR steam generators. In the affected plant two turbine trains with three pumps each are installed, with two out of each three pumps running simultaneously. The speed of the pumps can be adjusted by increasing the differential pressure of the main flow control valves that regulates the water level in the steam generators. Within the frame of a plant

uprate, pump impellers were replaced and the flow rate was increased of approximately 11-14%. Thereafter, high vibrations at and around the pumps were observed: six out of twelve pumps exhibited at certain structural vibration velocities over 5 mm/s. Analyses with different structural codes revealed that the corresponding frequencies of these vibrations lie between 500 and 550 Hz, which was in a good agreement with the measured values. The pressure fluctuations resulting from the pump were further investigated with the help of a CFD code.

High-resolution CFD analyses were performed to investigate the reason for the increased wear of the feedwater isolation check-valves after an extended power uprate (EPU) in Oskarshamn 3 NPP in 2009 [36, 37]. These showed unstable flow for 120% and 129% reactor power. The velocity field around the check valves showed a highly unstable behavior with large fluctuations of nearly ±10m/s close to the valve.

At 129% the axial forces on the valve plunger cause friction forces that are larger than the lateral forces caused by the unstable flow. At 120% the lateral forces could be higher than the friction forces, which could cause vibration and eventually the damage that has been found in the plant [36]. Steam-line vibrations after the EPU resulted in longer operation times at 120% reactor power. The check-valves in the feed-water system were originally designed for 7 m/s, while these were operated at 10 m/s. Further conclusion showed that numerical analyses could had helped to predict in advance the observed vibration issues in the aforementioned components.

1.4.4 FIV in steam lines

The steam generators at Ringhals 3 were replaced in 1995. After the installation of the new ones, high vibration levels were measured in the steam lines [33]. Root mean square vibration velocities of ~19 mm/s were measured. To reduce the steam line vibration levels, viscous dampers were installed. This reduced the vibrations levels by a factor of 10. However, the root cause of the problem was not solved. It was found that the root cause of the vibration appeared to be pressure pulsations generated in the steam generator outlet nozzle. To reduce the pressure pulsation levels a new design of the outlet nozzle was developed using experimental trials. Specifically, it was the venturi part of the outlet nozzle that had to be redesigned in order to reduce the pressure fluctuations in this region. The new design was successfully implemented 1998.

Vibrations were monitored in the main steam lines (MSLs) after the extended power uprate (EPU) from 109% to 129% power in 2009 was realized in Oskarshamn Unit 3 [36]. Concerning the MSLs vibrations, it was found that the measured high vibration levels in these lines at 110-120 Hz were caused by a resonance in the accelerometer clamps. These vibrations turned out not to be a problem for the piping system.

1.4.5 FIV in steam line valves

In a European NPP, power uprate plans were made in the late nineties and early 2000 [38]. This led to the need to update design loads and review plant components. Some internal reactor parts were replaced, and it was decided to change the main steam stop-control valves. Their housing was kept, while the internals were replaced. This activity was performed during a refueling outage. Approximately three weeks after recommissioning of the plant a pipeline to one actuator was broken. Therefore, accelerometers and vibration measurement devices were installed placed on the steam line and stop-control valve. Measurements revealed high vibration levels with

accompanying hammer strokes. Structural accelerations up to 50-60 g with frequencies up to 2 kHz were measured. As a consequence, the plant power had to be reduced down to 30 % of the nominal power for the rest of the operating season.

It was found the valve seat was damaged by a hammer stroke. This was believed to originate from a strong irregular flow field and very low static pressure. At the beginning plant staff and valve vendor could not believe that the vibrations stemmed from the valve design, until detailed CFD simulations were performed at the NPP.

Vibrations were monitored in the main steam isolation valves (MSIVs) after the extended power uprate (EPU) in 2009 was realized in Oskarshamn Unit 3 [36]. The reactor power was increased from 109% to 129%. The vibration frequency in the MSIVs was at around 660 Hz appearing at steam velocities of 71 m/s in the valve seats. The increased vibrations of the MSLs were not really a acute problem but in the long run could cause damage and should be mitigated.

Simulations and scaled experiments for the MSIVs showed that vortex shedding above valve cavities is coupled to acoustic modes in the valve cavity. The shedding vortices have a broad band of frequencies that are proportional to the steam velocity. Blocking cavities in the MSIV leads to the excitation of other acoustic modes. Both phenomena were decoupled in the NPP by breaking the coherence in the vortex.

In the end it was concluded that the proven design is very important. The new MSIVs that were installed had only been used for velocities up to ca 70 m/s, while in the plant steam velocities reached 90 m/s.

1.4.6 Core barrel vibration

FIV are also relevant for RPV internals. In a Nordic NPP, enlarged gaps between the core barrel and the RPV were found. The measured gaps were approximately five times larger than the design specification. The cause for these deviations was identified to be core barrel vibration that led to material wear and increased gap sizes. Numerical analyses with CFD and CSM codes were performed in order to better understand the nature of these vibrations. These helped to calculate the pressure field on the core barrel and the resulting on core barrel displacement [33].

1.4.7 Vibration of thermal sleeves

A thermal sleeve is made of stainless steel. During plant operation with no control rod movement, the thermal sleeve limits hot water flow from the vessel head to the control rod driving mechanism (CRDM). A guiding cone guides the drive shaft during reactor vessel head handling operation for closure. The thermal sleeve tube also guides control rod drives (CRD) through the adapter and inside the CRDM. In case of control rod drop, water flow from the bottom to the top of the CRDM lifts the thermal sleeve, which increases the flow area to improve the rod drop time. When the control rod is lifted, cold water at the top of the adapter moves down through the thermal sleeve tube, thus protecting the penetration weld.

In the last few years, an increasing number of industry events have revealed thermal sleeve wear issues as a result of flow-induced vibrations. Thermal sleeve flange wear is evidenced by a lowering of the thermal sleeve relative to the rest of the closure head. In certain cases, wear has led to the

thermal sleeve flange interfering with movement of the CRDM and ultimately failure of the thermal sleeve. In severe cases, wear on both the adapter and thermal sleeve stop causes loose parts, which could generate control rod blockage [39] [40]. Framatome has successfully replaced more than 30 thermal sleeves since 2018 in different NPP around the world.

1.5 Flow-induced vibrations in steam generators

Considering the important steam-water flow rate, the thousands of tubes composing the tube bundle and the specific tube configuration (long tubes of thin diameter with U shape), FIV phenomena occur in nuclear steam generators (SGs). Among all possible SG configurations (vertical U-tube, vertical once-through, horizontal, etc.), PWR U-tube SGs have been the ones historically more concerned by vibration issues. A status of reported SG tube degradation and failure due to FIV until 1996 can be found in [37]; the same document also lists all the reported Steam Generator Tube Rupture (SGTR) events, until 1996.

Turbulence-induced vibrations generated by the high velocity vapor-water mixture are characterized by small amplitudes. Nevertheless, even these small amplitudes can lead to long term fretting wear in the tube-to-support plate (SP) and in the tube-to-anti-vibration bar (AVB) contact regions. Excessive fretting can eventually result in tube failure. Moreover, fretting wear on tube-AVB contact point can lead to modification of the AVB support condition, decreasing AVB effectiveness versus FIV. According to [37], fretting/wear/thinning degradation was noted to some degree in all PWR SG designs, mainly (but not only) at the AVB contact points. As of December 1993, 116 NPPs with recirculating SGs were reported to experience tube failure due to AVB wear/fretting, resulting in the plugging of 4,663 tubes.

More severe and short-term tube rupture, compared to fretting, occurs in case of high-cycle fatigue, which features high vibration amplitude. This is the result of the so-called fluid-elastic instability (FEI) mechanism. FEI occurs when the amount of energy added per vibration cycle by the fluid-elastic displacement is greater than the amount of energy dissipated each cycle through damping [41]. Energy is dissipated due to the combined effects of frictional damping at the tube supports, tube material damping and fluid damping. FEI was the cause of SGTR occurred in the U-bend regions of the North-Anna NPP Unit 1, USA, in 1987 and at the Japanese Mihama NPP Unit 2, in 1991 [37].

FEI was found to be the root cause of the four reactor shutdowns due to primary-to-secondary reactor coolant leak occurred between 2004 and 2008 at the French Cruas NPP; the phenomenon was caused by a modified thermal-hydraulic of the steam-water secondary coolant, due to clogging of the tube support plates [42]. One of the most severe examples of FEI in SGs was observed at the SONGS NPP, USA, in 2012, where, following a shutdown due to a primary-to-secondary reactor coolant leak, wear on hundreds of tubes of the SGs were discovered [43]. This wear was unexpected, considering that both SGs had been recently replaced before the accident. The tube-to-tube wear mechanism observed was determined to be caused by in-plane FEI, associated with adverse secondary thermal-hydraulic and lack of effective in-plane tube support. In-plane FEI had never been observed before in operating NPP SGs.

1.6 Summary

Degradation from small amplitude, oscillatory motions between continuously rubbing surfaces, is generally termed fretting. Vibration of relatively large amplitude, resulting in intermittent sliding contact between two parts, is termed sliding wear, or wear. Fretting and wear are phenomena that must be avoided in NPP. These phenomena had led to numerous component failures in NPP around the world.

NPP FAs have historically been concerned by fuel leakage with GTRFW being one of the most common causes of fuel failure. GTRFW is generally caused by the axial turbulent coolant flow, that exerts fluid forces and eventually rod vibrations with consequent impacts between the rod surface and the spacer grid contact points. Improved grid design featuring a second spacer grid at the lowermost position largely increased the clamping factor of the fuel rods in that region, thus largely decreasing the turbulence induced vibrations in axial flow. It is important to mention that fuel rod vibrations also occurred in cross-flow conditions. Jets of water through the core baffles impinged laterally on the fuel assemblies and damaged fuel elements in various NPP. All these plants had a specific design of the RPV downcomer. Solutions included the use of modified fuel assemblies, which utilized stainless steel fuel rods at certain positions in the FA grid, as well as changes in the original downcomer construction.

FIV phenomena occurre also in nuclear SG. Among all possible SG configurations (vertical U-tube, vertical once-through, horizontal, etc.), the PWR U-tube SGs have been the ones historically more concerned by vibration issues. Turbulence-induced vibrations, generated by the high velocity vapor-water mixture, are characterized by small amplitudes. These can result in a long-term fretting wear in the tube-to-support plate and in the tube-to-anti-vibration bar contact regions. Vibrations, induced by vortex-shedding are mainly relevant for the highest, arc-type U-bend region of the U-tubes. More severe and short-term tube rupture, compared to fretting, occurred in case of high-cycle fatigue with high vibration amplitude, as a result of FEI. A number of plants experienced SGTR in the past, as a result of FEI in the U-bend region of the SG. Improved AVB and support plate designs help to reduce vibration phenomena in SG.

Vibrations have led also to issues in other NPP components. FIV occurred in feedwater as well as in steam lines and valves. Some of these were related to the change in the original component design, for example, as a result of plant power uprate programs. Vibration of core barrel and thermal sleeves are also worth of investigation. In the last few years, an increasing number of industry events have revealed thermal sleeve wear issues as a result of FIV, which might end with a control rod blockage. The damaged thermal sleeves were replaced with new ones.

1.7 References

[1] IAEA, "Assessment and Management of Ageing of Major Nuclear Power Plant Components Important to Safety: PWR Vessel Internals," *IAEA-TEDOC-1119*, 1999.

[2] M. Ramos, "EU Clearinghouse on NPP OEF Summary Report on Fuel Related Events," *JRC 60219,* Vols. ISBN 978-92-79-17529-9, 2010.

[3] W. Bailey and S. Wu, "Fuel performance annual report for 1986," *NUREG,* Vols. CR-3950 PNL-5210 Vol. 4, 1988.

[4] N. Utilities, "Millstone nuclear power station, Unit No. 2 failed fuel assemblies," *Docket No. 50-336 A03429,* 1983.

[5] "Recent fuel and core performance problems in operating reactors," *Nuclear Regulatory Commission information notice,* 1993.

[6] "Assessment of Ft. Calhoun fuel rod fretting history and root cause as it relates to implementation of ZIRLO^{TM} cladding material in fuel deisgned by {CE} Nuclear Power," *Westinghouse Electric Company LLC,* Vols. LD-2001-0028, 2001.

[7] K.-T. Kim, "A study on the grid-to-rod fretting wear-induced fuel failure observed in the 16x16 KOFA fuel," *Nuclear Engineering and Design,* vol. 240, pp. 756-76, 2010.

[8] "Le point de vue de l'IRSN sur la sûreté et la radioprotection du parc électronuclèaire français en 2009," *IRSN - Rapport DSR No 383.*

[9] IAEA, "Review of Fuel Failures in Water Cooled Reactors," *IAEA Nuclear Energy Series,* Vols. No. NF-T-2.1, 2010.

[10] IAEA, "Review of Fuel Failures in Water Cooled Reactors (2006-2015)," *IAEA Nuclear Series No. NF-T-2.5.*

[11] G. Gentet and et al., "AREVA product experience in support of EPR^{TM} fuel design," *Transactions of Top Fuel Reactor Fuel Performance 2012. Manchester, UK, 2-6 September 2012.*

[12] M. Kennard, D. Sunderland and J. Harbotte, "A Study of Grid-to-Rod Fretting Wear in PWR Fuel Assembly, vols. 1 and 2," *S.M. Stroller Co.,* 1995.

[13] Y. Fournier, C. Vurpillot and Y. Bechaud, "Evaluation of fluid flow in the lower core of a PWR with Code_Saturne," *Nuclear Engineering and Design,* vol. 237, pp. 1729-1744, 2007.

[14] B. D'Uston, "Non-linear vibrations of fuel rods under turbulent excitation," *IAEA-TECDOC-1454. Structural behaviour of fuel assemblies for water cooled reactors. Proceedings of a technical meeting held in Cadarache, France, 22-26 November 2004.*

[15] N. Baillon, "Grid to rod fretting wear in EDF PWR from operating problems to new designs qualification method," *IAEA-TECDOC-1454. Structural behaviour of fuel assemblies for water cooled reactors. Proceedings of a technical meeting held in Cadarache, France, 22-26 November 2004.*

[16] U. Bieder and A. Rashkovan, "Baffle Jetting: CFD Analysis of Plain Jets Impinging on Fuel Rods," *Progress in Nuclear Energy,* vol. 114, pp. 31-45, 2019.

[17] IAEA, "Fuel Failure in Normal Operation of Water Reactors: Experience, Causes and Mitigation," *IAEA TECDOC-2004.*

[18] IAEA, "Fuel Failure in Normal Operation of Water Reactors: Experience, Causes and Mitigation," *IAEA-TECDOC-2004,* 2004.

[19] NRC, "Information Notice No. 82-27: Fuel Rod Degradation Resulting from Baffle Water-Jet Impingement," *SSINS No.: 6835,* 1982.

[20] U. NRC, "Information Notice No. 82-27: Fuel Rod Degradation Resulting from Baffle Water-Jet Impingement," vol. SSINS No.: 6835, 1982.

[21] U. NRC, "Fuel Pin Damage Due to Water Jet from Baffle Plate Corner," vol. SSINS No.: 6830, 1980.

[22] U. NRC, "Licence Event Report: Failed Fuel Assembly at North Anna Power Station," Vols. Report No. 50-339, 2014.

[23] R. Gérard, D. Bertolis and S. Vissers, "Ageing Management of the Reactor Internals in Belgian Nuclear Units in View of Long Term Operation," *IAEA-CN-194-021.*

[24] E. P. Office, "Nuclear Reactor Core Containing Fuel Assemblies Positioned Adjacent Core Baffle Structure," vol. EP 0 290 865 A3, 1988.

[25] "European Patent Office, European Patent Application EP 0 290 865 A3 Nuclear Reactor Core Containing Fuel Assemblies Positioned Adjacent Core Baffle Structure," 1988.

[26] J. e. a. Stabel, "Advanced methodology to predict in reactor bow of PWR fuel assemblies for efficient design optimization: background, validation, examples," *Water Reactor Fuel Performance Meeting, Chengdu, China, Sept. 11-14, 2011.*

[27] A. Horvath and B. Dressel, "On numerical simulation of fuel assembly bow in pressurized water reactors," *Nuclear Engineering and Design,* vol. 265, pp. 814-825, 2013.

[28] S. King and et al., "Flow induced vibration and fretting wear in PWR fuel," *In: Proceedings of ICONE10, Arlington, VA, April 14-18, 200.*

[29] "Nuclear Fuel Safety Criteria Technical Review - Second Edition," *NEA OECD report. ISBN 978-92-64-99178-1,* 2012.

[30] S. Jacobson, "Incomplete Control Rod Insertion due to Extreme Fuel Element Bow," *In: Proceedings of {NEA} - Specialist meeting on nuclear fuel and control rods: operating experience, design evolution and safety aspects, Madrid, Spain,5-7 November 1996.*

[31] D. Degreve, H. De Baenst and J. Van Vyle, "Belgian Operating Experience with RCCA Behaviour," *In: Proceedings of {NEA} - Specialist meeting on nuclear fuel and control rods: operating experience, design evolution and safety aspects, Madrid, Spain,5-7 November 1996.*

[32] "Le point de vue de l'IRSN sur la sûreté et la radioprotection du parc électronuclèaire français en 2010," *IRSN - Rapport {DSR} N^{o} 466.*

[33] P. Veber and et al., "Flow Induced Vibrations at Ringhals NPP," *Proc. of the GO-VIKING Stakeholders' workshop, Chatou, France, February 16, 2023.*

[34] K. Angele, "Elimination of Cavitation Induced Vibrations in Orifice Plates," *Experimental and Computational Multiphase Flow,* vol. 4(3), pp. 310-317, 2022.

[35] P. Smeekes, "TVO OL1/OL2 Power Uprate Prestudy Risk Survey for Flow Induced Vibrations (FIV) OF RPV Internals," *Proc. of the GO-VIKING Stakeholders' Workshop, Chatou, France, February 16, 2023.*

[36] T. Probert and S. Ring, "Analysis of Flow-Induced Vibrations in MSIVs, MSLs and Feed-water Check-Valves in Oskarshamn Unit 3 (O3) by Using Acoustics, CFD and Coupled acoustics/CFD," *Proc. of the GO-VIKING Stakeholders' Workshop, Chatou, France, February 16, 2023.*

[37] P. MacDonald and et al., "Steam Generator Tube Failures," *NUREG/CR-6365 INEL-95/0383,* 1996.

[38] H. Lindqvist, "How Things Can Go Wrong, High Vibration Levels in Steam Lines," *Proc. of the GO-VIKING Stakeholders' Workshop, Chatou, France, February 16, 2023.*

[39] Framatome, "Thermal Sleeve Wear," *Framatome advertising material, 2023. https://www.framatome.com/solutions-portfolio/docs/default-source/default-document-library/product-sheets/a1795-b-us-g-en-725-9-21-thermal-sleeve-pdf.pdf?Status=Master&sfvrsn=5fcc6e16.*

[40] S. Maingot, "Flow induced vibrations - EDF operating experience or reactor vessel internals," *Proc. of the GO-VIKING Stakeholders' Workshop, Chatou, France, February 16, 2023.*

[41] H. Connors, "Fluidelastic vibration of tube arrays excited by cross flow," *The winter annual meeting of the ASME, New York,* 1970.

[42] IRSN, "REP - Fatigue vibratoire des tubes de générateurs de vapeur," *Avis IRSN N°2012-00539.*

[43] NRC, "San Onofre Nuclear Generating Station - NRC Confirmatory action letter response inspection 05000361/2012009 and 05000362/2012009," 2013.

2. Currently available experimental data and methods for FIV in FAs

K. Zwijsen, M. M. Hussain

2.1 Introduction

In most conventional FA designs, the mean flow is parallel to the tubes over the majority of the tube span. This is true for most Gen-II and Gen-III Light Water Reactors (LWRs), such as Pressurized Water Reactors (PWRs) and Boiling Water Reactors (BWRs), and most Gen-IV Heavy-Liquid Metal Cooled Reactors (LMRs). This axially directed flow is highly turbulent. For example, within a PWR FA, the average axial velocity is approximately 5 m/s, resulting in a Reynolds number, based on the hydraulic diameter of the FA, of about $5 \cdot 10^5$. The energy present in the turbulent flow, which is bounded by the surrounding structural elements, results in a fluctuating pressure force on the fuel rods. This fluctuating pressure force on its turn leads to flow-induced vibrations (FIV) of the fuel rods. As the turbulent flow is the driving force of the vibrations, this phenomenon is also referred to as Turbulence-Induced Vibrations (TIV).

The main concern for conventional fuel assemblies related to the flow-induced vibration is the potential for the damage of the fuel rod cladding at the points of their contact in the spacer grids cells caused by the motion of the fuel rods relative to spacer grids. This phenomenon, known as grid-to-rod fretting wear (GTRFW), is responsible for over 70% of all fuel rod leakages in US PWRs [1] and 58% of fuel failures in PWRs worldwide. Excessive fretting could lead to the cladding of the fuel rod be worn through, thereby releasing fission products into the primary coolant, which is a serious safety issue. Additionally, damaged fuel rods are a cause of expensive unplanned outages of the nuclear power plant (NPP). Hence, knowledge of the fuel rod vibrations, and ensuing wear, is of vital importance for the safe operation of NPPs.

2.2 Analytical models for FA FIV

The turbulence present in the flow that causes TIV could be generated locally by the fluid as it flows around the structure and gives rise to boundary-layer turbulence pressure fluctuations. This is termed as near-field excitation. On the other hand, turbulence could also be resulting from flow pulsations or vortex shedding over submerged objects, or be generated by upstream components such as inlet nozzles, elbows, pipe bends. This is termed as far-field excitation [3]. The intensity of the turbulence is further significantly increased by the presence of spacer grids and mixing vanes in the fuel assemblies. The spacer grids are responsible for keeping the fuel rods in place, while the mixing vanes are installed to enhance the mixing, and with that the heat transfer, of the coolant flowing along the fuel rods. The presence of these spacer grids and support plates intensifies the turbulence locally and ensures that the far-field excitation can be generally assumed to be of far less importance than near-field fluctuating pressure forces.

These fluctuating surface pressures vary randomly in time and space in the sense that (1) they are characterized by a broad band frequency excitation range, (2) their amplitudes vary along the structure surface, and (3) their correlation length is very small relative to the length of the structure. This means the resulting vibrations cannot be treated in a deterministic way; instead probabilistic methods must be employed [4]-[5].

It is possible to provide an analytical solution to TIV if one assumes that (a) the fluid pressures are independent of the motion of the structure and (b) the fluid pressures are stationary in the sense that averages made over many cycles of oscillation are independent of the start of the averaging interval [4]-[5]. With these assumptions, using the theory of random vibration, the mean of the squared response of the structure in a single mode is [4]:

$$\overline{Y^2} = \frac{CS_p(f_i)J}{f_i^3 \zeta_i m^2} \psi_i^2(z), \tag{1}$$

where m is the mass per unit length of the structure, f_i is the natural frequency for the i-th mode, ζ_i is the damping factor of the i-th mode and ψ_i is the mode shape. $S_p(f_i)$ is the turbulence spectrum at f_i and J represents the joint acceptance of the turbulence for the i-th mode. Joint acceptance is a measure of the efficiency of the pressure forces to excite a certain mode. C is a constant that depends on the definition of S_p and J. Two rational approaches to the random vibrations of structures have generally been employed in the literature [5]:

1. *Theory of Random Vibration*: This is to employ Equation (1) directly and then estimate the power spectra and joint acceptance of the turbulence to determine the mean square response. However, accurate estimates of power spectra and joint acceptance are rarely available for a particular system.
2. *Empirical Approach*: This is to by-pass the theory of random vibrations and empirically correlate observed vibration levels with known system parameters such as flow velocity and hydraulic diameter. However, this approach often neglects a parameter of fundamental importance, such as damping, and so can lead to erroneous results when applied to new systems.

2.2.1 Early semi-empirical models

The early equations to estimate the vibration amplitude were based on the empirical approach, correlating test data with system parameters. Burgreen et al. [6] was the first to propose an equation, using dimensional analysis to correlate the vibration amplitude y to three nondimensional parameters:

$$\left(\frac{y}{D_h}\right)^{1,3} = 0.83 \cdot 10^{-10} \kappa \left(\frac{\rho U^2 L^4}{EI}\right)\left(\frac{\rho U^2}{\mu f}\right), \tag{2}$$

with D_h the hydraulic diameter, L is the length of the tube, ρ is the fluid density, U is the fluid mean velocity, μ is the fluid viscosity, E is the Young's modulus of elasticity, I is the moment of inertia, f is the natural frequency of the tube and κ an end fixity factor.

Quinn [7], using data obtained from tests on single and multiple pipes in two-phase steam-water flow, and Basile et al. [8], based on experiments in air and water with different types of fuel element cans, proposed their own formula based on their own experiments. Païdoussis [9], [10] gathered all the experimental data available in [6], [7], [11]-[14] to establish a different expression, accounting also for the added mass effect:

$$\frac{y}{D} = \alpha_1^{-4}\left(\frac{(u^2\varepsilon^2 Re)^{4/5}}{1+2u^2}\right)\left(\frac{\beta^{2/3}}{1+4\beta}\right)\cdot 10^{-5}, \tag{3}$$

with

$$\varepsilon = \frac{L}{D}, \quad \beta = \frac{M}{M+m}, \quad u = UL\left(\frac{M}{EI}\right)^{0.5}. \tag{4}$$

Here, D is the tube diameter, M and m are the virtual mass and the mass of the cylinder per unit of length, respectively, and α_1 is the eigenvalue of the first normal mode of flexural vibration of the tube. Pavlica and Marshall [15] performed new tests and concluded that the expression given by equation (3) matches their data fairly well. Additionally, they found that the viscosity effect on the vibration amplitude is not as large as that predicted by Burgreen et al. (Eq. (2)) and Païdoussis (Eq. (4)). Following additional data, Païdoussis modified its expression, thereby reducing the influence of the Reynolds number, and with it the viscosity [16]:

$$\frac{y}{D} = \alpha_1^{-4}\left(\frac{u^{1.6}\varepsilon^{1.8} Re^{0.25}}{1+2u^2}\right)\left(\frac{\beta^{2/3}}{1+4\beta}\right)\cdot 10^{-5}. \tag{5}$$

Though this expression matched the available experimental data better than the first equations, a shortcoming of the semi-empirical approach is that there is no dependency on the driving forces in it. To overcome this, expressions for the vibration amplitude based on the random vibration theory have been established. This theory makes use of empirical expressions of the fluctuating pressure field in which the spatial correlations in axial and circumferential directions are taken into consideration [17]. Assuming the pressure field to be statistically stationary and homogeneous and being transported by a convective velocity U_c, Corcos [18] proposed the following relation for the cross-spectral density between two points of the wall pressure field ψ_{pp}:

$$\psi_{pp}(\omega, z_{12}, \vartheta_{12}) = \varphi_{pp}(\omega) A\left(\frac{\omega z_{12}}{U_c}\right) B\left(\frac{\omega \varphi_{12}}{U_c}\right) e^{-i\omega z_{12}/U_c}, \tag{6}$$

Here, z_{12} and ϑ_{12} are the distances between the two points in the axial (flow) and circumferential directions, respectively, $\varphi_{pp}(\omega)$ is the wall pressure power spectral density at a point and A and B are spatial functions describing the decay of the correlation in the axial and circumferential directions, respectively. While the correlation depends on both directions simultaneously, and hence some inter-dependency exists, separating it into the product of two separate functions does not introduce significant errors [19].

The convective velocity shows a small dependency on the frequency ω, though can generally be approximated by $U_c \approx 0.6U$ [20], [21]. Expressions for the wall pressure power spectral density $\varphi_{pp}(\omega)$ are obtained by fitting a curve to experimental data. While significant deviations are found between the various tests that have been performed, the spectral density is found to be proportional to $D_h\rho^2U^3$ [21]-[23]. Finally, the correlation of the pressure fluctuations have been found, using experimental tests, to decay exponentially in the two directions [21], [24]-[26], i.e.:

$$A\left(\frac{\omega z_{12}}{U_c}\right), B\left(\frac{\omega \varphi_{12}}{U_c}\right) \sim e^{-a_i \omega x_i / U_c}, \tag{7}$$

with $x_i = z_{12}, \varphi_{12}$ and a_i a constant depending on the direction.

The first to propose an expression for the root-mean square displacement of a cylinder subject to flow-induced vibrations using the random vibration theory was Reavis [27]. Discarding any influence of the spacer grids and mixing vanes on the turbulence, and assuming, amongst others, that beam motion has no effect on the flow field and that the first beam-bending mode is the dominant one, he found the following expression:

$$y = C\eta_D \eta_{D_h} \eta_L \frac{DN^{0.5}}{mf^{1.5}\zeta^{0.5}} U\rho\nu^{0.5}, \tag{8}$$

with η_D, η_{D_h}, η_L dimensionless scaling factors equal to fD/U , fD_h/U and fL/U, respectively, ζ the damping ratio, m the mass of the cylinder per unit length and N the number of tubes. The theory was found to underestimate the experimental data it was compared with. The underestimation was attributed to an incomplete representation of the pressure fluctuations. To overcome the disparity, a multiplication factor C was added to the expression.

Using a similar approach as Reavis, and accounting for shape deformation, Wambsganns & Chen proposed the following expression for the beam's RMS displacement response y_{RMS} in terms of beam natural frequency, damping factor, and intensity of the mean-square spectral density of the pressure field in the low-frequency range:

$$y_{RMS}(z, U) = 0.018\kappa \frac{D^{1.5} D_h^{1.5} U^2 \varphi(z)}{L^{0.5} f^{1.5} (m + m_a)\zeta^{0.5}}, \tag{9}$$

with $\varphi(z)$ the beam's model function, z the axial coordinate, m_a the added mass of the fluid per unit length of the cylinder and κ an empirical coefficient. Since the expression is based on results from a smooth cylinder in flow with minimal entrance effects, the computed RMS response represents a lower bound on the actual displacement. Blevins later on modified Equation (9) and placed it in a power law form [4]:

$$\frac{Y_{rms}}{D} = 0.036KD\sqrt{U}\left(\frac{\rho D^2}{m}\right)\left(\frac{U}{fD}\right)^{1.5}\left(\frac{D_h}{D}\right)^{1.5}\left(\frac{D}{L}\right)^{0.5}\left(\frac{1}{\zeta}\right)^{0.5}\sin\left(\frac{\pi z}{L}\right), \tag{1}$$

Where m is the mass per unit length, including added mass due to the fluid.

In general, all the theories presented express the characteristic vibration amplitude Y in the form

$$Y = K\rho^i U^j d^k D^e m^m f^n \zeta^o, \tag{2}$$

with i through o dimensionless exponents whose values are given in Table 1 for the various theories, and which have been approximated in many cases.

Table 1: Comparison of exponents in theories of parallel flow TIV of cylindrical structures [5].

Theory	i	j	k	e	m	n	o
Basile et. al. [8]	0.25	1.5	0.5	-0.5	-0.25	-1	0
Burgreen et. al. [6]	0.385	2.3	1	0.77	-0.65	-2.6	0
Chen [29]	1	2	0	1	0	-2	0
Païdoussis [16]	0.8	2.4	0.8	0.8	-0.66	-2	0
Reavis [27]	1	1.5	0.4	1.5	-1	-1.5	-0.5
Wambsganss & Chen [28]	1	2	1.5	1.5	-1	-1.5	-0.5

It can be easily seen that the variations of the exponents in Table 1 will result in large differences in the predictions of the various theories. Païdoussis [30] remarked that the best accuracy one can hope to achieve in the prediction of vibration with these theories is about one order of magnitude. Blevins [5] remarked that since the turbulent forces in a parallel flow are largely dependent on upstream turbulence generators, improvements in the theoretical work are unlikely to yield substantial improvements in accuracy unless the theories are tied to a specific system whose turbulence level can be accurately identified.

The theories described above have been extended and studied further by several researchers. Chase [31]-[33] and Chase & Noiseux [34] extended the work by Corcos by switching to the wavenumber domain and extending the model, making it more generally applicable. Gorman [35], [36] slightly modified Reavis' model to make it applicable to two-phase air-water mixture flows and compared model predictions with his own experimental data. Higher amplitudes of vibrations of a rod in two-phase flow are found than in single-phase flows. This is attributed to the higher peripheral spatial correlation of the pressure fluctuations on the surface of the rod in two-phase flows. Also, the proposed model was remarkably successful in predicting the amplitudes of vibration, finding agreement between theory and experiment of the order of 30 per cent or better. This could be due to the fact that in two-phase flows, far-field pressure fluctuations are quickly damped, and hence, the near-field pressure fluctuations may represent the total excitation field [30].

Finally, Ohlmer et al. [38] looked into simplifying the original model by Corcos and Bakewell by using the pressure difference fluctuations only in one single point to describe the driving forces, instead of considering the pressure fluctuation field in several points over the rod length. The simpler model was found to be able to describe in a satisfactory manner the flow-induced vibrations of rods in axis-parallel flow, however, the larger scatter in results showed the greater inaccuracy of the simplified model.

2.2.2 Later analytical models

Most of the analytical approaches proposed in the later years treat the fuel rods as an Euler-Bernouilli beam and derive a dynamic equation for its motion due to the surrounding fluid flow. The first to do so was Païdoussis, who considered a system consisting of a flexible cylindrical body of circular cross-section, immersed in an incompressible fluid of density ρ flowing with uniform

velocity U parallel to the x-axis, which coincides with the position of rest of the cylinder axis [39], [40]. The cylinder is considered to be either fixed at the upstream end and free at the other or supported at both ends. He derived a dynamic equation by dividing the force on the cylinder imposed by the flow into the inviscid force calculated with Lighthill's theory [41] and the viscous force calculated with Taylor's theory [42].

Chen & Wambsganss, in various studies [43]-[44], extended Païdoussis' model by including damping and a distributed random pressure loading as forcing. Païdoussis further improved the model by including internal dissipation and correcting the way the frictional forces were resolved [45]. This led to the following expression for small lateral motions y of the beam:

$$\begin{aligned} EI\frac{\partial^4 y}{\partial x^4} + \lambda I\frac{\partial^5 y}{\partial x^4 \partial t} + M\left(\frac{\partial}{\partial t} + U\frac{\partial}{\partial x}\right)^2 - \frac{1}{2}C_T\frac{MU^2}{D}\left\{\left(1-\frac{1}{2}\delta\right)L - x\right\}\frac{\partial^2 y}{\partial x^2} \\ -\left\{\delta T_0 + \frac{1}{2}(1-\delta)C_T' MU^2\right\}\frac{\partial^2 y}{\partial x^2} + \frac{1}{2}C_N\frac{MU}{D}\left(\frac{\partial y}{\partial t} + U\frac{\partial y}{\partial x}\right) \\ +\frac{1}{2}C_D\frac{M}{D}\frac{\partial y}{\partial t} + m\frac{\partial^2 y}{\partial t^2} = q(x,t), \end{aligned} \tag{10}$$

with EI the flexural rigidity of the cylinder, D its diameter, L its length, m its mass per unit length, λ the cylinder's internal viscous damping coefficient, M the virtual mass of the fluid per unit length, U the axial flow velocity, T_0 the initial axial tension, C_N and C_T the drag coefficient in normal and tangential direction, respectively, and C_D a viscous damping coefficient. Furthermore, $\delta = 0$ corresponds to the case where the downstream end is free to move axially, while for $\delta = 1$ it is not.

The above described equation was used by Chen & Wambsganns [44] and Païdoussis [45] to study the structural vibration response to axial turbulent flow. Hereto, generalized boundary conditions were used, and the dynamic equation was non-dimensionalized. Furthermore, the phenomenological model proposed by Corcos [18], see equation (6), was used to describe the forcing function $q(x,t)$.

It was established that, at low flow velocities, the cylinder is subjected to small, random vibrations, due to the mean axial flow not being purely axial, uniform and steady. Instead, the perturbations in the flow and pressure field induce stochastic vibrations of small amplitude ('sub-critical vibrations'). At high flow velocities, the fuel rods may be subject to fluid-elastic instabilities (divergence and flutter), as a result of interactions with the mean flow field. However, such instabilities occur at such high flow velocities that it is of little concern for most industrial applications. For most industrial cylindrical structures, including fuel rods in nuclear power plants, the mean axial velocity mainly (1) lowers the natural frequency of the rod compared to free rod vibration in air, and (2) introduces additional damping of the structure. The frequency of vibration was found to be essentially the first-mode of the cylinders.

The above-described approach was later enriched and improved in two different, related, directions. The first is in improving the description of the forcing function $q(x,t)$. Lin [46] used Fourier transforms and modal analysis of both the forcing and response to determine the rod vibration amplitude as a result of pressure fluctuations described as a stationary random process with zero mean. He found that only when the structure's dimensions are similar to the lengths of the turbulent eddies, in either longitudinal or circumferential direction, does the rod experience significant vibrations.

Later studies, also making use of modal analysis in the frequency domain, improved on the description of the forcing function by extracting the dynamical features of a flow-excited tube from a set of vibratory measurements [47]-[50]. This strategy, called source identification, allowed the identification of the structure modal parameters, as well as the spectral and spatial characteristics of the distributed flow excitation. Using the extracted forcing characteristics, random force sets in the time-domain can be generated, in order to simulate the excitation of rods by turbulent flows. While the first approached assumed linear behavior, Annules at al. later extended it to be applicable to non-uniform turbulent flows with nonlinear time-domain response [51]-[54].

The second improvement made to the above-described method was extending it from a solitary cylinder in axial flow to a cluster or bundle of cylinders in axial flow. Chen [55] showed that due to hydrodynamic coupling, the dynamics of clustered cylinders in axial flow are very different from a single cylinder and hence one cannot consider a cylinder in a bundle in isolation. The developed theoretical models [56], [57] predicted well both the behavior of cylinders in still fluid [58], as well as the stability characteristics of the system in axial flow [59], [60]. As, just as for single cylinders, the fluid-elastic instabilities are a result of the mean flow, it means the mean-flow effects have correctly been incorporated in the analytical model [57].

In regards to turbulence-induced vibrations of cylinders in a rod bundle, while some of the analytical models cited above and also some that were later on developed [61]-[63] are said to be for axial flow in bundles of cylinders, strictly, they really apply to solitary cylinders, rather than clusters, as two of the underlying assumptions are: (1) there is no correlation between the pressure fields on adjacent cylinders in the array; (2) the motion of a cylinder has no effect on the pressure field, nor on the motion of adjacent cylinders. Hence, inter-cylinder coupling was ignored in those studies. Through experiments, Païdoussis & Gagnon [64] found that hydrodynamic coupling is also important for turbulence-induced vibrations of clusters. They demonstrated that vibrations occur in prescribed inter-cylinder modal patterns, with both modal and spectral characteristics of vibration agreeing remarkably well with those predicted by the free-vibration analytical model of references.

Païdoussis & Curling [65] were the first to take hydrodynamic coupling into account in a forced-vibration model of rods in a bundle vibrating due to the random pressure fluctuations in the turbulent flow acting on the cylinders. The forcing function used was not only correlated on the same cylinder, but also on adjacent cylinders, using appropriate length scales. Hereto, correlation functions as proposed by Bakewell et al. were used. They found among others that the amplitude of vibration increases nearly as the square of the flow velocity. And even though a good qualitative agreement with measured characteristics of vibration was found, they state that the "quantitative aspect of the results obtained is clearly predicated on the degree of correctness with which the excitation field has been modelled".

To improve on the correctness of the forcing function, the same authors undertook an experimental campaign to measure and characterize the wall-pressure fluctuations on cylinders in a bundle in turbulent axial flow [66], [67]. With the generated experimental data, an improved analytical model was proposed [68]. Figure 6 shows the power spectral density of mid-cylinder displacements in radial direction in the four-cylinder system obtained with the model compared to that of the experiments. The excitation frequencies are well captured, however, the vibration response is clearly overestimated by the model. Normalizing the used differential pressure lateral

spectral density factors improved the results significantly, with the model predicting quantitatively a similar response as that found in the experiments.

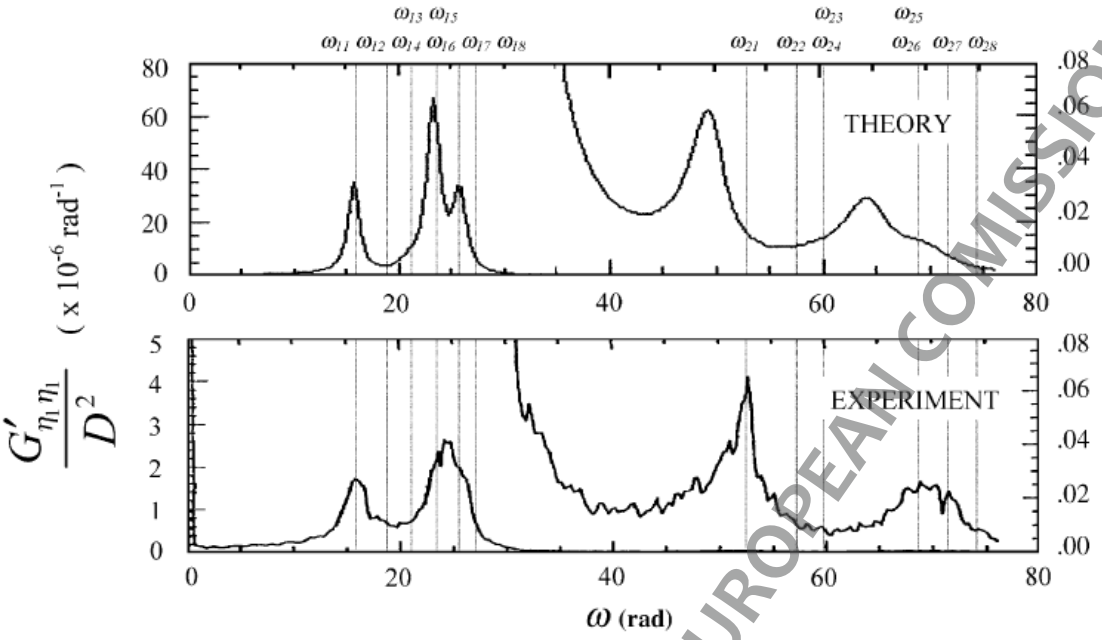

Figure 6: Comparison of theoretical and experimental power spectral densities of mid-cylinder displacements in radial direction in the four-cylinder system [68].

2.3 Experiments for FA FIV

2.3.1 Experiments of axial flow-induced vibrations of single cylinders and bundles

As illustrated, while significant progress has been made over the years in the modeling of turbulence-induced vibrations of a cluster of cylinders, all the theoretical methods or analyses are empirical, or at best, semi-empirical, meaning some empirical coefficients must be known a priori. Additionally, often the forcing function being used was obtained through measurements for conditions that may not be fully identical to the case under consideration. Finally, the case considered in the theoretical models is often a simplification from the actual fuel assemblies, in which structural elements such as spacer grids and mixing vanes induce significant additional turbulence. Hence, for correct use of the models based on the theory of random vibration, pressure field characteristics should be measured in situ. However, as stated by Païdoussis [69], "the proposition of having to measure the pressure field characteristics in situ in order to predict the vibration is not practical, for then the vibration amplitude itself might as well be measured in situ, with at least equal ease!".

This latter, direct measuring of the vibration amplitudes, was done by many researchers in the past. This section gives a short overview of the work done on measuring vibrations of single rods in axial flow, and those of bundles.

2.3.2 Early experimental work on single cylinders

Most of the earlier studies performed on measuring the vibrational amplitudes of fuel rods in axial flow had the purpose to predict the displacement of the rods due to the fluctuating pressure fields, and possibly provide input to analytical models of the same, as described above. Burgreen et al. [6] experimentally studied the type and magnitude of vibrations of fuel rods due to axial water flow, thereby varying the flow velocity and several other relevant variables. They observed the vibrations to be self-excited, resulting in the rods vibrating at their natural frequencies independent of the water velocity. Quinn [7] performed tests on single and multiple pipes in two-phase steam-water flow, and found the vibration behavior to be nearly independent of mass velocity for low values and to rapidly increase in intensity with higher values of mass velocity.

Basile et al. [8], based on experiments in air and water with different types of fuel element cans, demonstrated the additional effect of flow asymmetry and of some technological parameters (pumps, grids, clearances) on vibration amplitudes. Additionally, they emphasized that it is not sufficient to only look at the root-mean-square value of the displacement if the scatter is great, as values of amplitudes considerably greater than the mean may frequently be reached and exceeded. As these larger displacements are the main drivers for wear, hammering and fatigue of the rods, one needs to indicate not only the mean amplitudes of displacement, but also the variance of the sample of the values measured.

Kadlec & Ohlmer [37] also studied experimentally the influence of external parameters on the vibrations of fuel pins. They did this by varying the test loop design, and hence the inlet conditions of the flow, and using a subassembly mock-up. While pressure fluctuations could vary by as much as a factor of ten at the water inlet into the subassembly, this reduced to a factor of about four for the pressure fluctuations around the pins and to a factor of three of the vibrational amplitudes of the pin. So while it seems that the bundle stabilizes the fluctuating pressure field in the coolant, still a significant influence is found from the inlet conditions.

Païdoussis [10] was the first to look at dimensionless flow velocities larger than one, for which the vibrations are no longer sub-critical. Using an experimental facility of a flexible cylinder with pinned ends in axial water flow, he observed that at sufficiently high flow velocity the cylinder is subject to buckling and oscillatory hydroelastic instabilities, see Figure 7. However, these instabilities occur at such high flow velocities that they are not likely to be encountered in practice, unless the cylinder is made of very flexible material such as rubber. In regards to small amplitude vibration of the sub-critical regime, he postulates, and proves experimentally, that these vibrations are excited by cross-flow components of flow and other departures from steady, uniform and perfectly axial flow. In a later experimental study, buckling at higher velocities was also found to happen for cylinders clamped or pinned at the upstream end and free at the downstream end [40].

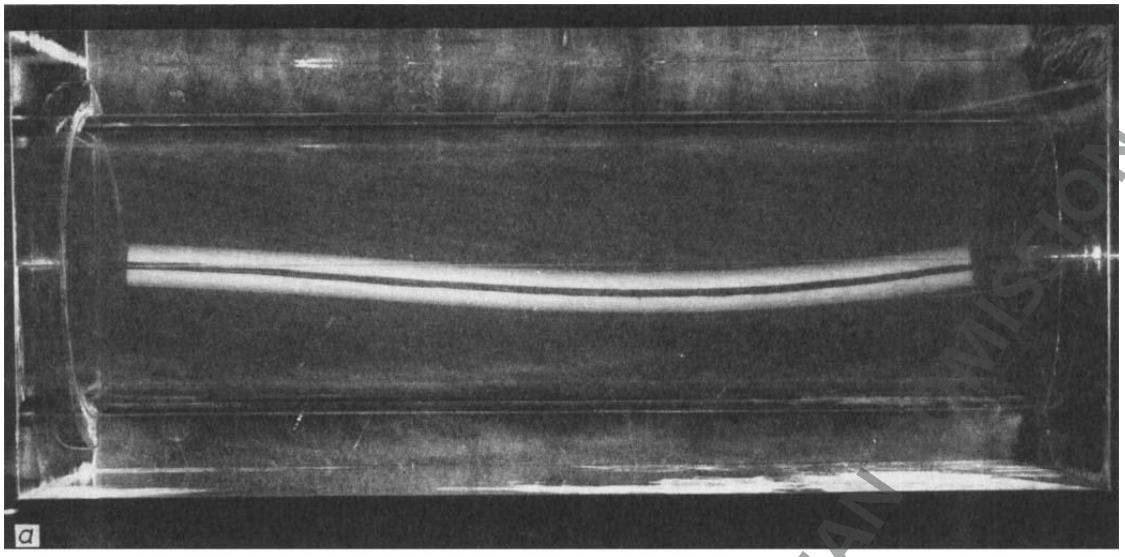

Figure 7: Buckling instability of a rubber cylinder with pinned ends; flow is from left to right [10].

Sogreah [11] performed experiments of a single rod in cold water in which the upstream turbulence and external excitation were reduced as much as possible. Using frequency spectral analysis, it is shown that the first and second mode natural frequencies are dominant. With the upstream disturbances reduced to a minimum, the found vibration amplitudes are considerably lower than those obtained in the other experiments, where no such care was taken, the main consideration being the realistic simulation of reactor conditions.

Pavlica and Marshall [15] performed vibrations tests in water of a 4x4 fuel assembly with spacer grids treated as a composite structure and observed that the behavior of such a structure in axial flow is quite similar to individual rod vibration in parallel flow; it tends to vibrate near its natural frequency and the amplitude increases proportional to the flow velocity to the second or third power. They also studied the effect of the number of spacer grids and temperature, for a limited range, on the vibrations. The vibrations decreased in amplitude with decreasing number of spacer grids, due to the decreased stiffness of the structure.

Païdoussis [16] in 1969 performed the most extensive experimental campaign of flow-induced vibration of cylinders till that point, running: 1) experiments with a single cylinder in the test section, in which the length, mass, flexural rigidity, and diameter of the cylinder, and the flow velocity were varied systematically, in order to obtain a measure of the dependence of vibration amplitude on these parameters; 2) ad hoc experiments with single cylinders on the effect of large-scale flow disturbances upstream of the cylinder; 3) experiments with a bundle of cylinders. Based on the results found, and all other experimental data available thus far, a new analytical model of the vibration amplitude was proposed, see Equation (5), which gives the amplitude $\delta \sim U^{1.85}(EI)^{-0.6}D^{0.4}L^{3.2}D_h^{0.65}$, see also Figure 8. To account for idealized conditions used in lab experiments, a multiplication factor of 5 is needed when applying the model to industrial conditions. Additionally, Païdoussis suggested that vibration at low flow rates is mostly induced by noise and not by the flow, i.e., by pump noise and by vibration transmitted to the cylinder through the supports. This view is reinforced by the fact that the amplitude of vibration with no flow, but with the pump turned on, is about the same as the amplitude at low flow velocities.

Gorman [35], [36] conducted a series of tests in which a single test element has been subjected to two-phase parallel flow in a circular annulus. As mentioned earlier, higher amplitudes of vibrations of a rod in two-phase flow are found than in single-phase flows. This is attributed to the higher peripheral spatial correlation of the pressure fluctuations on the surface of the rod in two-phase flows. Additionally, displacement increases rapidly and peaks at a simulated quality of 12%, before undergoing fairly rapid falloff.

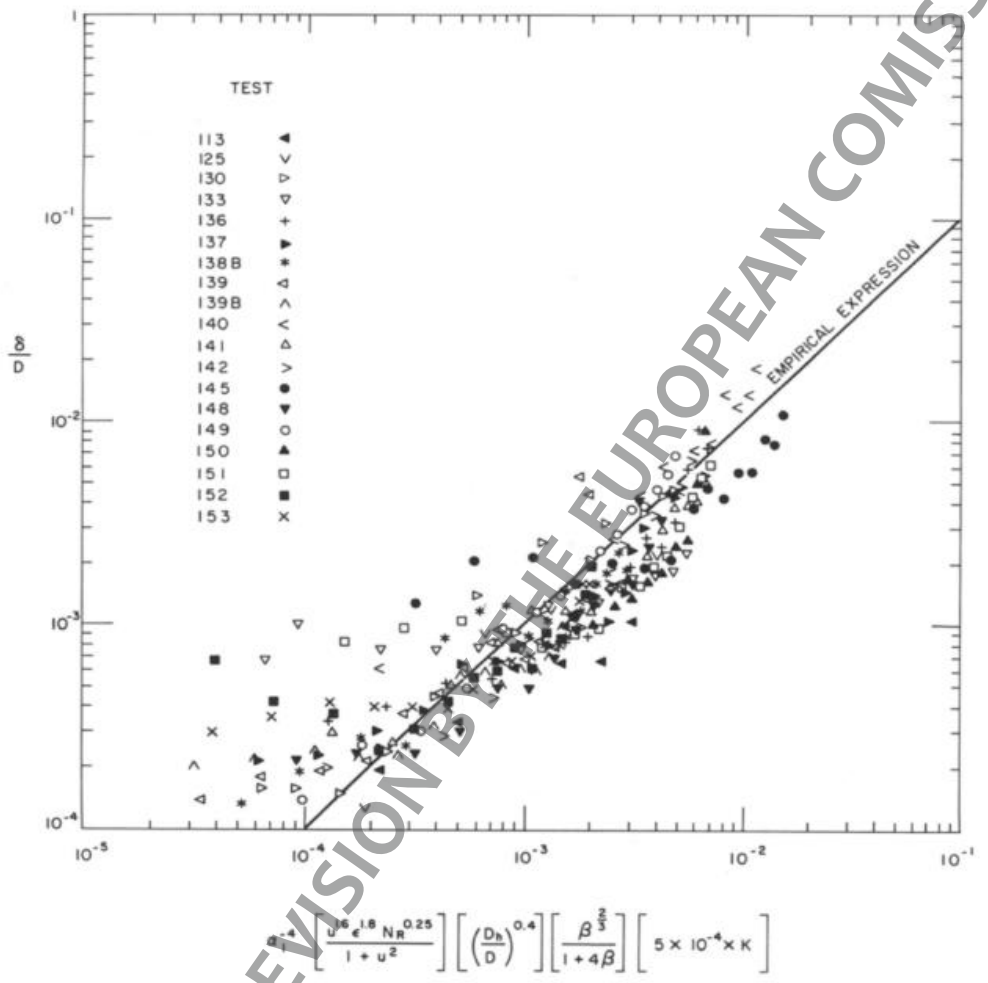

Figure 8: Experimental data from plotted against the empirical expression (K =1) [16].

Wambsganss & Zaleski [70] and Chen & Wambsganss [44] performed experiments of forced and axial-flow induced vibrations of a rod with arbitrary end conditions, i.e., fixed, pinned or cantilevered and investigated the influence of flow rate on the rod vibration amplitude, its fundamental frequency and the system damping. For a fixed or pinned rod, the fundamental frequency is found to decrease with increasing velocity. For a cantilevered rod, it is found to increase with increasing velocity. The system damping and vibration amplitude is found to increase with increasing velocity, for all end conditions considered.

2.3.3 Early experimental work on coupled vibrations in bundles

While some of the experimental work cited above performed tests with bundles, none of them looked explicitly at the coupled vibration of a cluster of cylinders. The first to do so were Chen & Jendrzejczyk [58], who performed three series of experiments on coupled tube/vibration in both still air and stagnant water, looking at a bundle of seven cantilevered rods. In both air and water, they first looked at uncoupled vibrations, by fixing all cylinders except one and exciting the free cantilevered rod by plucking at its free end. This allowed them to study the frequency and damping of all cylinders. Then, tests were performed with all rods free to vibrate, and plucking at the free end of one or more cylinders. These tests were done at various gap-to-radius ratios. They found, amongst others, that as the gap-to radius ratio decreases, the coupled natural frequencies become more widely spread; i.e., the lowest frequency becomes smaller while the highest frequency becomes larger. Additionally, they found that the coupling in air was quite small, while significant coupling exists when the cylinders are placed in water.

Such strong coupling was also found by Païdoussis [59], who studied experimentally the axial-flow induced vibrations of systems of two, three or four cylinders supported at both ends and positioned symmetrically in the cylindrical test section of a water tunnel. In a follow-up series of tests, [60], Païdoussis & Curling conducted experiments in a water tunnel with three- and four-cylinder clusters, monitoring the cylinders' behavior either optically or by instrumenting one of the cylinders with strain gauges. With increasing flow, the amplitude of small random vibrations of the cylinders increased; simultaneously, the natural frequencies, as a group, decreased, as the band of observed predominant frequencies of vibration shifts to lower frequencies, see also Figure 9. The cylinders eventually lost stability by buckling (divergence), and at higher flow by flutter.

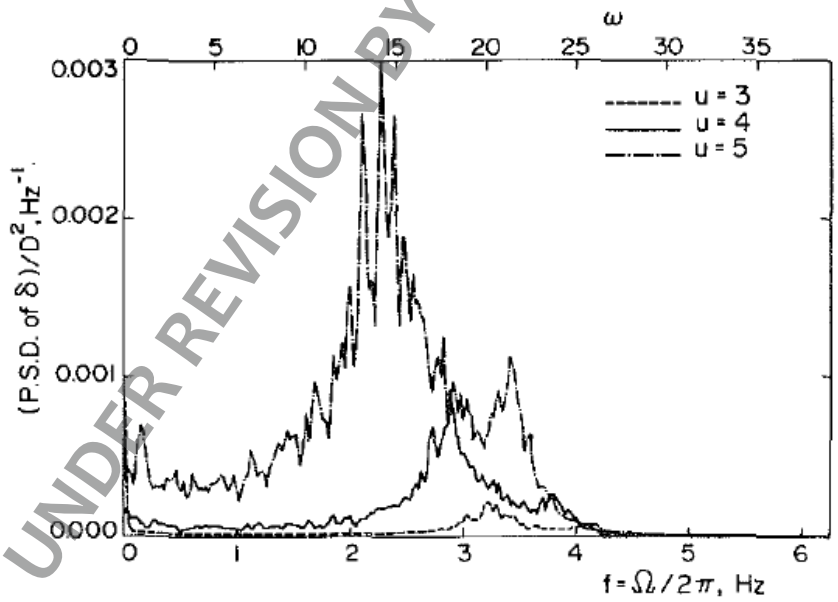

Figure 9: Observed power-spectral-densities for the mid-cylinder displacement of a cylinder in a cluster of four clamped-clamped cylinders, for three different dimensionless flow velocities u [60].

The broading of the vibration band-width and shifting of its center to lower frequencies with increasing flow velocities was confirmed by Païdoussis & Gagnon in another experimental campaign they performed [64], mainly with the aim of the development of a forced-vibration analytical model for the prediction of axial-flow-induced vibration of cylinder clusters. Additionally, in their experiments of a cluster of four cylinders, they also observed that there exist characteristic directions (planes) of motion, which correspond to the characteristic vectors of relative inter-cylinder motions: the so-called "radial" and "tangential" directions for the four-cylinder cluster. Though not presented, they mention the conclusions reached were backed by experimental evidence obtained with 2-cylinder and 19-cylinder clusters.

2.3.4 Later experimental work on vibrations of single and clusters of cylinders

The experimental work described above was mainly performed with the aim to develop and improve analytical predictive expressions for the vibration amplitude of cylinders in axial flow. With growing computer power and advancements in the numerical analysis methods and algorithms, see next chapter, the numerical simulation approach is becoming more an important tool in the analysis of flow-induced vibration of nuclear fuel assemblies. Hence, experimental vibrational studies performed in the later years were for a large part aimed at providing input and a validation basis for the development of numerical tools for the simulation of vibrations of fuel rods induced by axial turbulent flow, such as those done as part of the joint industry project VIKING [71].

One such experiment is the single vibrating rod experiment performed by Vattenfall Research and Development [72],[73]. In this experiment, a vertical slender rod with a roller boundary condition and a clamped bottom end is displaced and then released, after which its vibrations and damping under the influence of the, followed by tests in water with a flow rate of 1.0 m/s and 3.0 m/s. Boundary conditions were carefully controlled in order to make numerically modelling of it easier. The same test loop was used to study the vibrational behavior of an instrumentation guide tube [72]. The experimental geometry was adopted from the neutron flux detectors housing tube which is part of the core monitoring system in boiling water reactors. The geometry has been scaled down to fit the existing test section used for the single vibrating rod experiment, see Figure 10. Displacements were measured at various water flow velocities.

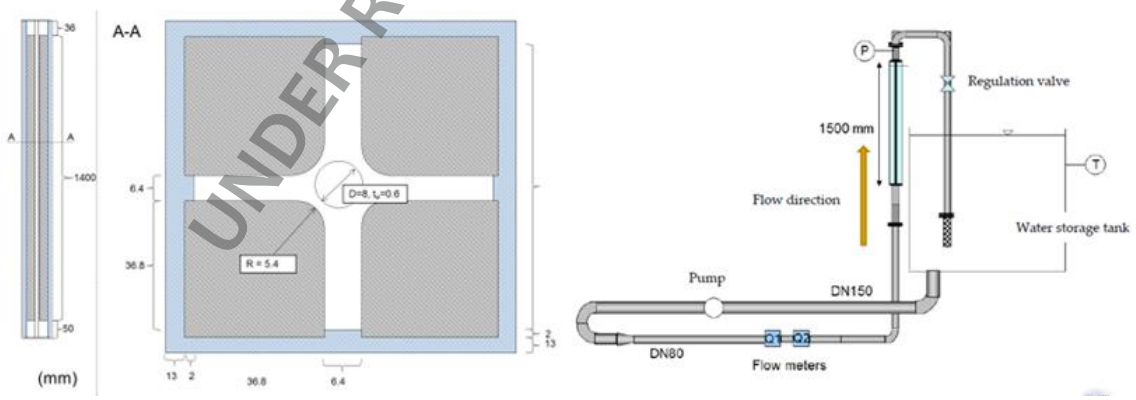

Figure 10: Dimensions of the instrumentation guide tube experiment (left) and a schematic of the complete test section (right) [72].

While both experiments performed by Vattenfall R&D involve cylinders fixed at both sides, Cioncolini et al. performed experiments of a cantilevered rod, with the downstream end fixed and the upstream end free to vibrate [74]. Series of tests were performed at different water flow velocities, as well as in stagnant air and water. The main goal in designing this cantilever beam experimental setup was to generate benchmark experimental data in controlled conditions with non-invasive simultaneous resolution of structural vibration (via non-contact optical tracking) and fluid flow (via Particle Image Velocimetry (PIV)). In particular the latter, detailed information of the flow field, is vital for validating numerical models for flow-induced vibration predictions.

Further experiments on a single cylinder were conducted by Modarres-Sadeghi et al. [75] for cylinders clamped at both ends, Païdoussis et al. [76] for cantilevered cylinders and Kheiri and Païdoussis [77] for pinned-free cylinders, while a very thorough systematic study of the nonlinear dynamical characteristics of a single nuclear fuel rod and clusters of fuel rods, both in quiescent and axially flowing water, has been conducted by Ferrari et al. [78]-[80].

A very recent study on the influence of spacer grids on the flow-induced vibrations in fuel bundles is that by Zhang et al. [81]. Using a 4x4 bundle, they find that turbulence and vortices generated by the spacer grids are the two main exciting sources of the rods. The vibration intensity increases with the increase of flow velocity. The vibration of the rods is found to be mainly due to the turbulence and the corresponding peak vibration frequency is low. However, the spacer grid generates vortices and the vortex induced vibration shows high frequency peaks.

2.3.5 Full scale experiments

As the numerical tools aren't mature enough to accurately predict flow-induced vibrations and the resulting fretting wear of full scale fuel assemblies, several industries have developed full scale experimental facilities housing full scale fuel assemblies to study the flow-induced vibrations and fretting wear of the fuel rods, with the facilities reproducing the operational flow conditions in terms of temperature, pressure and flow rate. Hereto, in France, the HERMES P Loop [82]-[84] was built, in the USA the VIPER test loop [85]-[87], in South Korea their own dedicated testing facility [88]-[90].

2.4 Numerical simulations of FA FIV

With the experimental work on FIV of fuel assemblies discussed in paragraph 2.3, the focus now shifts to numerical simulations of the same. Different approaches are available in literature for modelling the Fluid(s) and Structure(s) and eventually coupling the same. Before looking at literature on Fluid or Structure modelling, a brief but relevant discussion is made on the coupling.

2.4.1 FSI coupling

In the context of FIV of fuel assembly structures, the coupling may be done one-way (weak or de-coupled) or two-way (strong or fully coupled). This depends on whether the FIV has significant Fluid-Structure Interaction (FSI) effects, which could be indicated by density ratio of the solid to fluid where a low value ~O(1) indicates strong coupling [1]. In cases where the FSI effects are not

so significant, as in the case of TIV, one could obtain relatively accurate solutions with the one-way approach while for cases with significant FSI effects, such as in VIV or FEI, a two-way approach becomes mandatory to obtain accurate solutions.

The difference between the two approaches lies in whether both the fluid load and the structure displacement are exchanged between the fluid and solid solutions, as illustrated in Figure 11. In the one-way coupling, only the fluid loads are mapped onto the structure. The absence of structural displacements being mapped back to the fluid causes the flow field to not experience any change in the fluid domain boundaries [92]. Consequently, the fluid dynamics and structure mechanics could be performed separately and sequentially.

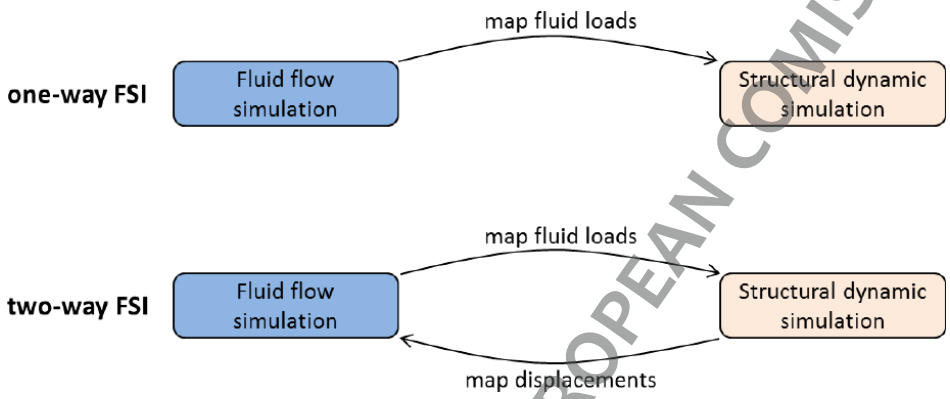

Figure 11: Illustration of coupling type

There are broadly two approaches to couple the fluid and structure governing equations: the monolithic approach and the partitioned approach. In the monolithic approach, the full set of equations (for the fluid, the structure and the interface) is built and solved simultaneously. In the partitioned approach, the system is set up individually for the fluid and the structure domain, while the coupling is established externally which involves mapping and exchange of data from one domain to the other.

In the partitioned approach, different ways of discretization both for space and time can be used for the fluid and structure domains, thus making it more suitable for coupling pre-existing CFD and CSM codes. Usually, the monolithic approach is able to handle greater coupling instabilities [93]. However, new partitioned coupling approaches have been developed recently which extend the range of applicability of the partitioned coupling approach to cases with stronger coupling [93],[94]. In this review, only the partitioned FSI approach is considered.

2.4.2 Fluid (Turbulence) Modelling

The fluid flow is governed by the Navier-Stokes equations. These are cushioned by a set of boundary conditions. Depending on the problem, there exist a number of possibilities in approximating the representation of turbulence in a CFD solver and solving the governing equations. These are:

2.4.2.1 Direct Numerical Simulations (DNS)

The most straightforward approach is direct numerical simulation (DNS). In DNS, the Navier-Stokes equations are discretized directly and solved numerically. Provided the mesh size and time step are fine enough to resolve all scales of turbulent motion, an accurate three-dimensional, time-dependent solution of the Navier-Stokes equations completely free of any modeling assumptions can be obtained. In the scientific realm, this would be the ideal in calculating turbulence-induced excitation forces. However, the enormous computational demands for resolving all spatial and time scales of turbulent motion make its application to fuel assemblies impractical in the industry and thus no relevant literature exists yet.

2.4.2.2 Large Eddy Simulations (LES)

The LES uses the approach of resolving the energy-containing large-scale turbulent structures on a mesh while modelling (or filtering) the small-scale turbulent structures. Assuming a universal behavior of small scales makes it possible to model them in a universal way. The required grid size Δx depends directly on the filter width Δ which is ideally smaller than the size l_{EI} of the smallest energy-containing motions (see Figure 12). The principal target of the LES is to resolve flow structures containing the bulk (~80%) of turbulent kinetic energy everywhere in the flow field, which should be achieved if the mesh spacing is smaller than l_{EI} [95]. Upon filtering the Navier-Stokes equations, a term remains that causes a numerical closure problem. This is the subgrid scale (SGS) tensor that represents the effect of the small scale structures on the larger ones. Quite a few SGS models exist, the earliest and the most commonly used being the Smagorinsky model [96].

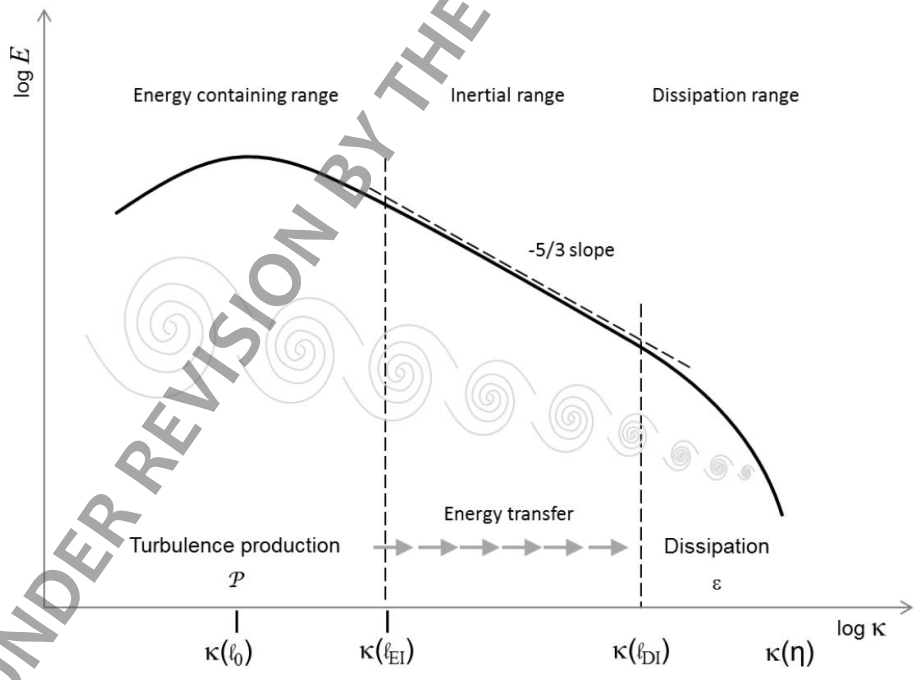

Figure 12: Turbulence energy spectrum and principal of turbulent energy cascade at high Reynolds number [95].

In the context of numerical simulations of fuel assemblies and its components using this approach, there exist quite some literature on the same. Zhang et al. [97] performed wall-resolved LES simulations using the Smagorinsky SGS model as available in ANSYS FLUENT with the aim to study and understand the flow induced excitation mechanisms within the CANDU fuel assemblies at an Re of 54000.

Elmahdi et al. [98] performed a CFD simulation to calculate the turbulence-induced forces along the fuel rod surface for a 2x2 sub-channel configuration with a spacer grid design with mixing vanes. The turbulent fluid forces calculated by wall-modelled LES using the WALE SGS model are used as the input for subsequent vibration analysis using the structural code to predict flow-induced vibration of the fuel rod and related wear. The main conclusion was that the coupled CFD-CSM solution provided a reasonable prediction of fuel rod TIV and an accurate representation of all the important physics and excitation forces was achieved compared to the experimental data.

Bakosi et al. [99] describe a wall-modelled LES approach to calculate the excitation forces for the GRTFW problem. The limitations of standard eddy-viscosity RANS models to predict turbulent fluctuations are outlined. LES is recognized as the viable approach for providing the flow-induced forces for FIV analysis. The authors considered it necessary to study the problem of FIV and GTRFW with LES before attempting the development of a GTRFW-specific RANS model.

In another paper, Christon et. al. [100] presented the results from a GTRFW analysis consisting of LES calculations to evaluate the excitation forces using Hydra-TH code and mechanical analysis to evaluate rod vibration response based on the CFD input. In these studies, an implicit LES method was used to solve the Navier-Stokes equations on several different meshes, which were optimized for wall-modeled LES in the fuel rod bundle region, with y+ values between 20 and 60. Within the spacer grid, fine mesh close to the wall was provided with y+ values close to 1.

In references [101], [102] and [103] Bhattacharjee et al. present the LES simulations performed using TrioCFD aimed at prediction of pressure fluctuations and fluctuating fluid forces in different single rod configurations investigated experimentally in the framework of development of methods for prediction of FIV and GTRFW of PWR fuel rods.

2.4.2.3 Reynolds Averages Navier-Stokes (RANS)

The most common way to deal with turbulence is by using a statistical approach for its modeling. In this case, the main interest is in calculation of temporal mean (averaged) flow quantities and the effects of turbulence on the mean flow are taken into account by a model. The most popular approach for statistical modeling of turbulence is based on the solution of Reynolds-averaged Navier-Stokes (RANS) equations. The main idea behind this approach is the decomposition of the flow variables into a time averaged (mean) and a fluctuating part called Reynolds decomposition (see e.g. [104], [105]). Like the LES filtered equations, there exists a term that causes a numerical closure problem. This is the Reynolds stress tensor. This term, which incorporates the effect of turbulent fluctuations on the averaged (mean) flow field, must be modeled to close the equation system. Common modelling approaches are the Eddy Viscosity Models, such as the k-epsilon and k-omega models and their variants, and the Reynolds Stress Model.

Since all the turbulence is modeled, the solution of RANS equations always provides as a result an averaged flow field in which the turbulent flow fluctuations are removed and the effect of the whole turbulence is represented by an additional diffusion term given by the Reynolds stress

tensor. This effect of turbulent diffusion is significantly higher in the case of RANS equations compared to filtered Navier-Stokes equations solved in LES.

The standard RANS models inherently have stronger tendency to damp the flow fluctuations, which limits their applicability to the evaluation of turbulence-induced fluid forces acting on the structure. As pointed out by Menter [106] and Acton et al. [107], special modifications of standard RANS models are needed in order to capture the unsteady flow features representing the turbulence specific structures. That being said, there still exists relevant literature where RANS or Unsteady RANS (URANS) have been applied either as standalone or as a precursor to an LES for fuel assembly simulations.

The steady RANS simulations are focused mainly on evaluation of global flow conditions within nuclear reactors or local flow conditions within a fuel assembly. Global and local flow distributions provide information about potential critical areas inside the reactor core or the fuel bundle giving important input for the FIV design assessment.

One possibility to utilize the steady RANS simulations is to use the flow distribution inside the fuel assembly to calculate excitation forces acting on the fuel rods using some empirical correlations as a function of averaged velocity [108]. An example of a steady fluid flow simulation of a quarter of a PWR core aimed to investigate flow conditions inside the core and derive conclusions for potential causes of GTRFW is presented by Hatman et al. [109] who used the standard k-epsilon model with a quadratic constitutive relationship as available in Star-CCM+. The steady state CFD solution provided in-depth understanding of the global flow field inside the reactor core, in particular of the uneven flow at the core inlet caused by the reactor core support hardware. The CFD simulation results enhanced the understanding of the physics behind flow-induced excitation, and identified the regions within the core exhibiting flow conditions conducive to FIV.

Steady and unsteady fluid flow simulations of a fuel assembly inlet region were performed by Yan et al. [110] who used the realizable k-epsilon model as available in Star-CCM+. The steady state simulations helped in understanding the temporal averaged flow field inside the fuel assembly that was subjected to uneven inflow rates. The unsteady forces on the fuel rods under typical reactor in-core conditions were calculated by unsteady analysis and used for the GTRFW assessment which aimed at predicting locations of vibrating fuel rods. Spectral analysis of the CFD results revealed synchronized excitation forces at the rod locations compatible with the locations of the failed fuel rods in the reactor.

De Santis et al. [111] and [112] investigated vibration of fuel rods subjected to axial flow induced by flow fluctuations between sub-channels of closely packed rod bundles. They investigated different configurations consisting of two and seven rods using URANS k-omega SST model and fully coupled FSI approach integrated in Star-CCM+ code. Bertocchi et al. [113] investigated FIV in a 7-rod bundle configuration. They performed coupled FSI simulations using two different simulation approaches and compared the results with experiments.

In the aforementioned work of Zhang et. Al. [15], the LES simulations used a RANS precursor simulation that used the k-epsilon model to generate the base mean field. Dolfen et al. [114] investigated the turbulence-induced vibrations of a wire-wrapped hexagonal fuel assembly of the Multi-purpose hYbrid Research Reactor for High-tech Applications (MYRRHA) cooled with lead-bismuth eutectic (LBE). They performed first coupled FSI simulations of a bundle consisting of seven pins to evaluate eigenfrequencies and damping ratios of the bundle in the LBE using RANS

approach. In the final step the turbulence-induced vibrations of the wire-wrapped rods were calculated in a decoupled one-way simulation. Fluid forces acting along the rods are calculated by LES assuming rigid rod geometry and the vibration response is calculated by a structural dynamic simulation using these forces as input.

2.4.2.4 Comparison of accuracy of (U)RANS and LES

The key to accuracy for capturing FIV of fuel assemblies and their sub-components lies in firstly accurately predicting the added mass and damping owing to the structures being immersed in a fluid. An example of successful application of coupled FSI simulations aimed at evaluation of fluid damping behavior of scaled fuel bundles subjected to axial flow using RANS turbulence models is presented by Dressel et al. [115]. Dressel and Kovacs [116] applied the coupled FSI simulation successfully to evaluation of added and coupled mass used in the accident analysis of BWR fuel assemblies by recalculating the experiments with full-scale fuel assemblies in a moving containment filled by water.

However, in the case of FIV, the proper capturing of these two essential fluid effects on dynamic structural response is not sufficient. The essential difference is that the structural motion is induced by the fluid flow itself and the models used for FIV must be able to reflect it. In the context of fuel assemblies and their sub-components which vibrate predominantly due to the turbulence of the flow, predictions of the pressure fluctuations over the structure and its evolution in time is also important.

The following example makes a comparison between different approaches of turbulence modelling (RANS vs LES). A coupled FSI analysis of flow-induced vibration of a slender rod exposed to axial flow is presented in the work of Bengtsson [117]. Coupled FSI simulations were performed in the framework of the commercial software ANSYS using partitioned approach based on coupling of ANSYS mechanical solver with FLUENT fluid flow solver. Different turbulence models were used which provide different degree of representation of turbulence: unsteady RANS models (e.g. in given case k-omega SST model of Menter [118]), LES and scale-adaptive simulation (SAS) [119], [120]. Among all models used in the study, only LES was capable to reproduce reliably the vibration response of the instrumentation tube measured in experiments. Unsteady RANS model used in this study was found to be too diffusive leading to strong damping of rod vibration while the SAS model significantly under-predicted the vibration amplitude. Although rather simple from the geometrical point of view, i.e., single rod without any supports (compared e.g. to the models of fuel bundles including spacer grids), this case demonstrates nicely the physical complexity of FIV and the difficulties related to its simulation. In particular, the importance of appropriate physical (turbulence) models for given application becomes clearer.

2.4.2.5 Alternative Approaches

Besides the classical (U)RANS and LES approaches, there are additional approaches available in literature. The first class of these are the so-called Hybrid or Scale-resolving methods that aim to combine the strengths of LES and RANS especially for highly separated flows. One such hybrid is the Detached-Eddy Simulation (DES) as proposed by Spalart et. al. [121]. DES uses RANS in the areas close to walls while using LES far away from the walls. Several flavors of this hybrid technique have

been developed since its conception in 1999 [122]. In the very first formulation [121], the one-equation Spalart Almaras eddy viscosity model [123] was used.

The main idea of detached eddy simulation is to limit the eddy viscosity in order to permit large-scale turbulent eddies to develop. This is done by replacing the distance to the wall, d, which is used as the length scale in the Spalart-Almaras model, by

$$\tilde{d} = \min(d, C_{DES}\Delta)$$

The bound on the length scale has the effect of bounding the turbulent viscosity. If the turbulent viscosity is kept low, natural instabilities within separated shear layers can evolve into turbulence. Like in LES, the turbulent eddies are resolved in DES. Hence, the simulation must be three-dimensional and it requires non-dissipative higher-order numerical schemes both in space and time [124].

Other variants of DES models have been developed using different eddy viscosity models as the basis. Among the most popular DES variants are those based on the k-omega SST model presented by Menter et al. [119] and on the k-epsilon elliptic blending model by Lardeau et al. [125]. Spalart [122] gives a comprehensive review of the progress in developments of DES including advantages as well as the main challenges of this approach.

Papukchiev [126] validated the FSI program ANSYS CFX - MOR on the Vattenfall Boiling Water Reactor (BWR) Instrumentation Tube Vibration Experiment, dedicated to vibration phenomena in a BWR core as part of the VIKING collaborative initiative. On the fluid side, the Zonal LES (ZLES) method was applied. The difference from DES is that the switch between URANS and LES is not on the mesh sizing but is manually prescribed by defining specific URANS and LES regions. For the URANS side, k-omega SST model was used while the SGS model for LES was not mentioned.

The aforementioned work of Bengtsson [117] also tests the so-called Scale-Adaptive Simulation (SAS) in predicting the FIV of a slender rod subjected to axial flow. While it is a hybrid method, its formulation is different from DES. The scale resolving nature of URANS is achieved by introducing a second derivative of the velocity source term into the specific turbulence dissipation (omega) transport equation. The derivation is based on a theory of Rotta [127] resulting in an exact equation for the turbulence length scale. Readers interested in the theory of different hybrid methods are directed to the review of Menter et al. [128].

Vivaldi and Pulicani [129] simulated the cantilever beam subjected to a water axial flow experiment by Cioncolini et al. [52], using two-way coupled fluid-structure simulations. The CFD employed wall-resolved URANS (based on the k-omega SST model) or wall-resolved Delayed Detached Eddy Simulation (DDES) (applied to the k-omega SST model). They found that URANS was unable to calculate the unsteady behavior of the flow, thus predicting practically zero beam vibration amplitude; on the other hand, DDES was found to predict significant unsteady fluid forces that, in turn, allowed to calculate beam vibration amplitudes of the same order of magnitude as the experimental measurements.

In order to use advantages of the RANS models with regard to computational effort but to be able to capture turbulent pressure fluctuations, an alternative approach to the scale-resolving methods was used by several authors (see e.g. [130]) by the name of Pressure Fluctuation Model (PFM). They used a hybrid method in which the turbulent flow fluctuations are added on top to the fluid flow solution based on steady [131] or unsteady ([130], [132]) RANS simulations. This approach is based

on the solution of an additional Poisson equation for pressure fluctuations which is derived from Navier-Stokes and Reynolds-averaged equations (see e.g. [95]):

$$\frac{\partial^2 p'}{\partial x_j \partial x_j} = -\rho \left[2 \frac{\partial U_i}{\partial x_j} \frac{\partial u_j'}{\partial x_i} + \frac{\partial^2}{\partial x_i \partial x_j} \left(u_i' u_j' - \overline{u_i' u_j'} \right) \right]$$

The velocity fluctuations appearing in the above equation are calculated by utilizing the turbulent kinetic energy spectrum. The time variation of the velocity fluctuations is represented by a discrete Fourier series. The coefficients of the Fourier series are calculated in a way to fulfill the von Karman turbulence energy spectrum (see [65]), using input information about turbulent kinetic energy and dissipation from RANS simulation results. Further development was made to deal with the anisotropic nature of turbulence, that is typically seen in fuel assemblies, in the form of the Ani-PFM model [133],[134].

2.4.3 Structure Modelling

The fundamental laws that govern the mechanics of solids are the same laws that describe the mechanics of fluids, namely, the conservation of mass, linear momentum and energy. While fluid mechanics are generally treated with an Eulerian approach, the solid mechanics equations are generally expressed in the Lagrangian frame, where the observer follows the solid material as it moves through space and time. This means that special consideration must be taken for FSI simulations since a middle ground must be achieved for the frame of reference. This is achieved with the Algebraic Lagrangian-Eulerian formulation [135]. Note that this holds for cases of two-way coupling. With respect to modelling the solid, the following methods are found in literature:

2.4.3.1 3D modelling

This is common for two-way coupled simulations. For such a setup, a choice can be made with regards to whether the geometry is "linear" or "nonlinear". This is concerning the strain where the infinitesimal strain approximation is used for the former while the latter uses the finite (nonlinear) approximation to describe the state of strain. The former is more suitable for small displacements and small strains while the latter is suitable for large displacements but small strains. In the context of TIV, the linear geometry is more suitable and has been used in literature [113]. Given the large domain size of general fuel assemblies, a reduced-scale fuel rod bundle is generally seen in literature [113],[136].

An example of FIV in a reduced-scale fuel rod bundle consisting of seven rods arranged in a hexagonal tightly packed rod matrix was recently published by Dolfen et al. [136] and Bertocchi et al. [113]. These studies were performed within the framework of SESAME project [138] aimed at benchmarking the tools and models developed by Ghent University and NRG against experimental data generated at Delft University of Technology as given by Bertocchi et al. [139]. The FIV mechanism of primary interest in this case was the vibration induced by large-scale coherent flow structures pulsations specific for tightly packed hexagonal rod matrix arrangement [140].

In the numerical simulation the flexible part of the silicone rod was considered as solid and it was represented by finite element structural models consisting of 3D linear elastic elements. Steel rods were considered as rigid in the simulations. The commercial codes Star-CCM+ and ANSYS FLUENT were used. In both results, the dominant frequency was found to be overestimated while the mean

vibration amplitude was found to be underestimated. This could be a direct consequence on relying on a pure URANS approach for modelling the fluid side which suffers from the aforementioned drawbacks.

2.4.3.2 1D Beam Model

For one-way or even two-way (with additional appropriate coupling effort) coupling approaches, it can be possible to select a 1D representation of fuel rods. The fuel rods can be represented by a beam subjected, for example, to the Euler-Bernoulli beam theory [141]:

$$\rho(z) \cdot S \cdot \frac{\partial^2 u_i(z,t)}{\partial t^2} + c\frac{\partial u_i(z,t)}{\partial t} + \frac{\partial^2}{\partial x_i^2}\left(EI\frac{\partial^2 u_i(z,t)}{\partial x_i^2}\right) = f_e(z,t) + f_{c,i}(u_i)$$

where $\rho(z)$ is the density of the beam, S is the area of the cross-section, c is the damping coefficient, E is the modulus of elasticity, I is the area moment of inertia of the cross-section, $u_i(z, t)$ is the lateral displacement along the rod, $f_e(z,t)$ is the excitation force, $f_{c,i}(u_i)$ represents the connecting forces describing the fuel rod support in the spacer grid cells.

Such an approach was taken by Dressel et. al. [115] who showed that the measured structural dynamic behavior of an 8×8 fuel design in the pluck excitations could be consistently and quantitatively reproduced in FSI coupled CFD simulations featuring the detailed flow geometry of the 8×8 FA. The FSI implementation was based on the user coding capabilities in the STAR-CD commercial CFD software with the FA structure treated by a FE beam modeling approach. A key feature of the approach was that the whole fuel assembly was represented by one beam.

Another example is that in the work of Christon et. al. [100] who presented a new approach for predicting GTRFW that used high-resolution implicit large-eddy simulation to drive nonlinear transient dynamics computations. The fluid-structure problem is separated into the simulation of the turbulent flow field in the complex-geometry fuel-rod bundles using implicit LES, the calculation of statistics of the resulting fluctuating structural forces, and the nonlinear transient dynamics analysis of the fuel rod that are modelled by the aforementioned beam theory.

An FSI two-way coupled approach based on an Euler-Bernoulli beam model was proposed by Vivaldi and Ricciardi [137]. The beam model was implemented inside the CFD code *code_Saturne*. The FSI approach was then used by Vivaldi and Pulicani to simulate FIV of a rod subjected to a water axial-flow [129].

2.4.3.3 Modal decomposition

A modal decomposition method is currently available as a mechanical Reduced Order Model (ROM) that has been tested in conjunction with ANSYS CFX [126],[142]. The principal idea of this method is a mode-superposition method, which uses the eigenfrequencies and mode shapes generated from a modal analysis to characterize the dynamic response of a structure to transient or steady harmonic excitations [143]. By performing key mathematical operations on the structural governing equation, the following decoupled set of equations are obtained:

$$\ddot{y}_i + 2\omega_i\xi_i\dot{y}_i + \omega_i^2 y_i = f_i,$$

where ξ_i is the fraction of critical damping for mode *i* and ω_i is its angular frequency. Since *i* represents any mode, the above equation denotes *n* uncoupled equations in the *n* unknowns y_i.

The advantage of the uncoupled system is that all the computationally expensive matrix algebra is preliminary done in the eigen-solver, and long transients may be analyzed inexpensively in modal coordinates with the above equation. The nodal displacements y_i are converted back into geometric displacements (the system response to the loading). That is, the individual modal responses are superimposed to obtain the actual response, and hence the name "mode-superposition".

In the recent works of Papukchiev [126] and Zwijsen et. al. [142], this approach has been tested against the Vattenfall BWR Instrumentation Guide Tube experiment as part of the collaborative VIKING initiative. Overall, the results obtained showed a good match for the eigenfrequency of the first mode of the guide tube with the one obtained from the experiment. Looking at the tube displacement, it was found that the method overpredicted the vibration amplitudes, which meant the solution was conservative. Considering the reduced computational costs of the used approach compared with high-resolution FSI approaches, the results, even though somewhat preliminary, were considered to be satisfactory. Further testing is suggested by the authors.

2.5 Summary

In an NPPs fuel assembly, the coolant flows axially along the fuel rod. The turbulent nature of this flow results in a fluctuating pressure force on the rods, giving rise to vibrations of the rods. In particular, at the points of contact of the rods with the spacer grids, this leads to local wear of the rods. If not managed adequately, this can result in grid-to-rod fretting wear, which is the main source of fuel failures in PWRs. As failure of the rods can lead to release of fission gases and expensive unplanned outages, NPP vendors have tried to estimate the vibration amplitudes of rods, and the associated wear, since the early NPP design.

Early on, analytical models were used to estimate the vibrations amplitudes. These models attempt to empirically correlate observed vibration levels with known system parameters such as flow velocity and hydraulic diameter. While the model's complexity grew with time, by increasing the number of system parameters included in the model and later on even switching to a dynamic equation of the rod's motion, all the theoretical methods or analyses are empirical, or at best, semi-empirical, meaning some empirical coefficients must be known a priori. Hence, some researchers concluded that if one is to measure particular model parameters in situ, one might as well measure the vibrations directly.

Measuring the vibrations directly was hence also done by a large group of researchers from the early days of NPP design. While the early measurements were performed for single rods, later experiments involved large clusters of cylinders, thereby taking into account the hydrodynamic coupling of the rods. Full scale experiments were even performed in the later years, where both the vibrations and fretting wear were measured. While the experiments, and later analytical models, obviously give good estimates of the vibration amplitudes, it is not straightforward to extrapolate the found results beyond the investigated range of system parameters. And performing experiments for a large range of these parameters is expensive.

Therefore, with the increase in computational power, numerical methods are more frequently used to estimate the fuel rod's displacements. As the problem at hand involves both fluid flow and structural motion, this generally means coupling accurate CFD solvers with structural mechanics solvers. To accurate resolve the pressure fluctuations, scale-resolving methods such as LES or DNS are generally used on the fluid side, though attempts are being made to use hybrid approaches or URANS solvers with additional models for the pressure fluctuations. On the structural side, most often 3D structural elements are used, though due to the relatively simple geometry of the rods, 1D beam elements and modal decomposition methods have been shown to also give good estimates for the rod's displacement.

Due to the interaction between the fluid and solid, the fluid flow and structural mechanics solvers generally need to be coupled. This could be either coupling in time, where data is exchanged between both solvers each time step, or by solving for the fluid flow first and prescribing the found pressure fluctuations as a boundary condition for the structural motion. This latter 1-way coupling saves considerable time and costs, and due to the rod's small displacements, can give a good estimate for the vibration amplitudes. Such one-way coupling has also been used in the full-scale models that not only estimate displacement, but also wear of the rods.

2.6 References

[1] EPRI, 2008, "Fuel Reliability Guidelines: PWR Grid-to-Rod Fretting", Technical report, 1015452. https://www.epri.com/research/products/1015452

[2] IAEA, 2019, "Review of Fuel Failures in Water Cooled Reactors (2006-2015)", IAEA No NFT-2.5, NE1864, Vienna, Austria.

[3] Pettigrew, M. J., Taylor, C. E., Fisher, N. J., Yetisir, M., & Smith, B. A. W., 1998, "Flow-induced vibration: recent findings and open questions", Nuclear Engineering and Design, 185(2-3), 249–276.

[4] Blevins, R. D., 1977, "Flow-Induced Vibration", New York: Van Nostrand Reinhold

[5] Blevins, R. D., 1979, "Flow-induced vibration in nuclear reactors: A review", Progress in Nuclear Energy, 4(1), 25–49.

[6] Burgreen, D., Byrnes, J. J., & Benforado, D. M., 1958, "Vibration of Rods Induced by Water in Parallel Flow". Trans. ASME 80(5), 991-1003.

[7] Quinn, E.P., 1962, "Vibration of fuel rods in parallel flow", GEAP-4069.

[8] Basile, D., Fauré, J., & Ohlmer, E., 1968, "Experimental study on the vibrations of various fuel rod models in parallel flow", Nuclear Engineering and Design, 7(6), 517–534.

[9] Païdoussis, M.P.,1965, "The amplitude of fluid-induced vibration of cylinders in axial flow", AECL-2225, Chalk River, Ontario.

[10] Païdoussis, M. P., 1965, "Vibration of flexible cylinders with supported ends, induced by axial flow", Proceedings of the Institution of Mechanical Engineers, Conference Proceedings, 180(10), 268-279.

[11] SOGREAH, 1962, "Study of vibrations and load losses in tubular clusters", Special Report No. 3, EUREAC-288, U.S.—Euratom Joint Research and Development Program

[12] Roström K. G. and Andersson N., 1964, "Boiler element for Marviken, vibration test with one rod", Ab. Atomenergi, (Stockholm), Arbetsrapport RPL-724.

[13] Roström K. G. and Andersson N., 1964, "Superheater element for Marviken, vibration test with one rod", Ab. Atomenergi, Arbetsrapport RPL-725.

[14] Roström K. G., 1964, "Seven-rod fuel element vibration tests", Ab. Atornenergi, Arbetsrapport RPL-726.

[15] Pavlica, R. and Marshall, R., 1966, "An experimental study of fuel assembly vibrations induced by coolant flow", Nuclear Engineering and Design, 4(1): 54-60.

[16] Païdoussis, M. P., 1969, "An Experimental Study of Vibration of Flexible Cylinders Induced by Nominally Axial Flow", Nuclear Science and Engineering, 35(1), 127–138.

[17] Kaneko, S. et al., 2014, "Flow-Induced Vibrations: Classifications and Lessons from Practical Experiences:, Elsevier, 2nd Edition.

[18] Corcos, G., 1963, "Resolution of pressure in turbulence". Journal of the Acoustical Society of America, 35(2): 192-199.

[19] White, F.M., 1964, "A Unified Theory of Turbulent Wall Pressure Fluctuations", USN Underwater Sound Lab. Report, 629, pp. 1-27

[20] Schloemer, H.H., 1967, "Effects of pressure gradients on turbulent-boundary-layers wall pressure Fluctuations", J. Acoust. Soc. Am. 42, pp. 93-113.

[21] Bakewell Jr., H.P., 1968, "Turbulent wall-pressure fluctuations on a body of revolution", J.Acoust. Soc. Am. 43 (6): 1358-1363.

[22] Willmarth, W.W., Wooldridge, C.E., 1962, "Measurements of the fluctuating pressure at the wall beneath a thick turbulent boundary layer", J. Fluid Mech. 14 (2) 187-210.

[23] Clinch, J.M., 1969, "Measurements of the wall pressure field at the surface of a smooth walled pipe containing turbulent water flow", J. Sound Vib. 9 (3),398-419.

[24] El Baroudi, M.Y. et al., 1963, "An Experimental Investigation of Turbulence-Excited Panel Vibration and Noise (Boundary-Layer Noise)", p. 19, AGARD-465, Advisory Group for Aeronautical Research and Development, Paris.

[25] Bakewell Jr, H. P., Carey, G. F., Libuha, J. J., Schloemer, H. H., and Von Winkle, W. A., 1962, "Wall pressure correlations in turbulent pipe flow," Technical report, Navy Underwater Sound Lab New London Ct.

[26] Bakewell Jr., H.P., 1964,. "Narrow-band investigations of the longitudinal space-time correlation function in turbulent air flow", Journal of the Acoustical Society of America, 36(1):146-148.

[27] Reavis, J. R.,1969, "Vibration Correlation for Maximum Fuel-Element Displacement in Parallel Turbulent Flow," Nuclear Science and Engineering, 38(1), 63–69.

[28] Wambsganss,M.W., & Chen, S. S., 1971, "Tentative Design Guide for Calculating the Vibration Response of Flexible Cylindrical Elements in Axial Flow", Technical Report ANL-ETD-71-7.

[29] Chen Y. N., 1970, "Flow-induced vibrations in tube bundle heat exchangers with cross and parallel flow, part I: parallel flow. Flow-Induced Vibration in Heat Exchangers", pp. 57-66, ASME, New York.

[30] Païdoussis, M. P., 1974, "The dynamical behaviour of cylindrical structures in axial flow", Annals of Nuclear Science and Engineering, 1(2), 83–106.

[31] Chase, D.M.,1969, "Turbulent boundary - layer pressure fluctuations and wavenumber filtering by non-uniform spatial averaging", Journal of the Acoustical Society of America 46, 1350-1365.

[32] Chase, D.M., 1980, "Modeling the wavevector-frequency spectrum of turbulent boundary layer wall pressure", Journal of Sound and Vibration, 70(1):29- 67.

[33] Chase, D.M., 1987, "The character of the turbulent wall pressure spectrum at subconvective wavenumbers and a suggested comprehensive model", Journal of Sound and Vibration, 112(1), pp. 125-147.

[34] Chase, D.M., and Noiseux, C.F., 1982, "Turbulent wall pressure at low wavenumbers: Relation to nonlinear sources in planar and cylindrical flow", Journal of the Acoustical Society of America, 72(3), pp. 975-982.

[35] Gorman, D.J., 1969, "The Role of Turbulence in the Vibration of Reactor Fuel Elements in Liquid Flow," AECL-3371, Atomic Energy of Canada Limited.

[36] Gorman, D.J., 1971, "An analytical and experimental investigation of the vibration of cylindrical reactor fuel elements in two-phase parallel flow", Nucl. Sci. Eng. 44, pp. 277-290.

[37] Kadlec, J., Ohlmer, E., 1971, "On the Reproducibility of the Parallel- Flow-Induced Vibrations of Fuel Pins", Nucl. Eng. and Design, 17, pp. 355-360.

[38] Ohlmer, E., Russo, S., and Schwemmle, R.,1972, "Investigation of an analytical model for parallel
flow induced rod vibrations", Nuclear Engineering and Design, 22(2), pp. 272-289.

[39] Païdoussis, M.P., 1966, "Dynamics of flexible slender cylinders in axial flow, part 1: Theory", J. Fluid. Mech. 26, pp. 717–736.

[40] Païdoussis, M.P., 1966, "Dynamics of flexible slender cylinders in axial flow, part 2: Experiments", J. Fluid. Mech. 26, pp. 737–751.

[41] Lighthill, M.J., 1960, "Note on the swimming of slender fish", J. Fluid. Mech. 9, pp. 305–317.

[42] Taylor, G., 1952, "Analysis of the swimming of long and narrow animals", P. R. Soc. Lond. A 214, pp. 158–183.

[43] Chen, S. S., and Wambsganss, H. W., 1970, "Response of a Flexible Rod to Near-Field Flow Noise", Proc. Conf. on Flow-Induced Vibrations in Reactor System Components, Argonne National Laboratory, May 14 and 15, ANL-7685, pp. 5-31.

[44] Chen, S.-S. and Wambsganss, M. W., 1972, "Parallel-flow-induced vibration of fuel rods", Nuclear Engineering and Design, 18(2), pp. 253-278.

[45] Païdoussis, M.P., 1974, "The dynamical behaviour of cylindrical structures in axial flow", Annals of Nuclear Science and Engineering, 1(2), pp. 83-106.

[46] Lin, W. H., 1984, "Buffeting of a slender circular beam in axial turbulent flows", AIAA journal, 22(5), pp. 690-695.

[47] Granger, S., and Perotin, L., 1999, "An Inverse Method for the Identification of a Distributed Random Excitation Acting on a Vibrating Structure. Part 1: Theory," Mech. Syst. Signal Process., 13, pp. 53–65.

[48] Perotin, L., and Granger, S., 1999, "An Inverse Method for the Identification of a Distributed Random Excitation Acting on a Vibrating Structure. Part 2: Flow- Induced Vibration Application," Mech. Syst. Signal Process., 13, pp. 67–81.

[49] Park, N.-G., Rhee, H., Park, J.-K., Jeon, S.-Y., and Kim, H.-K., 2009, "Indirect Estimation Method of the Turbulence Induced Fluid Force Spectrum Acting on a Fuel Rod," Nucl. Eng. Des., 239, pp. 1237–1245.

[50] Hwang, J.-S., Kareem, A., and Kim, W.-J., 2009, "Estimation of Modal Loads Using Structural Response," J. Sound Vib., 32, pp. 522–539.

[51] Antunes, J., Delaune, X., and Piteau, P., 2011, "Time-domain modeling of the random vibrations of tubes subjected to turbulence-conveying flows", ASME 2011 Pressure Vessels and Piping Conference, pp. 129-140.

[52] Antunes, J., Borsoi, L., Piteau, P., and Delaune, X., 2012, "The equivalent spectrum concept for turbulence conveying excitations", FIV-2012, Dublin, Ireland.

[53] Antunes, J., Borsoi, L., Delaune, X., and Piteau, P., 2014, "Identification of Random Excitation Fields From Vibratory Responses With Application to Multisupported Tubes Excited by Flow Turbulence", Journal of Pressure Vessel Technology, 136, pp. 051304

[54] Antunes, J., Piteau, P., Delaune, X., and Borsoi, L., 2015, "A new method for the generation of representative time-domain turbulence excitations", Journal of Fluids and Structures, 58, pp. 1-19

[55] Chen, S.-S., 1975, "Vibration of nuclear fuel bundles", Nuclear Engineering and Design 35, pp. 399-422.

[56] Chung, H., and Chen, S.-S., 1977, "Vibration of a group of cylinders in confined fluid", Journal of Applied Mechanics 44, pp. 213-217.

[57] Païdoussis, M.P. and Suss, S. ,1977, "Stability of a cluster of flexible cylinders in bounded axial flow", Journal of Applied Mechanics 44, pp. 401-408.

[58] Chen, S.-S., and Jendrzejczyk, J.A., 1978, Experiments on fluidelastic vibration of cantilevered tube bundles", Transactions of the American Society of Mechanical Engineers, Journal of Mechanical Design 100, pp. 540-548.

[59] Païdoussis, M.P., 1979, "The dynamics of clusters of flexible cylinders in axial flow: theory and experiments", Journal of Sound and Vibration 65, pp. 391-417.

[60] Païdoussis, M.P., Curling, Ll.R., and Gagnon, J.O., 1982, "Experiments on fluidelastic instability of cylinder clusters in axial flow", Transactions of the American Society of Mechanical Engineers, Journal of Fluids Engineering 104, pp. 342-349.

[61]Ohlmer, E., Russo, S., and Schwemmle, R., 1972," Investigation of an analytical model for parallel flow induced rod vibrations", Nuclear Engineering and Design, 22,pp. 272-289.

[62] Shin, Y.S., and Wambsganns, M.W., 1977, "Flow-induced vibration in LMFBR steam generators: a state-of-the-art review," Nuclear Engineering and Design, 40, pp. 235-284.

[63] Lin, W.H., and Wambsganns, M.W., 1981, "Analytical modelling of the buffeting of a rod bundle in axial flow:, 23. General Electric Report GEAP-24383, San Jose, California.

[64] Païdoussis, M. and Gagnon, J., 1984, "Experiments on vibration of clusters of cylinders in axial flow: Modal and spectral characteristics",. Journal of Sound and Vibration, 96(3), pp. 341-352.

[65] Païdoussis, M. and Curling, L., 1985, "An analytical model for vibration of clusters of flexible cylinders in turbulent axial flow", Journal of Sound and Vibration, 98(4): pp. 493-517.

[66] Curling, Ll.R., and Païdoussis, M.P., 1992, "Measurements and characterization of wall pressure fluctuations on cylinders in a bundle in turbulent axial flow. Part 1: spectral characteristics", Journal of Sound and Vibration, 157, pp. 405–433.

[67] Curling, Ll.R., and Païdoussis, M.P., 1992, "Measurements and characterization of wall pressure fluctuations on cylinders in a bundle in turbulent axial flow. Part 2: temporal characteristics", Journal of Sound and Vibration, 157, 1992, pp. 435–449.

[68] Curling, Ll. R.. and Païdoussis, M. P., 2003, "Analyses for random flow-induced vibration of cylindrical structures subjected to turbulent axial flow", Journal of Sound and Vibration, 264(4), pp. 795-833.

[69] Païdoussis, M. P., 1983, "A Review of Flow-Induced Vibrations in Reactors and Reactor Components", Nuclear Engineering and Design, 74, pp. 31-60.

[70] Wambsganss M.W., and Zaleski, P.I., 1971, "Measurement. Interpretation, and Characterization of Near-field Flow Noise", Proc. Conf. on Flow-Induced Vibrations in Reactor System Components, Argonne. Illinois. May 14-15, ANL-7685. pp. 112- 140.

[71] Zwijsen, K., et al, 2022, VIKING: A joint in-dustry project on Flow-Induced Vibrations, NU-RETH-19, Brussels, Belgium

[72] Lillberg, E. Angele, K., Lundqvist, G. and Edh, N., 2015, "Tailored Experiments for Validation of CFD with FSI for Nuclear Reactor Applications," in NURETH16, Chicago, IL.

[73] Lillberg, E., 2015, "Energiforsk FIV Experiment, Data for Computational Analysis".Technical Report Vattenfall Stockholm, Sweden.

[74] Cioncolini, A., Silva-Leon, J., Cooper, D., Quinn, M.K., and Iacovides, H., 2018, "Axial-flow-induced vibration experiments on cantilever rods for nuclear reactor applications," Nuclear Engineering and Design, 338, pp. 102-118.

[75] Modarres-Sadeghi, Y., Païdoussis, M.P., Semler, C., Grinevich, E., 2008, "Experiments on vertical slender flexible cylinders clamped at both ends and subjected to axial flow", Phil. Trans. R. Soc. A 366, 1275–1296.

[76] Païdoussis, M.P., Grinevich, E., Adamovic, D., Semler, C., 2002, "Linear and nonlinear dynamics of cantilevered cylinders in axial flow. Part 1: Physical dynamics", J. Fluids Struct. 16, pp. 691–713.

[77] Kheiri, M., Païdoussis, M.P., 2015, "Dynamics and stability of a flexible pinned-free cylinder in axial flow", J. Fluids Struct. 55, 204–217.

[78] Ferrari, G., Balasubramanian, P., Le Guisquet, S., Piccagli, L., Karazis, K., Painter, B., Amabili, M., 2018, "Non-linear vibrations of nuclear fuel rods", Nucl. Eng. Des. 338, pp. 269–283.

[79] Ferrari, G., Franchini, G., Balasubramanian, P., Giovanniello, F., Le Guisquet, S., Karazis, K., Amabili, M., 2020, submitted. Nonlinear vibrations of a nuclear fuel rod supported by spacer grids. Nucl. Eng. Design, 361, 110503

[80] Ferrari, G., Franchini, G., Faedo, L., Giovanniello, F., Le Guisquet, S., Balasubramanian, P., Karazis, K., Amabili, M., 2020, "Nonlinear vibrations of a 3×3 reduced scale PWR fuel assembly supported by spacer grids", Nucl. Eng. Des. 364, 110674.

[81]Zhang B., Gong S., Gan F., Zhang C., and Gu, H., 2022, "Flow induced vibration measurement for a 4x4 rod bundle with spacer grids by the Laser Doppler Vibrometer, Annals of Nuclear Energy, 166, pp. 108805

[82] Vallory, J., Tekatlian, A., Phalippou, C., and Viallet, E., 2000, "Wear of zirconium alloys within grid-to-rod interaction: review and analyses, current experiments and future prospects," Proc. Of the LWR Fuel Performance Conference, Park City, USA.

[83] Vallory, J., 2004, "Methodology of pwr fuel rod vibration and fretting evaluation in hermes facilities", IAEA-TECDOC-1454 Structural behaviour of fuel assemblies for water cooled reactors Proceedings of a technical meeting held in Cadarache, France, 22-26 November 2004.

[84] Collard, B., Clement, P., and Robert, Y., 2013, "CEA activities in support of the development and qualification of fuel assemblies", LWR Fuel Performance Meeting, Top Fuel 2013.

[85] Lu, R., Conner, M., Boone, M., and Marshall, R., 2001, "Nuclear fuel assembly flow induced vibration and duration wear testing", Proceeding of the ASME Symposium on Flow-Induced Vibration, PVP-2001, Atlanta, GA, July 22-26.

[86] King, S. J., Young, M. Y., Seel, D. D., Conner, M. E., Lu, R. Y., and Paramonov, D. V., 2002, "Flow induced vibration and fretting wear in pwr fuel", 10th International Conference on Nuclear Engineering, 1, 639-648.

[87] Aullo, M., Canencia, R., Chapin, D., Lu, R., and Rabenstein, W., 2009, "Fretting performance of the RFA fuel", Water Reactor Fuel Performance Meeting - WRFPM / Top Fuel 2009, Paris (France), 6-10 Sep 2009.

[88] Jang, Y. K., Kang, J. K., Choi, J. H., Kim, Y. H., and Kim, K. T., 2003, "An experimental study on the vibrations and grid-to-rod fretting wear in PWR fuel", Proceedings of the Korean Nuclear Spring Meeting, Gyeong Ju, Korea, May 2003.

[89] Kim, K.-T., Jang, Y.-K., Choi, J.-H., and Lee, S.-S., 2004, "A study of flow-induced grid-to-rod fretting wear in PWR fuel assemblies", Problems Involving Thermal Hydraulics, Liquid Sloshing, and Extreme Loads on Structures, 81-85.

[90] Kim, K.-T., 2010, "A study on the grid-to-rod fretting wear-induced fuel failure observed in the 16x16 KOFA fuel", Nuclear Engineering and Design, 240, 4, pp. 756-762.

[91]Ter Hofstede, E. (2015). *Numerical Study of Fluid Structure Interaction in Nuclear Reactor Applications.* Master Thesis, Delft University of Technology, http://resolver.tudelft.nl/uuid:f60d989c-9101-4f6a-8817-4da09b2075f6

[92] Benra, F. K., Dohmen, H., Pei, J., Schuster, S. and Wan, B. A. (2011). *Comparison of One-Way and Two-Way Coupling Methods for Numerical Analysis of Fluid-Structure Interactions*. Journal of Applied Mathematics. Doi: 10.1155/2011/853560

[93] Degroote, J., Bathe, K. J., and Vierendeels, J. (2009). *Performance of a new partitioned procedure versus a monolithic procedure in fluid–structure interaction*. Computers & Structures, 87(11-12), 793–801. doi:10.1016/j.compstruc.2008.11.013

[94] Küttler, U., and Wall, W. A. (2008). *Fixed-point fluid–structure interaction solvers with dynamic relaxation*. Computational Mechanics, 43(1), 61–72. doi:10.1007/s00466-008-0255-5

[95] Pope, S. B. (2000). *Turbulent Flows*. Cambridge University Press. ISBN 978-0-521-59886-6

[96] Smagorinsky, J. (1963). *General circulation experiments with the primitive equations; 1. The basic experiment*. Monthly Wether Review, Vol. 91, Number 3, 1963

[97] Zhang, X. and Yu, S. D. (2011). *Large eddy simulation of turbulent flows surrounding two simulated CANDU fuel bundles.* Nuclear Engineering and Design, 241, 3553-3572

[98] Elmahdi, A. M., Lu, R., Conner, M. E., Karoutas, Z. and Baglietto, E. (2011). *Flow Induced Vibration Forces on a Fuel Rod by LES CFD Analysis*. The 14th International Topical Meeting on Nuclear Reactor Thermal Hydraulics NURETH-14, Toronto, Ontario, Canada, September 25-29, 2011

[99] Bakosi, J., Christon, M. A., Lowrie, R. B., Pritchett-Sheats, L. A. and Nourgaliev, R. R. (2013). *Large-Eddy Simulation of Turbulent Flow for Grid-to-Rod Fretting in Nuclear Reactors*. Nuclear Engineering and Design, 262, 544-561

[100] Christon, M. A., Lu, R., Bakosi, J., Nadiga, B., Karoutas, Z. and Berndt, M. (2016). *Large-Eddy Simulation, Fuel Rod Vibration and Grid-To-Rod Fretting in pressurized water reactors.* Journal of Computational Physics, 322, 142-161

[101] Bhattacharjee, S. (2016). *Study and Modeling of Fluctuating Fluid Forces Exerted on Fuel Rods in Pressurized Water Reactors*. PhD Thesis, Aix-Marseille University

[102] Bhattacharjee, S., Ricciardi, G. and Viazzo S. (2017). *Comparative study of the contribution of various PWR spacer grid components to hydrodynamic and wall pressure characteristics*. Nuclear Engineering and Design, 317, 22-43

[103] Bhattacharjee, S., Ricciardi, G. and Viazzo S. (2015). *Modeling of fluctuating fluid forces excerted on the walls of a concentric annular pipe using large eddy simulation*. The 16th International Topical Meeting on Nuclear Reactor Thermal-Hydraulics, NURETH-16, Chicago, IL, August 30-September 4, 2015

[104] Wilcox, D. C. (1994). *Turbulence modeling for CFD*. DCW Industries, Inc. 1993, 1994, ISBN 0-9636051-0-0

[105] Celik, I. B. (1999). *Introductory Turbulence Modeling; Lecture Notes*. West Virginia University, Mechanical & Aerospace Engineering Department

[106] Menter, F. R. (2012). *Best Pactice: Scale-Resolving Simulations in ANSYS CFD, Version 1.0*. ANSYS Germany GmbH

[107] Acton, M. J. Lenci, G. and Baglietto, E. (2015). *Structure-Based Resolution of Turbulence for Sodium Fast Reactor Thermal Striping Application*. The 16th International Topical Meeting on Nuclear Reactor Thermal-Hydraulics, NURETH-16, Chicago, IL, August 30-September 4, 2015

[108] Okui, S., Kubo, Y., Kakinoki, S., Lu, R. Y., Karoutas, Z. and Ikeno, T. (2013). *Flow-induced grid-to-rod fretting test and simulation for NFI PWR fuel assembly*. Proceedings of the 2013 21st International Conference on Nuclear Engineering, ICONE21, July 29 - August 2, 2013, Chengdu, China

[109] Hatman, A., Williams, G., Martin, M., Keheley, T., Lascar, C., Goodheart, K. and Chatelain, A. (2013). *CFD analysis of reactor core flow field in support of FIV diagnosis*. The 15th International Topical Meeting on Nuclear Reactor Thermal - Hydraulics, NURETH-15, Pisa, Italy, May 12-17, 2013

[110] Yan, J., Yuan, K., Tatili, E., and Karoutas, Z. (2011). *A new method to predict Grid-To-Rod Fretting in a PWR fuel assembly inlet region*. Nuclear Engineering and Design, 241, 2974-2982

[111] De Santis, D. and Shams, A. (2019). *Numerical study of flow-induced vibration of nuclear fuel rods*. NURETH-18, Portland, OR, August 18-22, 2019

[112] De Santis, D., Kottapalli, S. and Shams, A. (2018). *Numerical simulations of rod assembly vibration induced by turbulent axial flows*. Nuclear Engineering and Design, 335, 94-105

[113] Bertocchi, F., Rohde, M., De Santis, D., Shams, A., Dolfen, H., Degroote, J. and Vierendeels, J. (2020). *Fluid-structure interaction of a 7-rods bundle: Benchmarking numerical simulations with experimental data*. Nuclear Engineering and Design, 356, 110394

[114] Dolfen, H., De Ridder, J., Brockmeyer, L., Merzari, E., Kennedy, G., Van Tichelen, K. and Degroote, J. (2019). *Numerical simulation of the turbulence-induced vibration of a wire-wrapped hexagonal fuel assembly*. NURETH-18, Portland, OR, August 18-22, 2019

[115] Dressel, B., Staude, U., Hofbeck, S., Münch, C. J. and Kovacs, Sz. (2017). *Investigations on the FSI characteristic of a scaled and integral fuel structure under axial flow*. Proceedings of the ASME 2017 International Mechanical Engineering Congress and Exposition, IMECE2017-70574, Tampa, Florida, USA, November 3-9, 2017

[116] Dressel, B. and Kovacs, Sz. (2019). *Structural and FSI Modeling Approach in Accident Analysis for a Framatome BWR Fuel Design*. The 18th International Topical Meeting on Nuclear Reactor Thermal Hydraulics, NURETH-18, Portland, OR, USA, August 18-23, 2019

[117] Bengtsson, K. (2016). *FSI-analysis on vibrations of a slender rod exposed to axial flow. Calculations for nuclear power applications*. Master thesis, Chalmers University of Technology, Göteborg, Sweden, ISSN 1652-8557

[118] Menter, F. R. (1994). *Two-equation eddy-viscosity turbulence models for engineering applications*. AIAA Journal, 32(8), 1598–1605

[119] Menter, F. R., Kuntz, M. and Bender, R. (2003). *A scale-adaptive simulation model for turbulent flow predictions*. AIAA Paper 2003-0767, American Institute of Aeronautics and Astronautics

[120] Menter, F. R. and Egorov, Y. (2010). *The Scale-Adaptive Simulation Method for Unsteady Turbulent Flow Predictions, Part 1: Theory and Model Description*. Flow, Turbulence and Combustion, 85, 113-138. Doi: 10.1007/s10494-010-9264-5

[121] Spalart, P. R., Jou, W. H., Strelets, M. and Allmaras, S. R. (1997). *Comments on the feasibility of LES for wings, and on a hybrid RANS/LES approach. Advances in DNS/LES*. Proceedings of the International Conference on DNS/LES, Louisiana, USA, August 4-8, 1997, pp. 137-147

[122] Spalart, P. R. (2009). *Detached-Eddy Simulation*. Annual Review of Fluid Mechanics, 41, 181-202

[123] Spalart, P. R. and Allmaras, S. R. (1994). *A one-equation turbulence model for aerodynamic flows*. La Recherche Aerospatiale, 1, 5-21

[124] Durbin, P. A. and Petersson, B. A. (2011). *Statistical Theory and Modeling for Turbulent Flows*. John Wiley & Sons, Ltd, ISBN 978-0-470-68931-8

[125] Lardeau, S. and Billard, F. (2016). *Development of an elliptic-blending lag model for industrial applications*. 54th AIAA Aerospace Sciences Meeting, p.1600

[126] Papukchiev, A. (2022). *FSI analysis of flow-induced vibrations in a BWR instrumentation tube experiment*. Proceedings of the 19th International Topical Meeting on Nuclear Reactor Thermal Hydraulics (NURETH-19), Brussels, Belgium, March 6-11, 2022

[127] Rotta J. C. (1972). *Turbulente Strömumgen*. BG Teubner Stuttgart.

[128] Menter, F. R., Schütze, J. and Gritskevich, M. (2012). *Global vs. zonal approaches in hybrid RANS-LES turbulence modelling*. In Progress in Hybrid RANS-LES Modelling: Papers Contributed to the 4th Symposium on Hybrid RANS-LES Methods, Beijing, China, September 2011 (pp. 15-28). Springer Berlin Heidelberg.

[129] Vivaldi, D. and Pulicani, R. *Fluid-structure interaction simulations of a rod subjected to a water axial flow in a nuclear core relevant configuration*. Proceedings of the ASME Pressure Vessels & Piping Conferences PVP 2023, July 16-21, 2023, Atlanta, Georgia, USA.

[130] De Santis, D. and Shams, A. (2019). *An advanced numerical framework for the simulation of flow induced vibration for nuclear applications*. Annals of Nucl. Energy, 130, 218–231

[131] Senthooran, S. A. (2002). *Computational Model to Calculate Flow-Induced Pressure Fluctuations on a Bluff Body*. PhD Thesis, Texas Tech University, August 2002

[132] Kottapalli, S., Sharma, S., Shams, A., Zuijlen, A. H. and Porquie, M. J. B. M. (2017). *Numerical simulation of Turbulence Induced Vibrations from URANS models using the Pressure Fluctuation Model*. The 17th International Topical Meeting on Nuclear Reactor Thermal-Hydraulics, NURETH-17, Qujiang, September 3-8, 2017

[133] van den Bos, N., Zwijsen, K., van Zuijlen, A. H., Frederix, E. M., and Roelofs, F. (2023). *Turbulence-induced vibrations prediction through use of an anisotropic pressure fluctuation model*. EPJ Nuclear Sciences & Technologies, 9, 7.

[134] van den Bos, N. (2022). *Turbulence-Induced Vibrations Prediction: Through Use of an Anisotropic Pressure Fluctuation Model*. Master Thesis, Delft University of Technology, http://resolver.tudelft.nl/uuid:74381b81-fe30-4177-a4b7-9d77a735f038

[135] Donea, J., Giuliani, S. and Halleux, J. P. (1982). *An arbitrary lagrangian-eulerian finite element method for transient dynamic fluid-structure interactions*. Comput. Methods Appl. Mech. Eng., 33(1), 689–723

[136] Dolfen, H., Bertocchi, F., Rohde, M. and Degroote, J. (2019). *Numerical simulations of vortex-induced vibrations in a 7-rod bundle compared to experimental data*. SESAME International Workshop, Petten, The Netherlands, 19-21 March, 2019

[137] Vivaldi, D. and Ricciardi, G. *Assessment of an Euler-Bernoulli beam model coupled to CFD in order to perform fluid-structure simulations*. Proceedings of the ASME 2022 Pressure Vessels & Piping Conferences PVP 2022, July 17-22, 2022, Las Vegas, Nevada, USA

[138] Roelofs, F. (2019). *Thermal Hydraulics Aspects of Liquid Metal Cooled Nuclear Reactors*. ISBN: 978-0-08-101980-1, Elsevier 2019

[139] Bertocchi, F., Rohde, M. and Kloosterman, J. L. (2019). *Experimental investigation on the influence of gap vortex streets on fluidstructure interactions in hexagonal bundle geometries*. Int. J. Heat Fluid Flow, 79. Doi:10.1016/j.ijheatfluidflow.2019.108443

[140] Tavoularis, S. (2011). *Rod bundle vortex networks, gap vortex streets, and gap instability: a nomenclature and some comments on available methodologies*. Nucl. Eng. Des., 23, 4612–4614. Doi:10.1016/j.nucengdes.2011.09.043

[141] Craig Jr., R. R. and Kurdila, A. J. (2006). *Fundamentals of Structural Dynamics*. John Wiley & Sons, Inc., second edition

[142] Zwijsen, K., Tajfirooz, S., Roelofs, F., Papukchiev, A., Edh, N. and Lillberg, E. (2023). *Modelling of Flow-Induced Vibrations of a BWR Instrumentation Guide Tube Experiment*. The 20th International Topical Meeting on Nuclear Reactor Thermal-Hydraulics, NURETH-20, Washington DC, USA, August 20-25, 2023 (In press)

[143] ANSYS CFX 17.2 User's Manuals, 2016

3. Currently available experimental data and methods for FIV in SGs

W. Benguigui, S. Benhamadouche

3.1 Introduction

In PWRs, the heat from the primary circuit is used to boil water in the secondary loop. Thanks to a tubular heat exchanger, called steam generator (SG), power is transferred from primary to secondary loop. This hence produced steam is dried before entering the turbine through swirl separators and steam dryers.
PWRs can have two, three or four SGs. Their height might be up to 20 m and weight as much as 800 tons. The tube bundle is composed from 3000 to 16 000 U-tubes with a diameter of approximately 20 mm for French SGs. A sketch of the EPR steam generator is exposed in Figure 13.

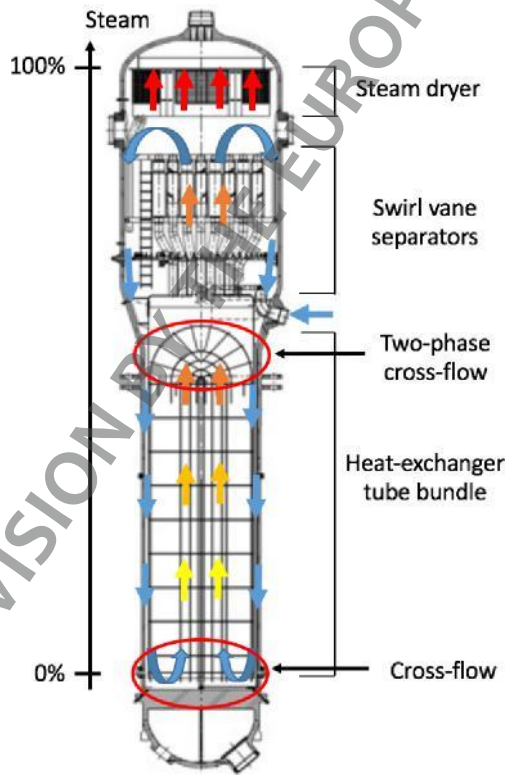

Figure 13: Cross-sketch of an EPR steam generator. The production of steam is sketched by blue to red arrows. Vibration due to cross flows are located in the red circles.

In a PWR recirculating SG, the primary loop flows through thousands of U-shaped tubes with a tube sheet at the bottom and U bends at the top of the tube bundle. Primary coolant water enters the steam generator usually between 315 - 330°C for the hot leg side and leaves at about 288°C for the cold leg side.

The secondary coolant water enters through a feedwater nozzle, the distribution is then performed by a ring into the downcomer, where the water from the separators is drained. Then, it flows to the bottom before going upward through the tube bundle, where phase-change occurs. About 25% of the water is converted into steam in the tube bundle, the other part being recirculated.
SG integrity is extremely important both for economic and safety reasons as degradation over time might occur. Consequently, during scheduled maintenance outages or shutdowns, steam generator tubes are inspected. SG problems are of primary interest since they might lead to unscheduled or extended maintenance operations. Unfortunately, these maintenance and replacement operations are expensive.
One of the main tube degradation mechanisms is flow induced vibration. [1] identified two locations of the steam generator where there is a cross-flow: at the bottom of the bundle under single-phase flow and at the top under two-phase flow with high void fractions (see Figure 13). There are two kinds of degradation mechanisms that might occur due to flow-induced vibration: fretting wear and high cycle fatigue. It might affect anti-vibration bars, tube support plates or tubes leading to SG maintenance.
According to [2], three main categories drive flow-induced vibration in single-phase flow: Tubulence-Induced-Vibrations (TIV); Vortex-Induced-Vibrations (VIV); Fluid-Elastic Instability (FEI). Vibration regimes are clearly highlighted in published experimental data with fluid-elastic instability as the most violent regime for a structure since it might cause vibration of high amplitude.
To characterize the three regimes, a velocity, called "reduced velocity", is defined to quantify the relation between characteristic length from fluid and solid.

$$V_R = \frac{U}{f_0 D}$$

with U the fluid velocity, D the characteristic length of the structure, and f_0 the natural frequency of the structure. Moreover, different other dimensionless numbers are used to characterized fluid-structure interaction in single phase-flow, as described by [5], and in two-phase flow [6].

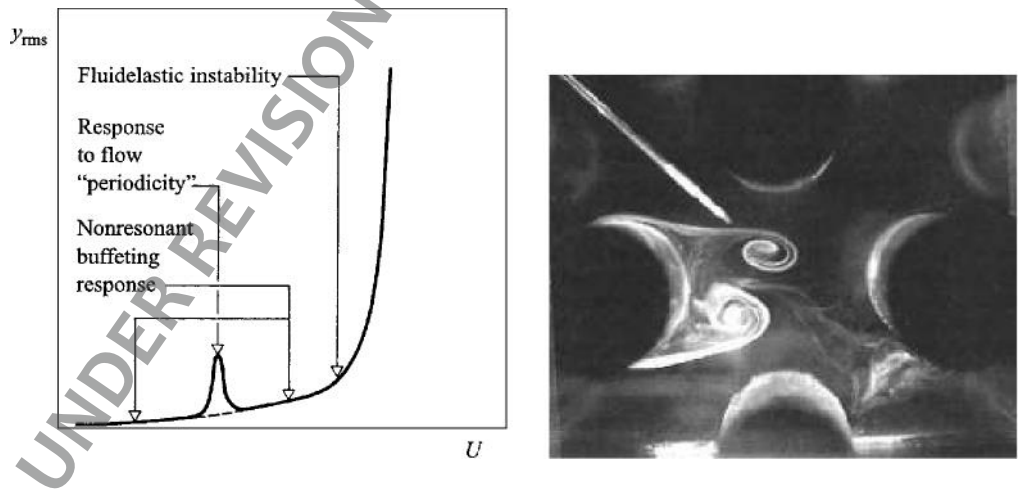

Figure 14: Idealized response with increasing flow reduced-velocity of a cylinder from [3] (left) and downstream vortices of a cylinder [4] (right).

Turbulence-induced vibration is defined by random turbulent forces leading to pressure fluctuations at structure wall. The structure can be seen as a filter taking energy from the fluid. In fact, the solid begins to vibrate with reasonable amplitude driven by the Reynolds number. In SGs, turbulence is essential to increase heat transfers. Despite low vibration magnitudes, it is crucial to take TIV into account for its influence on the tube duration. Periodic vortices in the wake of the cylinder is responsible for the increase of magnitudes when its frequency is close to the natural frequency of the cylinder (see Figure 14). Vortex-induced vibrations are stable due to the non-linearities of the system. Outside these range of reduced velocity, the structure motion is governed by turbulent excitation until a critical reduced velocity. Fluid-elastic instability is a result of fluid forces which are generated by the vibration itself. This self-amplified phenomenon appears above a critical velocity that was extensively modeled in last decades in single and two-phase flows.
When two-phase cross flows appear (half of the heat exchangers utilized in industry [6, 7]), the phenomenon is even more challenging since two-phase phenomena affect the dynamic of the tube, thus its response. Three main two-phase flow patterns are identified in literature:

- Bubbly flow, low void-fraction, where the response of the tube is similar to the one in single phase flow;
- Intermittent flow, with only few local scale description, where the two-phase damping (highest damping for this pattern) appears to be not well understood when reducing the slope of FEI and increasing critical reduced velocity;
- Annular flow, high void fraction, where the tube response comes back to something similar to single-phase flow.

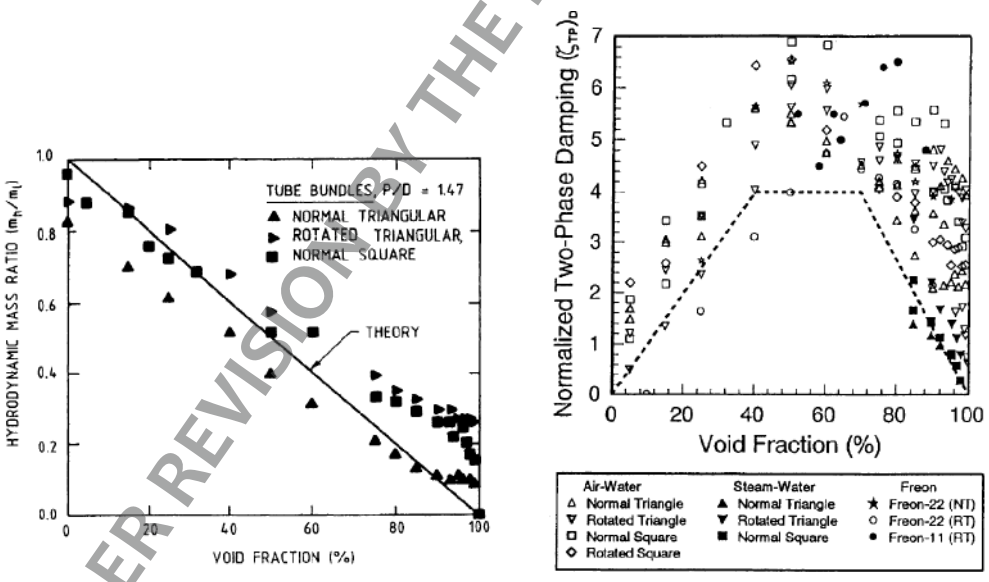

Figure 15: a) Comparison between the theoretical model of hydrodynamic mass [8] with experimental data. The decrease of the hydrodynamic mass is responsible for the increase of the critical reduced velocity. b) Comparison between the theoretical model from [9] and experiments for different mixtures and configurations. The variations of two-phase damping with void fraction are responsible for the variation of the slope of fluid-elastic departure.

Unfortunately, steam-water flow is complex to reproduce in labs to study its role on FIV, consequently simulant fluids are used such as: water/air or adiabatic freon for example. These mixtures introduce distortions in terms of mass ratio, viscosity ratio, or surface tension. Most of the time, geometric parameters of reduced-size experiments are similar to the ones in SGs, consequently dimensionless parameter such as the Weber number cannot be respected. The transition in terms of flow pattern, gas structure size, or wetting properties are consequently different and affect their ability to be representative of a steam-water flow-induced vibration in a tube bundle.
The tube response is characterized by its inertia, stiffness and damping. Illustrated in literature, these two-phase dynamic parameters, added mass and damping, are different from single-phase flow ones due to the change of physical properties.
The equivalent mass of external fluid vibrating with the structure [10] is known as the added mass. In two-phase flow, it decreases linearly with void fraction increment, see Figure 15 a). It explains the increase of critical velocity when void fraction increases.
Damping is the energy dissipation due to the flow or the structure. In two-phase flow, there is a significant dependency on the pattern as seen in Figure 15 b): the damping reaches a maximum for void fraction between 40% and 70%. The relationship between local void fraction fluctuations and damping ratio is probably explained by the temporal fluctuations in the momentum because of gas and liquid slugs alternatively impinging the tube. Damping is consequently of primary interest to predict fluid-elastic instability departure.

3.2 Experimental review of FIV in tube arrays

There are many configurations of flow through tube arrays also called cross-flow in tube bundles. One may also find different names for the same configuration. Figure 16 gives the two main generic configurations, the in-line and the staggered one. *L*, *T*, *D* are the longitudinal pitch, the transverse pitch and the tube diameter. U_∞, U_g and T_u are the upstream velocity, the gap velocity and the turbulent intensity upstream the bundle. $U_g = T/(T - D) \times U_\infty$. The normal, rotated and rotated square triangular configurations are obtained for a = 30°, a = 60° and a = 45°, respectively. They will be noted *NR*, *RT* and *RST*, respectively. The in-line square configuration is obtained when $L = T = P$. Table 2 gives *L* and *T* as a function of the distance between the tubes *P* for the particular triangular configurations. Note that in these cases, the distance between the cylinders centers is constant and usually instead of giving *L*/*D* and *T*/*D*, only the pitch-to-diameter ratio *P*/*D* is given.

Several experimental configurations exist as is shown in Tables 2 and 3. Square and triangular configurations are separated due to the large number of available experimental data. There are experiments with flexible tubes (moving tubes), sometimes just one single or a group of tubes, and experiments with fixed (rigid) cylinders. We will avoid here the nomenclature "flexible" to avoid talking about the possible deformation of a tube in the span-wise direction; we consider only rigid fixed or flexible (moving) cylinders. We clearly see from the tables that experiments dealing with both fluid and solid measurements are rare.

Experiments dealing with tube motions measure several variables, the most important ones being:

- The critical velocity U_{pc} at which the fluid elastic instability occurs (usually based on the gap velocity); this gives instability maps of U_{pc}/f_nD as a function of the mass-damping parameter δ_r (see below). An example is given in Figure 17 (left). This velocity can be obtained by interpolating linearly the r.m.s. of the tube displacement (as a function of the imposed gap velocity) using the points where there is a sharp increase. The intersection of this line with the abscissa line gives U_{pc}.

- The tube displacements usually expressed as r.m.s. of the displacement relative to the diameter of the tube as a function of the gap velocity.

- The dominant frequency of vibration of the flexible tube. An example of these two latter quantities is given in Figure 17 (right).

Additional data can be provided such as spectra, forces, etc.

When the tube is not moving we often find in the old literature fluid measurements such as the velocity and turbulence intensities using hot wires of films. We might also find *LDA* and *PIV* data and pretty fine pressure measurements as it will be shown. Another more pragmatic way to understand flow physics is visualisation using dyes or particles. [11] (see Figure 18) shows that vortex shedding emanates from the tubes of the first row and then proceed into the flow lanes of the second row and promote vortex formation from the tubes of this row. This phenomenon has been observed independently of the Reynolds number. More generally, identifying the flow patterns depending on different non-dimensional parameters is still a challenging task (see [12] containing several observations). As it will be shown later, isolating flow patterns doesn't seem to be an easy task because of the possible bifurcation (or bi-stability or jet switching) phenomena in all the configurations.

For a flexible tube configuration where one assumes that all the tubes are similar, all the targeted variables (fluid quantities, tube displacements, forces on the tubes, ...) are function of several parameters. In addition to the previous variables and for a single phase-flow configuration, let call L_z and H the tube length and the channel width, ν and ρ the kinematic viscosity of the fluids and its density, m, f_n and ζ the mass of the cylinders per unit length including the added mass due to the fluid, the natural frequency and the damping ratio (these data can be obtained experimentally). Thus, whatever the sought quantity is, it should be expressed as a function of L, T, D, H, L_z, U_g, T_u, ν, p, m, f_n and ζ. U_∞ is a function of U_g and one has to choose between the two as these two parameters are dependent. We could also add the number of tubes n_x and n_y in x and y directions (which reflect the width and length of the bundle). There also might be a redundancy between H and n_x, this depends on the distance of the side tubes to the confining walls. Using Vaschy-Buckingham theorem and if we search for example for the critical velocity U_{pc} at which the instability occurs, we have 13+1 dimensional parameter and three units (note that T_u, n_x and n_y are already non-dimensional). Thus U_{pc}/f_nD is a function of 9 non dimensional independent parameters. We have actually:

$$\frac{U_{pc}}{f_n D} = \phi\left(\underbrace{\frac{U_g D}{\nu}}_{Re_g}, Tu, n_x, n_y, \underbrace{\frac{L}{D}}_{X_L}, \underbrace{\frac{T}{D}}_{X_T}, \frac{L_z}{D}, \frac{H}{D}, \frac{m}{\rho D^2}, \zeta\right)$$

Re_g, X_L and X_T are the Reynolds number based on the gap velocity, the longitudinal pitch-to-diameter ratio and the transverse pitch-to-diameter ratio. We usually define δ as the logarithmic decrement of the damping. We have $\delta = 2\pi\zeta/(1-\zeta^2)^{0.5}$, which may replace ζ in the above equation. $\delta \approx 2\pi\zeta$ if $\zeta << 1$, which is often the case.

This is the rigorous dimensional analysis but we often find for example $U_{pc} = K \times \delta_r^{\alpha}$, where K and α are constant; here two non-dimensional numbers have been considered with the same power. The combination of these two dimensional numbers gives the Scruton number or the mass-damping parameter also called δ_r; $Sc = \delta_r = m\delta/\rho D^2$. [13] studied mixed configurations (staggered and in-line) and found a formula for the critical velocity $U_{pc}/f_n D = 2.51(2\pi\zeta m/\rho D^2)^{0.52}$.

We may find in the literature more sophisticated expressions; for example in [14] where U_{pc} is expressed as a function of $m\rho D^2$ and P/D, separately. This analysis shows that the expected quantities might depend on much more than one non-dimensional parameter, and this makes the analysis complex.

The next two sections give separately the gathered available experimental data for the in-line and staggered general configurations, separately (although some comments are sometimes given for both configurations). This is a non-exhaustive list and some more references are added in the comments. The reader can also find additional older but very instructive experiments mentioned in [14] and [15] among others. In the present document, we try to give some major statements found thanks to the experiments. The configurations which have less than 4 and 3 tubes in the longitudinal and normal directions, respectively, are not considered in the present work. As acoustic resonance is not our main target this phenomenon is not analysed in the present work. Heat transfer is also not considered and the effect of the temperature is not taken into account. The temperature may vary experimentally and this information is often not reported ([13] reported a sensitivity of the data to the temperature). Here are some indications to read the tables:

- When (*) is mentioned in the Reynolds number column, the latter is calculated using the upstream velocity and not the gap one.
- When (*) is mentioned after the tubes number $n_x \times n$, column, it means that half tubes are used on the side walls. The half cylinders might be used to decrease the boundary effects.
- When (-) is mentioned in a column, it means that the information has not been provided or not found by the authors.

Tube array configuration	L	T
Normal triangular (NT)	P	P cos(π/6)
Rotated triangular (RT)	P tan(π/3)	P
Rotated square triangular (RST)	P tan(π/4)	P cos(π/4)

Table 1: *L* and *T* as a function of *P* in the particular triangular configurations.

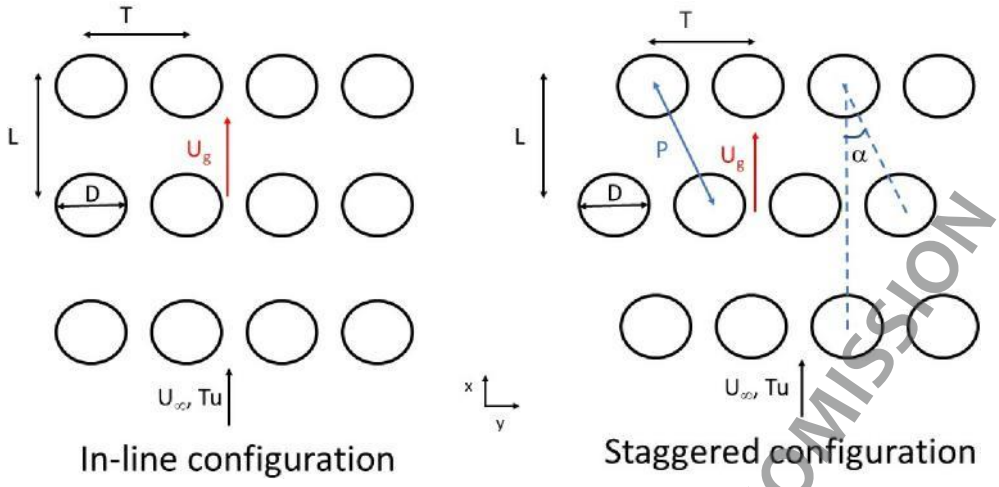

Figure 16: General configurations of the flow through tube arrays, (left) in-inline configuration, (right) staggered configuration, inspired from [16].

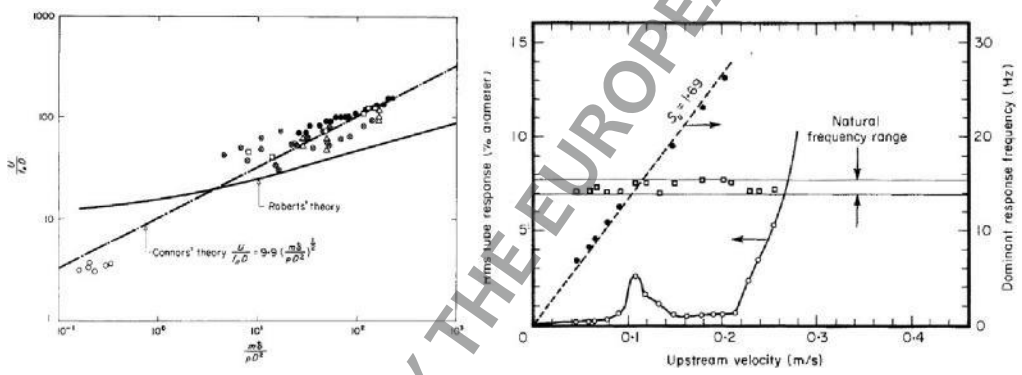

Figure 17: (Left) Critical velocity (or threshold) for FEI, image taken from [14] who compiled several data, Robert's and Connors' work can be found in [17] and [18] (right) Example of tube amplitude and frequency response for a normal triangular array at P/D = 1.5 in water, taken from [19].

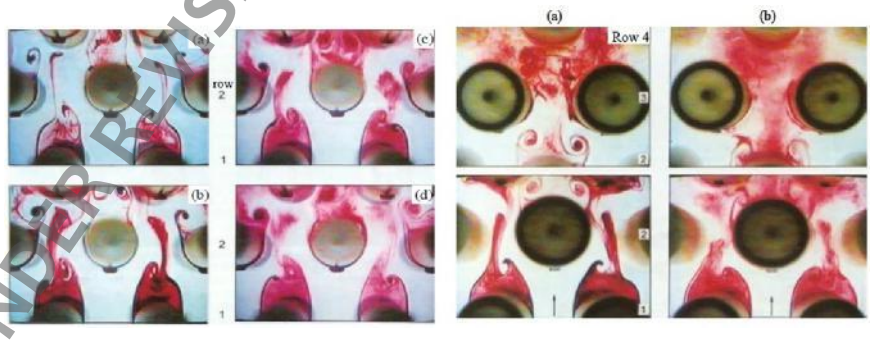

Figure 18: Flow visualisations from [11] for normal triangular configurations, (left) behind the first two rows at Reynolds number (a) 1000, (b) 1800, (c) 5000, and (d) 7000, (right) behind the first three row for P/D = 1.61 and at Reynolds number 3050 and Re=15250.

3.3 Experiments for single-phase flows

3.3.1 Experiments for the in-line configuration

Table 2 gives the major experiments for the in-line configuration chosen by the authors[1]. We start first by giving some outcomes from a structural point of view, then we move to experimental data more related to the fluid flow.

Note that upstream velocities are always well controlled in the experiments and will not be precised in the tables.

We mainly deal herein with turbulent flows. [20] observed that the laminar regime goes up to Re = 150 based on the upstream velocity. This regime is characterized by a stable symmetric vortex shedding. The wake becomes unstable (loss of apparent coherence) and fully turbulent at Re = 400.

In order to predict FEI, we clearly distinguish between vortex shedding and turbulence buffeting phenomena. The first one usually occurs at the first rows with reasonable upstream turbulence and may lead to resonance. The second one, characterised by large turbulent structures, is considered as responsible for FEI departing from a certain velocity [14]. According to [13], vortex shedding does not affect the onset of FEI. [19] noticed that for both staggered and inline configurations, the critical velocities are very similar for different tube mass ratios and that the tube response curves increase more abruptly as the mass ratio increases, what makes the definition of the stability threshold easier. [19] also gave estimations of the averaged critical reduced velocity for the four usual main patterns (normal, rotated, rotated square and in-line) for different pitch-to-diameter ratios. However, [16] tested 4 configurations with various pitch-to-diameter ratios and showed the limitations of stability diagrams not taking into account the pitch-to-diameter dependency. [21] using the experiment detailed in table 2 improved Roberts [17], Connors [18] and Blevins et al. [22] predictions of the critical velocities by considering unsteady fluid dynamic forces measured experimentally. They also found that the critical velocity in a low density fluid like air is proportional to $(m\delta/\rho D^2)^{0.5}$ as predicted in the past but is less influenced by the mass-damping parameter for high density flows. The number of rows and upstream turbulence may also play an important role. [13] found that, generally speaking, upstream turbulence stabilizes tube arrays as they found that the critical velocity increases while increasing upstream turbulence. However, [23] showed that added upstream turbulence has little effect deeper in an array than on the first row of cylinders.

Generally speaking, FEI is observed for vibrations perpendicular to the main flow direction also called cross-flow direction. However, this phenomenon can occur in the flow direction. [24] argued that vortex shedding resonance leads to large stream-wise displacements (about 6% of *D*). This shedding is due to pairs of vortices emanating from the first tube row and this phenomenon persists up to at least the third row, the second tube row response being the largest. In [23], for all positions of the flexible tube in the array, the flexible cylinder was found to become fluid-elastically

[1]: In Weaver and Yeung (1984), there were also normal and parallel triangular configurations. In Chen and Jendrzejcyk (1981) few points go up to 100 for the mass-damping ratio. In da Silva et al. (2018), 35 configurations are also reported. A better description of wind and water tunnels experiments are given in Price et al. (1986) and Price et al. (1986) for Price and Paidoussis (1989).

unstable, with its motion predominantly in the cross-flow direction. [25] also identified two distinct motion-dependent excitation mechanisms for a cylinder: a single-mode flutter phenomenon and a symmetric vortex shedding resonance. According to the authors, the first one is responsible for the on-set of fluid-elastic instability in the cross-flow direction.

[26] performed flow visualization study of an in-line array in water flow to reveal the nature of the flow instability, which dominates away from resonance effects. They showed that the flow structure is dominated by the instability of the jet issuing between the tubes. The jet impingement on the downstream tubes enhances the symmetric mode and suppresses the anti-symmetric mode of the jet instability. Later, [27] performed deeper investigations with flow visualisation for the in-line configuration in water or in air. They observed that large-scale vortices are formed on both sides of the flow lanes between adjacent cylinders after a development through the first few rows. The vortex-shedding is due to the jet instability and looks like a pulsating flow emanating from the gaps between the cylinders. The gaps must be small enough involving relatively packed bundles (P/D in the order of 1.5). This instability is π out of phase with those of the neighboring cylinder, which leads to an anti-symmetric phenomenon, but not comparable to the vortex shedding of an isolated cylinder.

Flow field measurements have received less attention than mechanical responses in the early years. With the growth and enhancement of measurement techniques, we have more and more data that allow us to better understand the FSI mechanisms and to validate numerical approaches such as simplified mechanical models or CFD. The measurements, in particular concerning the surroundings of a flexible tube, are difficult. We find much more data in the literature with fixed tubes. Concerning the involved frequencies, [28] studies deep tube arrays and showed that Strouhal numbers associated with peaks in the turbulence frequency spectrum of flows in tube arrays can be functions not only of the bank geometry, but also of measurement location and Reynolds number. Thus, the practice of assuming broadband turbulent excitation of tubes for vibration design could be limited.

Author(s)	fluid	$n_x \times n_y$	Flexible cyl.	Re	Upstream Turb.	D (mm)	(L/D,T/D) or (P/D,P/D)	L_z (mm)	H (mm)	$m\delta/\rho D^2$	Fluid Meas.	Mech. Meas
Tanaka & Takahara [21]	water & air	4×7	(2,4) in (x,y)	6×10^3 to 2.4×10^4	(-)	30	(1.33,1.33)	300	280	5-200 (air), 0.003-0.3 (water)	(-)	fluid dyn. forces in (x, y) dir. in water (strain gauges), displacements
Chen & Jendrzejczyk [13]	water	5×5	all	19^5 to 4.6×10^5	Fully Turb. (20 diameters)	15.9	(1.42,1.5,) (1.42,1.35) (1.515,1.6) (1.5,1.5) (1.6,1.515)	127	5T	$0.2 - 2$	(-)	displacements in (x,y) dir. (accelerometers), pictures (small light)
Weaver & Yeung [19]	water	4×8	4×3 flexible	up to 6×10^3	"low"	12.7	(1.5,1.5)	150	150	0.15 to 0.25	(-)	displacements of 2 central tubes (Strain gauges)
Weaver & Abd-Rabbo [24]	water	4×7	(*)4×3 in (x,y)	110 to 6.5×10^3	(*)$< 0.5\%$	25	(1.5,1.5)	300	300	0.07	Flow visualisations (Aluminum lighted particles)	displacements (strain gauge)
Fitzpatrick et al. [28]	water	20×7	none	4×10^3 to 1.3×10^4	0.3 to 0.6%	6.35	(1.73,1.73) (1.73,1.97) (1.97,1.97)	6T	200	(-)	upstream velocity (Pitot static tube with a Betz manometer), turbulence at six locations (hot wire)	(-)
Price & Païdoussis [23], see also [31] and [32]	air	6×5	1 flex. at different rows	600 to 1.1×10^4	7% using grid turbulence	25.4	(1.5,1.5)	609.6	(-)	0.1 to 10^3	Velocity along a line (hot wire)	displacements in (x,y) (accelerometers)
Price & Païdoussis [23]	water	6×5	1 flex at different rows (not the upstream one)	(-)	1%	12.7	(1.5,1.5)	260.35	(-)	0.1 to 10^3?	(-)	displacements in (x,y) (strain gauges)
Ziada et al. [26]	air	10×8 (*), 10×6 (*), 10×4 (*)	(-)	(-)	$< 1\%$	31	(1.35,1.6)	200	450, 350, 250	(-)	microphones, hot wire (velocity & fluctuations)	(-)

Author(s)	fluid	$n_x \times n_y$	Flexible cyl.	Re	Upstream Turb.	D (mm)	(L/D,T/D) or (P/D,P/D)	L_z (mm)	H (mm)	$m\delta/\rho D^2$	Fluid Meas.	Mech. Meas
Ziada et al. [26]	water	13×6	up to 1.2×10^4	none	$< 0.1\%$	20	(1.4,1.5)	200	390	(-)	dye injection in the wakes, hot films	(-)
Ziada & Oengören [27]	air	10×10 (*)	none	10^4	$< 1\%$	20	(1.75,2.25)	200	495	(-)	fluctuating & upstream vel. (Disa anem.), fluctuating vel. (hot wire)	(-)
Ziada & Oengören [27]	water	10×5 (*)	none	7×10^3 to 2×10^4	$< 0.1\%$	25	(1.75,2.25)	400	(-)	(-)	dye injection, fluctuating & upstream vel., fluctuating velocity (hot film)	(-)
Granger et al. [25]	water	7×7	1 or 3 rows $\times 5$	3.4×10^4 to 9.6×10^4	(-)	22	(1.44,1.44)	250	227	0.4 to 400	(-)	displacements in (x,y) dir. (strain gauge)
Lever & Rzentkowski [33]	air	c	variable	up to 2×10^5	(-)	60	(1.433,1.433)	600	430	1.9 to 23	(-)	displacements (x,y) (strain gauges)
Austermann & Popp [16]	air	18×4	one in (x,y)	up to 2×10^5	1%	80	(1.25,1.25)	800	(-)	11.7 to 500	(-)	displacenement in (x,y) dir. (strain gauges)
Endres & Möller [29]	air	5×5	none	4×10^4 to 7×10^4	2%	32.1	(1.05,1.05) (1.16,1.16) (1.26,1.26) (1.6,1.6)	146	up to 193	(-)	Velocity & fluctuations (hot wire anemometry)	wall pressure (piezo-resistive pressure transducer)
Iwaki et al. [30]	water with 56.9% sodium iodide	20×3 (*)	none	0.54×10^3 to 2.97×10^4 (*)	(-)	15	(1.5,1.5)	427.5	90	(-)	mean & fluctuating Vel. (PIV)	(-)
Yahiaoui et al. [34]	air	7×7(*)	none	3.55×10^4	(-)	40	(1.44,1.44)	460	460	(-)	(-)	surface pressure (pressure taps)
Da Silva et al. [12]	water	5×5	none	1960 & 3220	10.1% using a grid	10	(2,1.5) (4,1.5)	80	107	(-)	mean & fluct. vel. (LDA)	(-)

Table 2: Experiments for the in-line tube array configuration.

[29] measured r.m.s. of the wall pressure fluctuations. They found that they scale with the gap velocity and give the same magnitudes for triangular and in-line arrays. In triangular arrays, there is no local maximum around the tubes. However, with the in-line configuration, the authors found pronounced local maxima at 30° and 45°. They also analysed pressure and velocity spectra. They found, for example, that the energy of the small scales increases with decreasing the pitch-to-diameter ratio. [30] analysed in-line and staggered configurations. For the in-line configuration they showed that turbulence increases gradually from the first row to the fourth. The flow was characterized by two flow regions; (a) a vortex region behind the tubes, (b) a straight flow region of high velocity in space between adjacent tubes. The wake structure at the first row was different from the other ones which were open. In the staggered array, the turbulence grows highly behind the second row in comparison to the in-line configuration and becomes homogeneous more rapidly, compared to the in-line configuration. The flow was characterized only by symmetric pairs of vortices behind all the tubes. The wakes were also close behind all the tubes.

Finally, [12] tried to identify persistent flow patterns in the in-line configuration. The same regime did not always persist along all cylinder rows for a given spacing ratio. For the smallest *T/D* ratio, a quasi-steady behavior associated with a biased flow pattern was noted and flip-flopping was observed in one case. Additional considerations made the authors conclude that there is a need to extend flow pattern investigations to arrays with more cylinder rows.

3.3.2 Experiments for the staggered configuration

Table 3 starts by giving the major experiments for the in-line configuration chosen by the authors[2].

First concerning the laminar regime, [24] used flow visualization to show that for Reynolds numbers up to about Re = 870, based on the gap velocity, the flow development in the array is laminar and looks like the one obtained for an isolated single cylinder characterized by regions of unseparated flow, then stable attached vortices and finally alternate vortex shedding.

[41] found with a triangular array configuration and *P/D* = 1.375 that the critical tubes for fluid-elastic instability are in the third and fourth rows. It is thus recommended to use six tube rows.

Obtaining FEI is not straightforward as it is shown with the examples below. [32] found, for example, that a single flexible cylinder in the studied array does not become fluid-elastically unstable. Vibrations both from turbulent buffeting and from resonance were however observed. [42] (same experiment as [32]) showed later that it is possible to obtain FEI when the array has three or more flexible tubes, at least when the flexible cylinders are positioned at the first few rows. [43] observed FEI with air-flow, predominantly in the flow direction, in the first two or three rows. In water-flow, oscillatory FEI never developed. [44] obtained FEI in air-flow at a pitch-to-diameter ratio *P/D* = 1.375 for a single flexible cylinder. FEI is obtained in the cross-flow direction and instabilities in the flow direction were also observed. [45] found that a single flexible tube located in the third row (this does not apply for rows 1, 2, 4, 5) of a rigid parallel triangular array becomes

[2] [35] analyzed vortex shedding mechanisms and turbulent forces exerted on the tubes. Other work from the same authors can be found in [36] for a parallel triangle tube bundle. In [37], additional configurations of rotated and normal triangular configurations are studied. [38] used electromagnetic shaker for additional force to change the damping. [39] also studied parallel triangular configuration. For [40], other configurations exist.

fluid-elastically unstable at essentially the same threshold as for the fully flexible array. Thus, tube location significantly affects its fluid-elastic stability behavior when tested as a single flexible tube in a rigid array.

In [42], the experimental results show that increasing mechanical damping has a very small effect on the critical flow velocity at which instability occurs. However, increasing non-dimensional mass can result in a large increase of the critical flow velocity. [46] showed that a fully flexible array undergoes FEI despite the unidirectional flexibility constraint, the critical instability velocity being of the same order of magnitude when compared with previous tests on an unconstrained fully flexible array. A single flexible tube, on the other hand, is found to be stable.

[47] showed that in case of instability due to galloping (fluid-damping-controlled instability) the correlation length of the forces acting along the tube axis increases suddenly to large values. The fluid forces are well correlated for the whole tube when galloping is dominant.

Following [37] and [16], [48] showed among other findings that for normal (P/D=1.375) and rotated (P/D=1.25) configurations and by using grid turbulence with variable geometric properties leading to variable high turbulence intensity and length scale at the inlet of the bundles, a stabilization occurs with increasing turbulence in case of single flexibly mounted tube (in the first few rows).

[24] performed experiments with single flexible tube and a fully flexible array. They provide valuable information on the flow unsteadiness through a deep analysis of the Strouhal numbers based on flow velocity. The excitation phenomenon for a single flexible tube had a lower Strouhal number than the full flexible bundle and the turbulence spectrum was quite different. This implies that the shape of the turbulence spectrum is significantly influenced by very small tube motions (less than 0.5% of D). FEI in the transverse direction occurred at a slightly lower critical reduced velocity than that for the full flexible bundle. The flow visualization studies allowed also performing comparisons with observations made with the in-line configuration. They showed that flow development in the staggered array exhibits alternate vortex shedding which does not occur in the in-line array. On the other hand, the associated symmetric vortex shedding observed in the in-line array did not occur in the staggered array.

[39] provided very useful surface pressure measurements for a tube in the third row of three normal triangular arrays. Pressure measurements were also made with various static displacements applied to the tube. The fluid forces did not scale with the upstream velocity as assumed by models in the literature. It was found also that the fluid forces are dependent on Reynolds number and pitch ratio. A non-dimensional relationship between drag coefficient and Reynolds number is proposed for the three arrays.

[40] provided a widely used experiment for CFD validation as it will be shown later. Velocity and Reynolds stress measurements at several locations are provided. The success of this experiment comes probably from the fact that the tube bundle is deep enough to consider a statistically periodic flow at the last rows. As computing power was rather limited in particular twenty years ago, a lot of contributors assumed numerically periodic boundary conditions using a minimal pattern. [49] also provided valuable LDA data but on shorter tube bundle.

Author(s)	fluid	$n_x \times n_y$ *type*	Flexible cyl.	Re	Upstream Turb.	D (mm)	(L/D,T/D) or (P/D,P/D)	L_z (mm)	H (mm)	$m\delta/\rho D^2$	Fluid Meas.	Mech. Meas
Grover & Weaver [50]; Weaver & Grover [51]	air	27×5(*)	19 Flex.	(-)	$< 0.2\%$	25	(1.375,1.375)	305	1000	1.5 to 30	(-)	Velocity (hot wire probes), displacements (vibration meters)
Weaver & Yeung [19]	water	4×8 [4]	4×3 Flex.	up to 6×10^3	"low"	12.7	(1.5,1.5)	150	150	0.15 to 0.25	(-)	displacements of 2 central tubes (Strain gauges)
Abd-Rabbo & Weaver [24]	water	5×6 RST	all or one	up to 1.6×10^4	$< 0.5\%$	25	(1.41,1.41)	305	305	(-)	Flow visualisation (light with aluminium particles)	displacements (x,y) (strain gauges)
Simonin & Barcouda [40]	water	21×7, SRT	(-)	1.8×10^4 (*)	f	21.7	(2.07,2.07)	100	280	(-)	Vel. and Reynolds Stress (LDA)	(-)
Price et al. [32] later Païdoussis et al. [43]	air	7×6 or 7×8 RST & RT	non or single	up to 3.6×10^4	$< 0.5\%$ and 17%	24.5	(2.12,2.12) (1.5,1.5)	610	910	variable	Air velocity (constant temperature hot wire anemometer)	displacements (x,y) (accelerometers)
Price et al. [32] later Païdoussis et al. [43]	water	7×6 or 7×8 RST & RT	non or single	up to 5×10^3	0.4% to 0.5%	12.7	(2.12, 2.12) (1.5,1.5)	260	260	variable	Velocity (constant temperature hot film conical probes), turbulence measurements	displacements (x,y) (strain gauges)
Ziada et al. [26]	air	10×8 (*), 10×7 (*) 10×4 (*)	(-)	none	$< 1\%$	31	(2.7,1.6)	200	450, 375, 225	(-)	microphones, hot wire (velocity and fluctuations)	(-)
Andjelić & Popp [37], Austermann & Popp [16] Lever & Rzentkowski [33]	air	18×4	one in (x,y)	up to 2×10^5	1%	80	(1.25,1.25) (1.35,1.35)	800	(-)	10 to 80 then 11.7 to 500	(-)	displacement in (x,y) dir. (strain gauges)
	air	5×10 (*)	variable	up to 2×10^5	(-)	60	(1.375,1.375)	600	430	1.9 to 23	(-)	displacements (x,y) (strain gauges)
[44] similar to [32]	air	7×25 or 26, NT	single	(-)	(-)	25.4	(1.375,1.375)	590	(-)	(-)	(-)	(-)
Mureithi et al. [52]	water	$7 \times (8, 9), RT$	single	(-)	$< 0.5\%$	12.7	(1.375, 1.375)	238	260	(-)	(-)	tube disp. & vel. (x,y) (Optron noncontacting optical motion follower)

Author(s)	fluid	$n_x \times n_y$ type	Flexible cyl.	Re	Upstream Turb.	D (mm)	(L/D,T/D) or (P/D,P/D)	L (mm)	H (mm)	$m\delta/\rho D^2$	Fluid Meas.	Mech. Meas
Polak and Weaver [53] same wind tunnel as [50]	air	3×4(*)	none	5.6×10^2 to 7.6×10^4	$< 0.2\%$	g	(1.14,1.14) to (2.67,2.67)	305	305	(-)	hot wire, flow visualisation (ammonium sulphite)	(-)
Oengören and Ziada [35]	air	variable NT	none	5.3×10^4	$< 1\%$	variable	(1.61,1.61) (2.08,2.08) (3.41,3.41)	variable	variable	(-)	vel. (hot-film)	surf. pressure fluc. (taps / microphones), C_L and C_D simultaneously (two piezo-electric transducers)
Oengören and Ziada [35]	water	variable NT	none	3.5×10^4	$< 0.1\%$	variable	(1.61,1.61) (2.08,2.08) (3.41,3.41)	variable	variable	(-)	dye injection, velocity measurments (hot-film)	(-)
Endres & Möller [29]	air	5×5 RT	none	4×10^4 to 7×10^4	2%	32.1	(1.05,1.05) (1.16,1.16) (1.26,1.26) (1.6,1.6)	146	up to 193	(-)	Velocity and fluctuations (hot wire anemometry)	wall pressure (piezo-resistive pressure)
Meskell & Fitzpatrick [38]	air	5×5 (*) NT	single (central) in y dir.	5×10^3 to 5×10^4 (*)	$< 1\%$	38	(1.32,1.32) (1.58,1.58)	300	300	10 to 400	(-)	tube acc. and vel (piezo-ceramic accelerometer & laser vibrometer), tube disp. (transducer)
Iwaki et al. [30]	water with 56.9% sodium iodide	20×3 (*) RST	none	0.54×10^3 to 2.97×10^4 (*)	(-)	15	(1.5,1.5)	370.5	90	(-)	mean and fluctuating Vel. (PIV)	(-)
Mureithi et al. [46]	air	8×3 (*) RT	fully flexible, single, finit number in x dir.	up to 2.2×10^4	(-)	40.4	(1.37,1.37)	305	305	2.2 to 3.6	(-)	displacements in x dir.
Mahon & Meskell [39]	air	5×5 (*) NT	static disp. single cyl (x,y)	up 5×10^3 to 4.5×10^4 (*)	$< 1\%$	38	(1.32,1.32) (1.58,1.58) (1.97, 197)	299	300	(-)	Velocities (Hot wire)	36 pressure taps located in the mid-plane of a tube
Mahon & Meskell [54]	air	5×5 (*) NT	single (central) in y dir.	up 5×10^3 to 2.5×10^4 (*)	(-)	52.8	(1.375,1.375)	298	272	(-)	(-)	36 pressure taps located in the mid-plane

Table 3: Experiments for the staggered tube array configuration.

3.4 Experiments for two-phase flows

In two-phase flow, an additional parameter is the two-phase behavior of the flow, which is still a challenge to characterize in a tube bundle. The description of the incoming flow is no longer based on a velocity or a pitch-velocity, but on pitch superficial velocities or on a homogeneous velocity. The superficial velocity of phase i is defined as:

$$j = \frac{m_i}{\rho_i S}$$

with *i* the liquid or gas phase, m_i the mass flow rate of phase *i*, *S* the section of interest (test section for the inlet or gap section in the tube bundle for examples) and ρ_i the phase density. The void fraction is commonly defined as:

$$\alpha = \frac{j_G}{S j_L + j_G} = \frac{\rho_L x}{S\rho_G(1-x) + \rho_L x}$$

with *S* is the slip ratio between phases and *x* the flow quality. In most of the two-phase FIV literature, the homogeneous void fraction (β) is used, the slip ratio is considered equal to 1 and thus:

$$\beta = \frac{j_G}{j_L + j_G} = \frac{Q_G}{Q_L + Q_G}$$

with *Q* the volumetric mass. Then, the homogeneous incident velocity U_o is obtained by dividing the total flow rate by the test section area. Then, it can be projected at the gap by with $U_g = U_0 \frac{P}{P-D}$. Moreover, the mixture can be composed either by one single fluid (like with pressurized water or freon for examples), or like most of the time, by a simulant gas and a simulant liquid. Indeed, the physical properties of the gas and the liquid have to be taken into account since they are responsible of the two-phase regime, the size of the inclusions/interfaces or the slip ratio. Consequently, in addition to the previous parameters of the phenomena in single-phase, a characteristic size defining the liquid or gas inclusions is of interest since it has been shown that the cylinder to bubble size ratio plays a role. Usually, the Eotvos, the Morton, the Weber, the Richardson or the Capillary numbers are used to describe a two-phase flow, respectively:

$$Eo = \frac{\Delta\rho g D^2}{\sigma};\ Mo = \frac{g\mu_L^4\Delta\rho}{\rho_L^2\sigma^3};\ We = \frac{\rho U D}{\sigma};\ Ri = \frac{\Delta\rho(P-D)g}{G_p^2};\ Cap = \frac{\mu_L U_g}{\sigma}$$

In terms of two-phase flow regime in tube bundles, it depends on the geometric configuration and also on how the two-phase flow is generated. Theses regimes are of primary interest when it comes to characterize the flow-induced vibration.

3.4.1 In-line tube bundle

In square tube bundle, a lot of knowledge has been shared since the 70s, as can be seen by looking at the review of literature in Table 6, 7 and 8. An extensive variety of configuration in square is available in literature where the pitch ratio is most of the time between 1.4 and 1.5, the diameter around 20 mm, and the mixture is often air-water due to its ease to use.

In terms of two phase flow, the main interest is the flow pattern which is defined based on visual observations or with quantitative approaches with optical probes. Xu et al. 1998 [55] proposed a

sketch of the different flow patterns in a square tube bundle in Figure 19. In Figure 20, pictures of two-phase flow inside a square tube bundle are presented from:

- Ulbrich & Mewes (1994) [56], where an air-water flow is observed with a side view for bubbly, intermittent and quasi annular flow;
- Murakawa et al. (2018) [57], where an air-water flow is observed in front view for bubbly and churn flow;
- Fichet et al. (2022) [58], where a comparative study is performed between air-water and air-ISL (improved simulant fluid - leading to a reduced surface tension and liquid density) for an equivalent flow rate.

It is possible to notice that one is churn flow, while the other is still in bubbly regime. This is a first illustration of the role that can be played by the choice of the mixture.

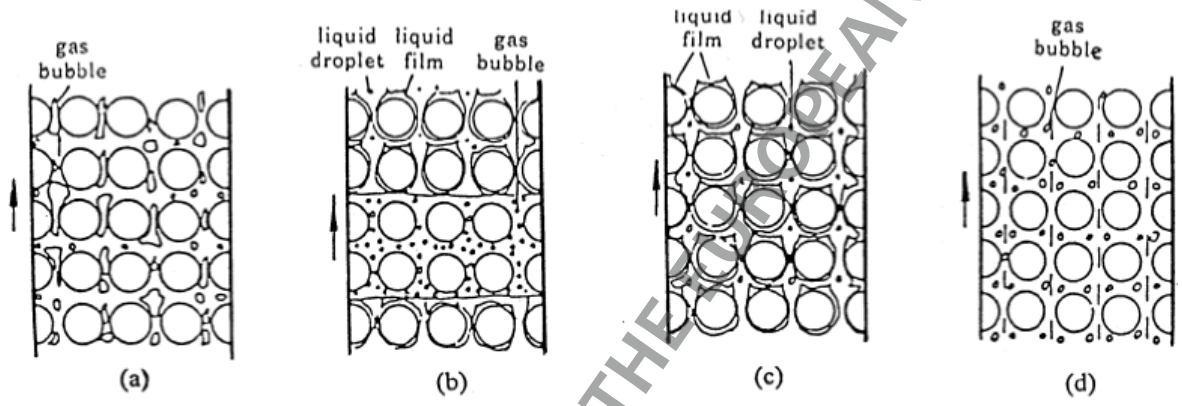

Figure 19: Flow patterns accross a square tube bundle: (a) churn fow; (b) intermittent fow; (c) annular fow; and (d) bubbly fow from [55].

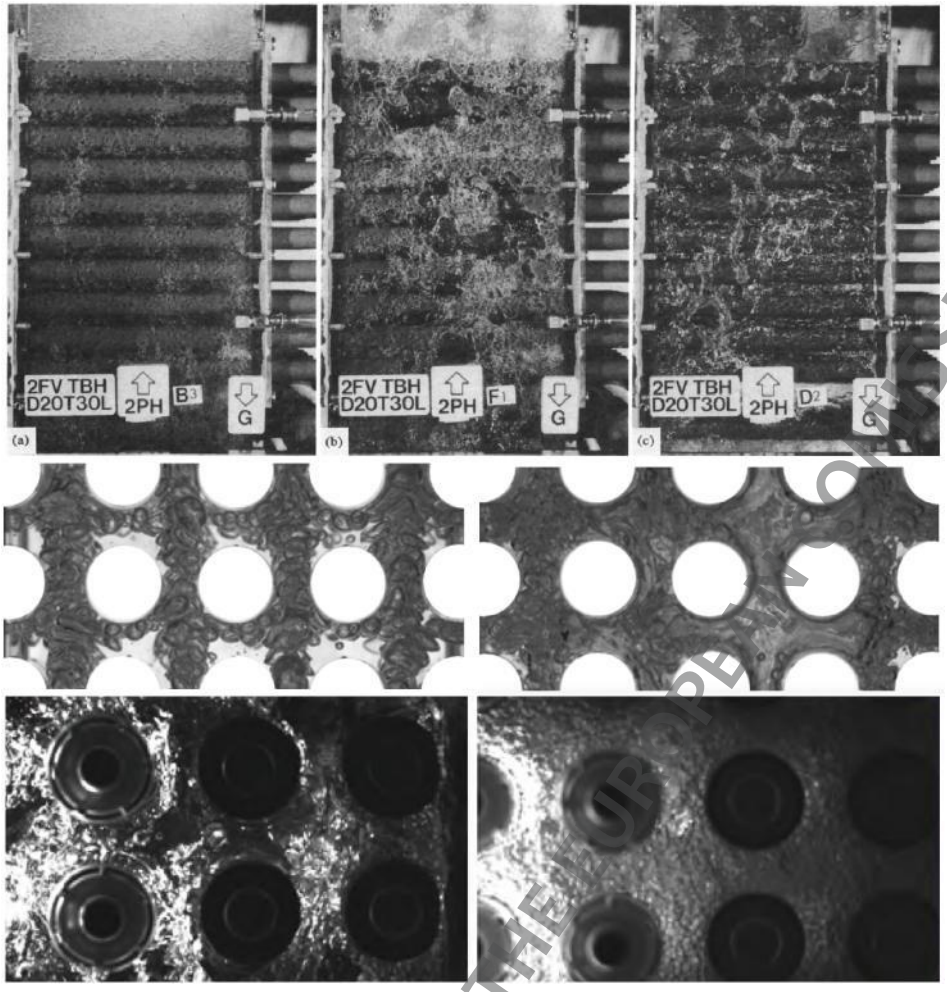

Figure 20: Examples of two-phase flow in a square tube bundle. Top, sides views from dispersed to annular flow from Ulbrich & Mewes (1994) [56]. Mid: dispersed and churn flow from Murakawa et al. (2018) [57]. Bottom: comparative study of the two-phase regime for two different liquid/gas mixtures from Fichet et al. (2022) [58].

In fact, the flow pattern can significantly change the amplitude of vibration (i.e. the damping). That's why, different authors tried to derive a flow pattern or flow regime map based on superficial velocities. For square tube bundles, a concatenated flow regime map is presented in Figure **21**, where data from Table 4 are presented. There are tube diameters from 9.79 mm to 30 mm, pitch ratio from 1.25 to 1.80, but the mixture is still air-water for each reference. For the transition from bubbly to intermittent regime, there is a correct agreement (especially around j_l close to 0.1 m/s) between most of the references (it is important to consider that the axis are in log-scale). For the transition from intermittent to annular flow the range is larger. These observations are interesting, for example [56],[59] and [60] used the same diameter and a similar pitch ratio. There is an agreement for the first transition with low liquid velocity. However, for the second transition results are quite different. The differences in the configurations of [56] and [59] are only the number of rows according to the Table 4, and the method of determination. It is surely not the reason for such discrepancies.

Authors	n_xxn_y (-)	D (mm)	P/D (-)	Fluids (-)	Method (-)
Ulbrich & Mewes (1994) [56]	5 x 10	12.7	1.50	Water/Air	Visual observations
Xu et al. (1998) [55]	3 x 20	9.79	1.28	Water/Air	Visual observations
Noghrehkar et al. (1999) [59]	5 x 24	12.7	1.47	Water/Air	PDF of local void fraction
Hong & Liu (2010) [60]	4 x 10	20.0	1.80	Water/Air	Visual observations
Hong & Liu (2010) [60]	6 x 10	12.7	1.30	Water/Air	Visual observations
Murakawa et al. (2018) [57]	3 x 8	15.0	1.50	Water/Air	Visual observations
Murakawa et al. (2022) [61]	3 x 8	18.0	1.25	Water/Air	Visual observations
Piteau et al. (2022) [62]	3 x 5	30.0	1.50	Water/Air	PDF of local void fraction

Table 4: References from literature with a two-phase flow regime map for square tube bundle.

One main discrepancy with reality is that the flow is at atmospheric pressure with a higher density ratio and surface tension. If we take a look at the previous two-phase characteristic dimensionless number, the shape of gas structure is consequently affected. With air-water, spherical bubbles and gas structures can be larger and consequently their inlet size is of great interest. It depends on the kind of mixer, and length prior to the first row. For example, in [56] and [59] they are respectively 200 mm and 300 mm after the mixer, and the characteristic size of the mixers is not given. They used a flow straightener to avoid 3D effects, but their length seems a bit short to have a stabilized diameter of bubbles. Especially when it comes to higher void fraction, where the discrepancies are much larger on the flow regime map. Moreover, the number of rows is of primary interest when studying the flow regime. The two-phase pattern does not have sufficient time to stabilize and consequently the outlet also plays a role when the number of rows is low.

This last observation is mainly dedicated to square tube bundle since a large gas structure can easily cross 3 rows by the in-line gap.

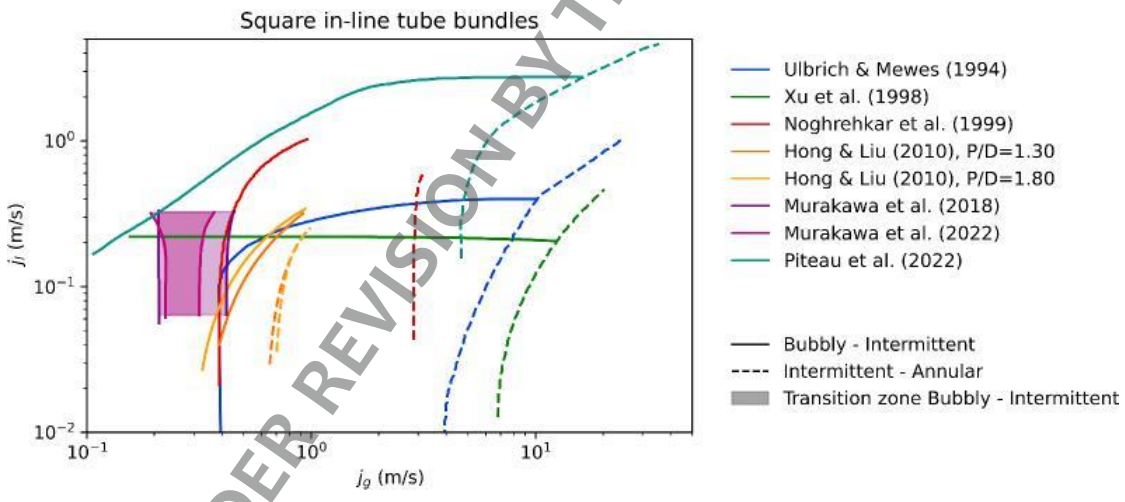

Figure 21: Flow regime map for air-water flow across a square tube bundle based on available data from literature.

If most of the flow regime maps in square tube bundles are from air/water experiments, there were also experimental tests performed with:

- steam/water from 5.0 to 58.0 bar [63, 64, 65, 66, 67, 68, 69, 70];

- refrigerant such as R114, R12, R113, or R11 operating between 5 and 10 bar [71, 72, 73, 74, 75, 76, 77, 78, 79];
- refrigerant for the gas and water for the liquid operating between 5 and 10 bar [80, 71, 81, 82];
- an "improved simulating liquid" and air such as [58] at atmospheric pressure.

These mixtures are compared in terms of density ratio, viscosity ratio and surface tension in Table 5. The respect of the viscosity ratio appears to be at the second order to influence the pattern whereas the density ratio and surface tension might significantly affect the flow:

- the lighter is a gas structure compared to the liquid, the more it will follow the liquid stream. On the contrary, a reduction of the density ratio increases the role played by the gas in the fluid stream;
- lowering the surface tension induces weaker gas-liquid interfaces and consequently lowers the size of gas structures.

Regarding the use of a single gas-liquid component without any additional heat or two components (one for the gas and one for the liquid), it is difficult to discuss these choices. However, regarding the use of adiabatic condition with a given void fraction for the whole tube bundle instead of steam generated at tube wall, Jatzlau & Mayinger (1989) [73] showed that it was conservative in terms of vibration to not take into account heating tubes in square tube bundle for different homogeneous void fractions.

Mixture	Constituant	P (bar)	T (K)	$\frac{\rho_L}{\rho_g}$	$\frac{\mu_L}{\mu_g}$	$\sigma(N/m)$
Steam/Water	1	45-70	Sat.	20 - 35	47.0	0.015 - 0.025
Air/Water	2	1	293	833	55.6	0.075
R13B1/Water	2	7-9	293	20 - 25	58.0	0.072
R116/Water	2	7-9	293	20 - 25	70.0	0.072
R114	1	9	Sat.	20.2	14.9	0.006
R12	1	10	Sat.	22	14	0.0067
R113	1	9	Sat.	150	20	0.017
R11	1	1.75	Sat.	100	31	0.017

Table 5: Comparison of mixtures used in experiment in terms of physical properties.

Before that, first publications were mainly in air-water. For example, Heilker & Vincent (1981) [83] proposed a sensitivity to the arrangement and to the inlet homogeneous void fraction. This study is one of the first to show the effect of the void fraction on the amplitude of vibration. Then, Remy (1982) [84] performed a similar investigation with a first time measurement of local void fraction behind a row of cylinder to characterize the flow. The effect of the two-phase flow on vibration was found in agreement with the works from [83] or [85].

In 1984, Axisa et al. (1984) [63] proposed a first comparison of flow-induced vibration between an air-water and a steam-water flow at 25 bar. The two-phase damping appeared to be similar in both mixtures but slightly higher in air-water for homogeneous void fractions over 90%. Fluid-elastic instability was recorded with both mixtures. The work from Axisa and co-authors ([63, 64, 65]) is the first highlighting a similar behavior in terms of damping between steam-water and air-water

flow, but also one of the first to assess the effect of void fraction, and thus of flow pattern. Then Boivin et al. (1987) [71] compared a two-phase flow with two non miscible fluids water/R13B1 with a freon at adiabiatic condition in terms of flow. Moreover, they measured void fraction locally with an optical probe when tubes are heated or not and highlighted that the main discrepancy was the increased void fraction in the vertical gap area. Pettigrew et al. (1989) [86] proposed a comparison of vibration response for different void fractions when there is a single flexible tube or all flexible tubes. The critical velocity was found significantly lower with all flexible tubes. Moreover, they first illustrated the role of the regime on vibration, since they found that continuous flow (homogeneous bubbly flow) was in agreement with Connor's formulation whereas the intermittent flow was not. Cornwell et al. 1990 [74] compared an air-water bubbly flow and an adiabatic R113 bubbly flow. They illustrated the discrepancies in terms of size distribution with some large bubbles in air/water compared to many small bubbles on the other side. Ulbrich & Mewes (1994) [56] proposed then a flow pattern map based on their own experiment and a review of literature, which is still a reference today.

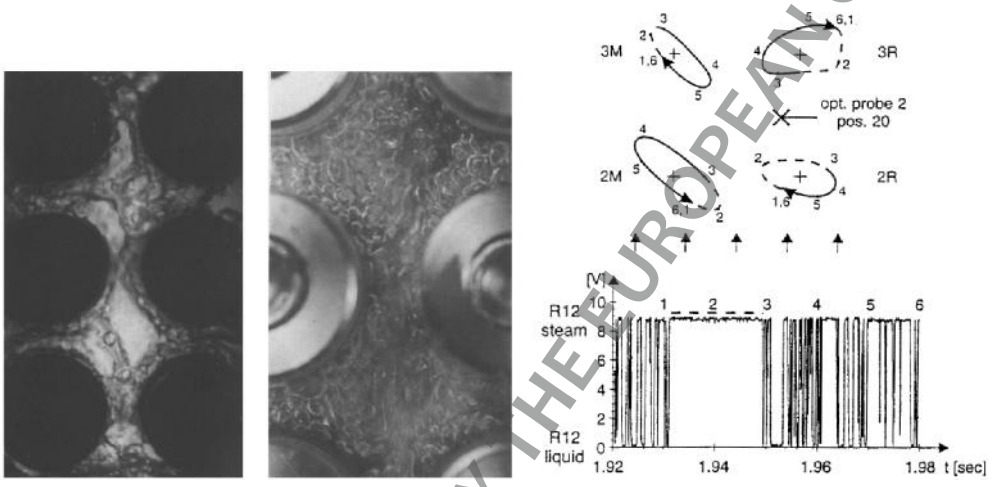

Figure 22: a) (left) View of an air/water and (right) a R113 bubbly flow illustrating the discrepancy in terms of size distribution [74]. b) Motion of 4 flexible tubes related to the void measured simultaneously with an optical probe [75].

Serizawa et al. from 1994 to 1997 [87, 88, 89] studied the trajectories of bubbles for different liquid velocities. They also illustrated the effect of the gap on the horizontal void fraction. It was also finely studied by Mann & Mayinger (1995) [75] with two optical probes in between to see the shift in void fraction between two rows. For the first time, they linked the local void distribution to the vibration by performing simultaneously a void and a vibration measurement (see Figure **22**).

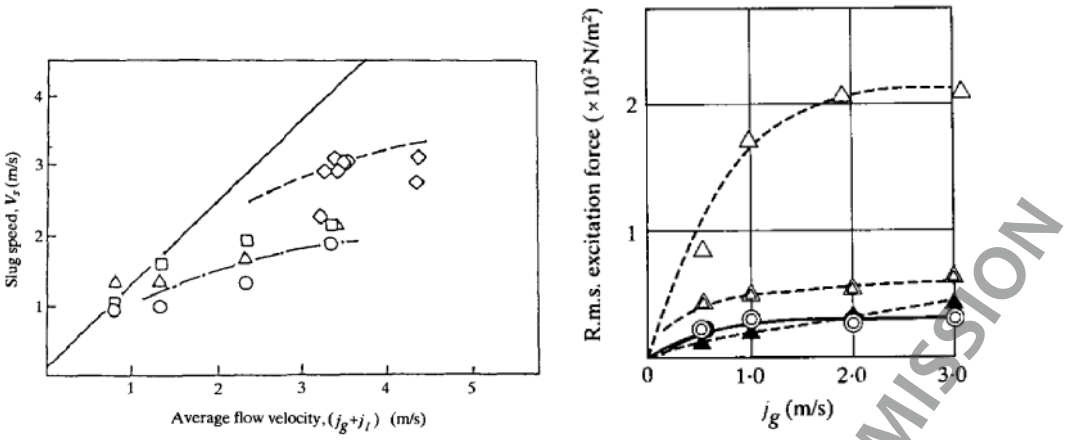

Figure 23: a) Slug speed versus gas flow velocity for a constant liquid velocity of 3.0 m/s with 0.1 MPa (rotated square), 0.5 MPa (square), 3.0MPa (triangle) and 5.8MPa (circle) b) Variation of RMS excitation forces for a constant liquid velocity (3.0m/s) when increasing the gas velocity for 0.5 MPa (white), 3.0 MPa (white with small symbols) and 5.8 MPa (black) with in triangular and circular symbols for drag and lift respectively [66, 67].

Nakamura et al. (1995) [66, 67] proposed an analysis of two specific two-phase flow patterns with air/water, and steam/water for 4 operating pressures and their role on vibration. They analysed the speed of gas slugs for different tests, it is consequently possible to link it to the excitation force on tubes. In Figure **23**, it is possible to see that by increasing pressure, the slug speed is reduced (thus its size), as well as the RMS excitation force especially in drag direction. This work highlights the role played by the size of gas structures at high void fraction on the excitation.

Delenne et al. (1997) and Gosse et al. (2001) [81, 82] proposed a comparison of vibration amplitude functions of the position in the bundle for a single or 3x3 flexible tubes for few homogeneous void fractions dedicated to be used to assess the stability of a SG tube bundle.

Then Caillaud et al. (2000, 2003) [90, 91] proposed a method based on an active control of the vibration to determine the damping of a single flexible tube for velocities beyond the fluidelastic instability for an air-water flow with different inlet void fraction.

Nakamura et al., Mureithi et al. and Hirota et al. (2002) [68, 70, 69] analyzed other test run with the steam-water loop previously discussed. They showed that the tube inclination resulted in a slightly higher damping. Moreover, damping was higher in the drag direction and decreased with pressure in the lift direction. The inhomogeneous behavior of the flow for intermittent regime was also described as a complicated phenomenon to model compared to homogeneous flow (bubbly flow).

Then, Feenstra et al.n (2003) [79] proposed another experiment with R11 illustrating that there was no obvious vortex shedding in two-phase flow. With a fully flexible tube bundle, the FEI was observed whereas for a single flexible one it was not, demonstrating the coupling between neighboring tubes.

Iwaki et al. (2005) [92] analyzed bubbly flow for low void fraction with a PIV method illustrating the slip in square and triangular tube bundle between rows. In square, they analyzed the distribution of void and velocity for two different bubbly regimes when bubbles were contained in the main

flow or when for higher liquid velocity were entrained into the wake behind the tubes. The slip ratio in the inline array was found larger than the staggered array, even if the difference remained low.

Then Sasakawa et al. (2005) [93] showed that fluidelastic instability occurs in air-water flow whatever the flow pattern is. They illustrated similarities in vibration mechanisms for bubbly flow with single-phase flow as previously mentioned, but not in churn flow. The main result is regarding FEI in churn flow, which occurs when the Power Spectrum Density (PSD) of void (gas structure passing) highlights a strong peak close in frequency to the natural frequency of the tube. For high void fraction, the FEI is no more due to the statistic character of liquid flow but to the two-phase flow dynamic.

Delaune et al. (2018) [94] performed an analysis of vibration in the drag direction of a flexible tube depending on the number of flexible tubes around. They illustrated the coupling between different tubes through PSD for various void fraction and velocities. No FEI was found during these tests. Thus, in drag direction the two-phase fluid forces are not sufficiently high to destabilize the tube until FEI.

Fichet et al. (2022) [58] proposed a comparison of an air/water and an other mixture with different physical properties to illustrate the discrepancy in terms of void distribution around the central tube, and also in terms of vibration.

Spina et al. (2022) [58] proposed an experiment dedicated to local characterization of the flow with an accurate characterization of the inlet in order to derive more information on the onset of instability in bubbly and churn flows.

3.4.2 Staggered tube bundle

For the triangular configuration, like for the square one, a lot of knowledge has been shared since the 70's illustrated by the present review of literature in Tables 6-8 and 10-12. For this configuration, the two-phase pattern is thus different due to the forced modification of the flow trajectory with geometry. Therefore, the gas structures and all two-phase properties are affected.

Authors	Tube bundle characteristics			Experimental conditions			Measurements
	Rows x Col.	D (mm)	P/D	Fluids	P (bar)	T (°C)	
Pettigrew & Gorman (1973) [85]	3 x 3 3 x 3	12.9	1.47	Water-Air	1	20	Strain gauges
Heilker & Vincent (1981) [83]	9 x 8	19.05	1.50	Water-Air	-		accelerometer Strain gauges
Remy (1982) [84]	-	-	-	Water-Air	-	-	-
Axisa et al. (1984,1985,1988) [63, 64, 65]	6 x 10	19.05	1.44	Water-Air	-	-	Gamma ray accelerometers & Strain gauges
				Water-Steam	25	210	
Taylor et al. (1986) Axisa et al. (1998) [95?]	5 x 3	30	1.50	Water-Air	-	-	force transducers
Hara (1987) [96]	1 x 5	25	1.33	Water-Air	1.00	20	-
Pierotti & Bussy (1987) [80]	14 x 7 14 x 7	25	1.44	Water-R13B1	7.4	20	-
Boivin et al. (1987) [71]	14 x 7	25	1.44	Water-R13B1	7.5	25	Gamma ray
	30 x 5	9.5	1.44	Freon R114	4	45	Optical probes
Campan & Bouchter (1988) [72]	15 x 184	9.31	1.48	Freon R114	8.94	78.43	Bi-optical probes Piezoelectric accelerometer
Schrage et al. (1988) [97]	27 x 5	7.94	1.30	Water-Air	1-3	10	Visual observations Pressure gauges Manometers
Pettigrew et al. (1989a,b) [98, 86]	8 x 5	13	1.47	Water-Air	1	20	Visual observations Strain gauges
Jatzlau & Mayinger (1989) [73]	5 x 3 1 x 3	22	1.50	Freon R12	10-32	T_sat	Displacement transducers
Cornwell (1990) [74]	17 x 2	19.05	1.33	Freon R113	1	47.6	Visual observations
Dowlati et al. (1990) [99]	20 x 5	19.05	1.30	Water-Air	1.01-1.80	-	Gamma ray densitometer
	20 x 5	12.7	1.75				
Ulbrich & Mewes (1994) [56]	10 x 5	12.7	1.50	Water-Air	1.01-1.40	20-30	Visual observations Differential pressure transducer Pressure transducers
Serizawa et al. (1994) (1995) (1997) [87, 88, 89]	9 x ?	10	2.00	Water-Air	-	-	Visual observations Electrical resistivity probe Hot-film probe Pitot tube
Mann & Mayinger (1995) [75]	5 x 3	22	1.50	Freon R12	1	41	Optical probes Inductive displacement transducers
Haquet & Gouirand (1995) [76]	24 x 4	9.31	1.48	Freon R114	9	78	Bi-optical probe
Nakamura et al. (1995a,b) [66, 67]	20 x 5	19	1.42	Water-Air	1	20	Strain gauges
				Water-Steam	5-58	150-273	
Dowlati et al. (1996) [77]	20 x 5	12.7	1.30	Freon R113	1.03-1.55	T_sat	Visual observations Load cells Gamma ray densitometer Differential pressure transducer

Table 6: References from literature with a two-phase flow in a square tube bundle Part 1.

Authors	Tube bundle characteristics			Experimental conditions			Measurements
	Rows x Col.	D (mm)	P/D	Fluids	P (bar)	T (°C)	
Delenne et al. (1997) [81]	9 x 7	22	1.44	Water-R13B1	7.45	25	Visual observations Strain gauges
Xu et al. (1998) [55]	20 x 3	9.79	1.28	Water-Air	1-2	25	Visual observations U-tube manometers
Noghrehkar et al. (1999) [59]	24 x 5	12.7	1.47	Water-Air	1.00	22	PDF of local void fraction fluctuations Electrical resistivity probe Gamma ray densitometer
Caillaud et al. (2000) (2003) [90, 91]	5 x 3	30	1.50	Water-Air	-	-	Strain gauges Accelerometer
Gosse et al. (2001) [82]	9 x 7	22	1.44	Water-R13B1	7.45	25	Strain gauges
	7 x 7	22	1.44				
Soussan et al. (2001) [78]	40 x 4	9.31	1.48	Freon R114	9	78	Bi-optical probes
Inada et al. (2002) [**?**]	11 x 5	22	1.42	Water-Air	-	-	Strain gauges
Nakamura et al. (2002) [68]	30 x 5	22.23	1.46	Water-Steam	5-58	150-273	Void sensor probe
Mureithi et al. (2002) [70]							Strain gauges
Hirota et al. (2002) [69]							-
Feenstra et al. (2003) [79]	4 x 3	7.11	1.485	Freon R11	1.70	40	Gamma ray densitometer Optical probe
Mitra et al. (2003) [100]	10 x 3	16	1.40	Water-Air	1	20	Visual observations Gamma ray densitometer Strain gauges
Iwaki et al. (2005) [92]	20 x 5	15	1.50	NaI-Nitrogen	1	25-28	PIV Visual observations
Sasakawa et al. (2005) [93]	5 x 3	22	1.45	Water-Air	1	-	Power spectra of local void fraction fluctuations Electrical resistivity probe Strain gauges Pitot tube
Chung & Chu (2006) [101]	20 x 3	12.7	1.633	Water-Air	1	20	Visual observations
	28 x 5	12.7	1.633				
Bamardouf et al. (2009) [102]	10 x 1	38	1.32	Water-Air	1	20	Strain gauges
Sadikin et al. (2010) [103]							- Accelerometer
Hong & Liu (2010) [60]	10 x 4	20	1.80	Water-Air	1-2	10-20	Visual observations
	10 x 6	20	1.30				

Table 7: References from literature with a two-phase flow in a square tube bundle Part **2.**

Authors	Tube bundle characteristics			Experimental conditions			Measurements
	Rows x Col.	D (mm)	P/D	Fluids	P (bar)	T (°C)	
Delaune et al. (2011) [104]	5 x 3	30	1.50	Water-Air	-	-	Piezoelectric force transducers
Delaune et al. (2018) [94]	5 x 3	30	1.50	Water-Air	-	-	PDF of void fluctuations Sapphire bioptical probe Strain gauges
Murakawa et al. (2018) [57]	8 x 2	15	1.50	Water-Air	1	20-25	Visual observations X-ray radiography
Murakawa et al. (2022) [61]	3 x 8	18	1.25	Water-Air	1	22	Visual observations
Fichet et al. (2022) [58]	48 x 6	19	1.44	Water-Air	1.5	20	Visual observations
				Improved Simulating Liquid (ISL)-Air	1.5	15	Dual optical probe
Spina et al. (2022) [105]	5 x 5	30	1.44	Water-Air	-	-	Dual optical probe Strain gauges High speed camera Accelerometer Wire Mesh Sensor Accelerometer

Table 8: References from literature with a two-phase flow in a square tube bundle Part 3.

Kanizawa et al. (2016) [106] illustrate 6 different flow patterns for the present configuration. Bubble regimes are different depending on the density and size of bubbles. For higher void fraction, a chaotic classical pattern is observed: churn flow. The intermittent flow is also observed, it appears when there are successive passages of gas and liquid. This regime is most of the time observed in air/water flow, and might come from the inlet zone where large gas structures might occur and accumulate at the inlet of the tube bundle. Finally, there is also for very high void fraction in the annular flow where a liquid film is observed around tubes and liquid droplets in the stream.

Figure 24: Side view of a disped flow in a triangular tube bundle from Kanizawa et al. (2016) [106] and view of the test section from Darwish et al. (2023) [107] for a high void fraction.

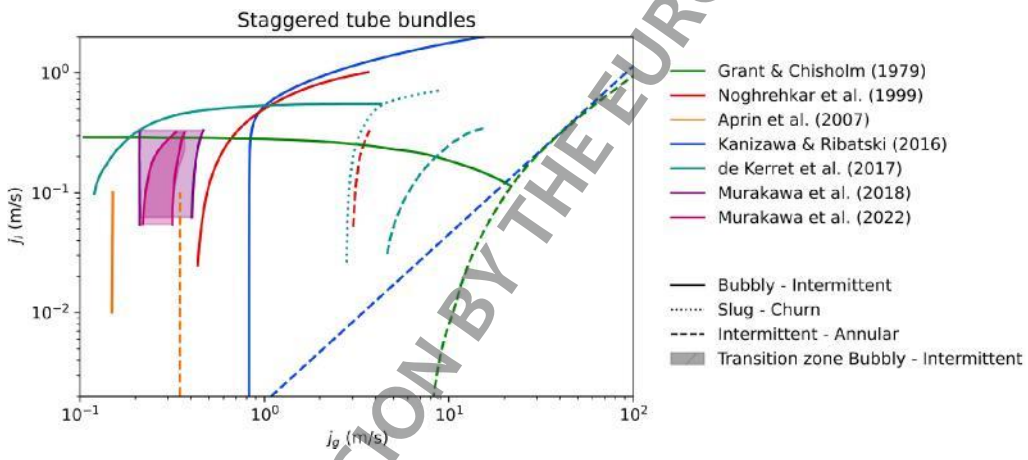

Figure 25: Flow regime map for air-water flow across a triangular tube bundle based on available data from literature.

Pictures of such kind of flow are available in their publication, but one is presented in Figure **24** with another one from Darwish et al. (2023) [107]. The flow pattern is consequently also a concern in triangular configuration. Few authors proposed a classification depending on superficial velocities. Configuration and properties of the mixture are given in Table 9. Most of these contributions were performed with air/water, but the contribution from Aprin et al. (2007) [108] was done with n-pentane, propane, and iso-butane in order to have more realistic simulant fluids in terms of surface tension and mass ratio. Regarding diameters, they are between 12.7mm and 38mm but most of them are around 20mm. By taking a look at Figure **25**, it is possible to notice that the different

transitions from bubbly to intermittent and from intermittent to annular are very different. Thus, the geometry seems to have a more significant effect on the pattern. The most significant result to notice here is the reduced zone of intermittent flow with the fluids from Aprin et al. (2007) [108]. The use of boiling hydrocarbons allows in fact to reach a correct volumetric mass ratio and surface tension. Their work was performed with 3 different fluids for different operating pressures. A PSD of the void distribution was performed on each test to determine the regime. Based on all these tests, they derived the present flow regime map, which is significantly different from air-water ones. As for the square regime map, no clear conclusion can be derived from Figure 14, it highlights the complexity to reproduce same behavior in terms of inlet two-phase flow in particular and probably a significant role played by the geometric configuration (which was not the case in square configuration).

First experiments were performed on similar loop mentioned in the square configuration section: Pettigrew & Gorman (1973) [85]. They performed a first comparison of configuration, illustrating FEI in most of them and some discrepancy in vibration regime depending on the configuration.

Like Weaver & El Kashlan (1980) [41] worked on the number of rows required to study cross flow-induced vibration in tube banks, Kondo & Naka¬jima (1980) [111] did a similar study based on air-water flow for 3 pitch ratio with 7, 9, 13, 15 and 20 rows by comparing the bubble distribution. They identified 4 two-phase flow patterns for triangular configuration, determined the minimum number of rows in air-water for 3 pitch ratio, and highlighted the significant role played by the inlet and the outlet which was reduced by a sufficient number of rows. Before that, a first description of the flow pattern was done and given as a first map by Grant & Chisholm (1979) [112].

Heilker & Vincent (1980) [83] performed one of the first extensive work to compare vibration from the first to the last rows for different triangular configurations in single-phase flow and one in two-phase flow. They showed that FEI was possible for different void fraction and its onset was different depending on the void.

Axisa et al. (1984 to 1988) [63, 64, 65], Pierotti & Bussy (1987) and Boivin et al. (1987) proposed a work on fluids and their impact on the vibration. Their conclusions were similar in triangular configuration as the square one.

Gay et al. (1988) compared with two loops the effect of the mixture on FEI onset, with air/water and R13B1/water. They found for similar condition an early onset with R13B1/water, but similar one when taking into account the density difference. Moreover, they highlighted different behavior of the flexible tube depending on the choice of the support.

Conclusions from Pettigrew et al. (1989) [98, 86] were similar to the square configuration section. In 1995 [9], they proposed a R22 loop to study the response of different tubes in a triangular tube bundle in drag and lift direction. After 65% of void fraction, they highlighted a reduced onset of FEI, authors found that it was due to a change of flow pattern; to the dependency of damping to the void fraction, thus to the flow pattern; and to a reduced turbulent excitation in boiling freon compared to air/water flow. Then, Taylor et al. (1996) [113] compared results from different air-water loops in order to understand the behavior of the flow for various tube bundle geometries. PSD of the excitation force was highlighted to be proportional to D^2,whereas the effect of the pitch ratio between 1.32 and 1.47 was demonstrated to be low. Moreover, for churn flow the effect of mass flux or void fraction was low on the PSD in comparison to its significant effect for the bubbly regime. This behavior was also reported by Pascal-Ribot et Blanchet (2005) or Benguigui et al.

(2023) [114, 115] for a single cylinder. It appears that the PSD was unchanged for churn flow whereas the change was significant before. It shows one more time the role played by the flow pattern.

At the same time, Feenstra et al. (1995) [116] proposed an analysis of their recent experiment in R11 compared to others in air/water and steam/water. Some discrepancies were found on the stability threshold for different mass fluxes attributed to physical properties of R11. The critical reduced velocity was found to be slightly dependent on the mass ratio whereas the effect was larger in air/water. Flow pattern was found to be responsible of this change between the different analyzed tests. Based on their void measurement, they assessed that it was not possible to remain on a homogeneous void fraction with an assumption of no slip due to the high discrepancy between the measured void and the homogeneous void. On the same test section, Gidi et al. (1997) [117] analyzed the effect of surface boiling. The vibration amplitude was found to be reduced when surface boiling appeared especially in the transverse direction. This was found to be probably due to larger steam structures, thus to the flow pattern, when vapor is generated at tube surfaces.

Taylor et al. (2001) [118] proposed an analysis of void fraction and flow regime effect by coupling void measurement. Void fraction is for example increasing along tube bundle whereas depending on the flow pattern the liquid gas distribution behind a tube is not the same. Depending on the flow pattern, they showed a significant dependency of mass and damping ratio with void fraction.

For the present configuration, one of the first quasi-CFD scale experiment was performed by Pettigrew et al. (2005) [119] and Zhang et al. (2008) [120]. The objective was to characterize the two-phase flow in terms of void fraction, size distribution and gas velocity. They used optical probes in 4 different locations of a narrow triangular channel with probably wall effect (1 tube + 2 halves). Two tests were presented, 50% and 80% of homogeneous void fraction (which seems very high to have accurate results with an optical probe on the diameter and the velocity). Force was also generated and were unexpectedly quasi periodic, which was probably due to the homogeneous behavior of the flow with the gas streamed between cylinder with a very low slip.

Violette et al. (2006) [121] proposed an extensive work on two-phase flow-induced vibration in a triangular tube bundle with an air/water flow for different repartition of 7 flexible tubes highlighting the coupling between flexible tubes. They highlighted:

- the motion of a cluster of adjacent flexible tubes at the onset of instability for different void fractions and the role of flexible adjacent tubes in the instability;
- no fluidelastic instability for a single flexible tube or a single flexible column of tubes.

Ricciardi et al. (2011) [122] showed that the normal configuration was more stable than the rotated one, and found no FEI in drag direction. They observed with increasing void fraction very large amplitude of vibration, their conclusions were that the local behavior of the flow was still not well understood but surely responsible for this kind of phenomenon, due to void, size and gas velocity distribution.

Sawadogo & Mureithi (2014) [123, 124] dedicated their experiment to enrich FEI model by analyzing air-water quasi static lift coefficients for void fraction from 40% to 90%. For this range, probably for the same regime, no significant discrepancy was found in terms of amplitudes. The unsteady force in the lift direction was found to be a single valued function of the reduced flow velocity, which differs from the conclusions from [70] (which was in steam/water with a different geometry). It highlights again the complexity of these flows and the role played by physical properties in the flow

pattern and thus in the fluid excitation. The same apparatus was then used to study streamwise fluidelastic instability in Olala & Mureithi (2017) [125].

Deri et al. (2014-2018) [126, 127] proposed a water-R116 triangular tube bundle with a cell of 9 flexible tubes able to be at the inlet, exit or middle of the tube bundle. No FEI in drag direction was found neither for lift direction with a single flexible tube above 40% of void fraction. Flow pattern influence was probably seen in the critical reduced velocity since its evolution was recorded to be dependent on the void fraction. Modes of vibration were highlighted before and at the onset of instability to show the coupling between tube displacements. It was found that the most responding mode at incipient FEI is always the same for all the explored void fractions.

Kanizawa & Ribatski (2016) and Alvarez-Briceno et al. (2017, 2018, 2023) [106, 128, 129, 130] proposed an air-water triangular tube bundle with a fine description of flow patterns based on a pressure drop analysis. Bi-stability was observed for intermediate liquid velocities and low gas velocities. This phenomenon is related to the fact that the flow is similar to a liquid single-phase flow for these conditions. They proposed transition law which agreed well on their tests but also on the flow-regime map from [56] (in square arrangement) and others. After that, the vibration response in drag and lift was studied. In terms of hydrodynamic mass and damping, results were in agreement with the reviewed literature excepted for the highest two-phase damping, which was found for low void fraction (around 30%). Moreover, vibration amplitude of a tube subjected to high mass velocity but low homogeneous void fraction was found to be lower than when subjected to low mass velocity but high homogeneous void fraction illustrating one more time that flow patterns play a significant role in tube vibration.

More recently, Lai et al. (2019-2022) [131, 132, 133, 134, 135, 136] proposed an extensive work on the relation between critical reduced velocity and void fraction.

Authors	n_xxn_y (-)	D (mm)	P/D (-)	Fluids (-)	Method (-)
Grant & Chisholm (1979) [109]	7 x 11	19.0	1.25	Water/Air	Visual observations
Noghrehkar et al. (1999) [59]	9 x 26	12.7	1.47	Water/Air	PDF of local void fraction
Aprin et al. (2007) [108]	5 x 18	19.05	1.33	n-pentane propane iso-butane	PDF of local void fraction
Kanizawa et al. (2016) [106]	7 x 20	19.05	1.26	Water/Air	Visual observations k-means clustering
Murakawa et al. (2018) [57]	7 x 8	15.0	1.50	Water/Air	Visual observations
Murakawa et al. (2022) [61]	7 x 5	18.0	1.25	Water/Air	Visual observations
De Kerret et al. (2017) [110]	2.5 x 66	38.0	1.50	Water/Air	PDF of local void fraction Pressure Fourier transform

Table 9: References from literature with a two-phase flow regime map for triangular tube bundle.

Piteau et al. (2022) (drag) and Panunzio et al. (2022) (lift) [62] proposed an experiment to study the FEI onset for different configurations of flexible tube in the bundle. For cross-flow FEI, a higher

Connor's constant was found, and the FEI above 30% of void was also found to appear for at least 2 flexible tubes. Regarding in-line FEI, it was found to not occur with 2 to 7 flexible tubes. They highlighted that streamwise instability might occur only through the vibration coupling of tubes.

Darwish et al. (2023) [107, 137] performed a similar experiment on a more confined tube bundle and got similar results: no FEI for a single flexible tube in the streamwise direction, or for void fraction above 30% for transverse direction. With fully flexible tube bundle, the conclusion on the Connor's constant are however different in both directions.

The present review of literature on two-phase flow-induced vibration in tube bundle is probably not complete due to the very high number of contributions in the field. The evolution of the interest over the years is illustrated in this section, however the need to study locally two-phase flow appears to still be of primary interest to understand discrepancies between similar experiments, to understand better the role played by simulant fluids. Some authors tried to address this point ([84, 119, 105] for example) by giving a local distribution, however the confinement increases the difficulty to have measurements. As mentioned by [122], a concrete understanding of gas structures in the flow is needed to describe FEI mechanisms in two-phase flow, therefore having a single point of void measurement as often proposed is not enough. Local scale simulation, so CFD, could help to reach this objective, by detailing void distribution, size distribution, gas velocities, and if possible the motion depending on local fluid behavior such like [75]. This is one of the main objective of the European project GO-VIKING to improve CFD models with a local-scale validation in order to better address the behavior of two-phase damping.

Authors	Tube bundle characteristics			Experimental conditions			Measurements
	Rows x Col.	D (mm)	P/D	Fluids	P (bar)	T (°C)	
Sutherland & Murray (1969) [138]	5 x 3 (7 tubes)	19	-	Water-Air	1.15	3-11	Visual observation
Grant & Murray (1972) [139]	11 x 7 (39 tubes)	19	1.25	Water-Air	1.03-1.65	4-20	Visual observation
Pettigrew & Gorman (1973) [85]	5 x 7 (13 tubes)	12.9	1.47	Water-Air	1	20	Strain gauges
	7 x 5 (13 tubes)						
Grant & Chisholm (1979) [112]	11 x 7 (39 tubes)	19	1.25	Water-Air	1.00	20	Visual observation
Kondo & Nakajima (1980) [111]	(7 to 20) x 5	25	1.08	Water-Air	1.20	18-20	Visual observation
			1.28				Pressure transducers
			1.40				Manometers
Heilker & Vincent (1981) [83]	5 x 9	22	1.36	Water-Air	1	20	Biaxial piezoelectric accelerometer
	9 x 8	19.05	1.50				Strain gauges
Axisa et al. (1984) [63]	7 x 19	19.05	1.44	Water-Air	1	20	Gamma ray densitometers
				Water	25	210	Biaxial piezoelectric accelerometers
Axisa et al. (1985) (1988) [64] [65]							Strain gauges
	11 x 11						
Pierotti & Bussy (1987) [80]	14 x 7	25	1.44	Water-R13B1	7.4	20	
Boivin et al. (1987) [71]	20 x 5	25	1.44	Water-R13B1	7.5	25	Optical probes
							Gamma ray densitometer
							Pressure transmitters
Gay et al. (1988) [140]	11 x 19	10	1.44	Water-Air	1	20	Piezo-resistiv accelerometers
				Water-R13B1	7.5	25	
Pettigrew et al. (1989a,b) [98, 86]	10 x 11	13	1.32	Water-Air	1.00	20	Visual observations
	10 x 11	13	1.47				Strain gauges
	10 x 6	13	1.47				
Dowlati et al. (1992a,b) [99]	20 x 5	19.05	1.30	Water-Air	1.01-1.80	20	Gamma ray densitometer
	20 x 5	12.7	1.75				Differential pressure transducer
Serizawa et al. (1994) (1995) (1997) [87, 88, 89]	9 x ?	10	2.00	Water-Air	1	20	Visual observations
							Electrical resistivity probe
							Hot-film probe
							Pitot tube

Table 10: References from literature with a two-phase flow in triangular tube bundle Part 1.

Authors	Tube bundle characteristics			Experimental conditions			Measurements
	Rows x Col.	D (mm)	P/D	Fluids	P (bar)	T (°C)	
Pettigrew et al. (1995) [9]	11 x 6	12.7	1.50	Freon R22	10	23.3	Strain gauges
Taylor et al. (1995) [141, 113]	6 x 10	12.7	1.50	Water-Air	1	20	Strain gauges
Janzen et al. (2005) [142]							Displacement probes Piezoelectric force-transducer
Feenstra et al. (1995) [116]	7 x 4	6.35	1.44	Freon R11	1.70	40	Visual observations Optical light probe
Joo & Dhir (1995) [143]	5 x 7	22	1.40	Water-Air	1.4-1.9		Strain gauges
	5 x 7	23.7	1.30				
Noghrehkar et al. (1999) [59]	26 x 5	12.7	1.47	Water-Air	1.00	22	PDF of local void fraction Gamma ray
Taylor & Pettigrew (2001) [118]	11 x 6	12.7	1.50	Freon R134a	10	30	optical probes
Pettigrew et al. (2002) [144]					7.40	34	Strain gauges
Pettigrew et al. (2005) [119]	13 x 1	38	1.50	Water-Air	1	20	optical probe
Zhang et al. (2008) [120]							Strain gauges
Iwaki et al. (2005) [92]	20 x 7	15	1.50	NaI-Nitrogen	1	25-28	PIV Visual observations
Violette et al. (2005) (2006) [145, 121]	13 x 3	38	1.50	Water-Air	1	20	Strain gauges
Chung & Chu (2006) [101]	28 x 5	12.7	1.633	Water-Air	1	20	Visual observations Strain gauges, Accelero.
Aprin et al. (2007) [108]	18 x 5	19.05	1.33	n-pentane	0.2-0.5	T_sat	PDF of local void fraction
				propane	6-12	T_sat	
				iso-butane	4-6	T_sat	
Pettigrew & Taylor (2009) [146]	6 x 11	12.7	1.50	Freon R22	12-20	23.3	Strain gauges
Senez et al. (2010) [147]	20 x 9	17.5	1.42	Water-Air	1	20	Strain gauges Accelerometer
Ricciardi et al. (2011) [122]	9 x 7	38	1.50	Water-Air	?	?	Strain gauges
Sadikin et al. (2014) [148]	22 x 7	19	1.32	Water-Air	1	20	Gamma-ray densitometer
Deri et al. (2014) [126]	22 x 9	19.05	1.44	Water-R116	0.8	20	Strain gauges

Table 11: References from literature with a two-phase flow in triangular tube bundle Part 2.

Authors	Tube bundle characteristics			Experimental conditions			Measurements
	Rows x Col.	D (mm)	P/D	Fluids	P (bar)	T (°C)	
Kanizawa & Ribatski (2016) [106]	20 x 7	19.05	1.26	Water-Air	1	20	Visual observations k-means clustering method from pressure drop and capacitance
Sawadogo & Mureithi (2014a,b) [123, 124]	13 x 3	38	1.50	Water-Air	1	22	Force transducer
Olala & Mureithi (2017) [125]							Strain gauges
de Kerret et al. (2017) [110]	2 1/2 x 66	38	1.50	Water-Air	1	20	PDF of local void fraction Fourier transform Optical probe
Azuma et al. (2018) [149]	156 x 6	9.53	1.33	Ethanol-SF6	6.8	30	Isotropic and anisotropic beams Strain gauges
	126 x 6	9.53	1.33				Accelerometers
Tan et al. (2018) [150]	15 x 7	17.48	1.48	Water-Air	1	20	Strain gauges
Murakawa et al. (2018) [57]	8 x 7	15	1.50	Water-Air	1	20-25	Visual observations
Lai et al. (2019a) [131]	15 x 7	12	1.40	Water-Air	≤16	20	X-ray Strain gauges
Lai et al. (2019b,c,d) [132, 133, 134]	15 x 7	17.45	1.48				
Lai (2019)							
Lai et al. (2020) [135]							
Lai et al. (2022) [136]							
Murakawa et al. (2022) [61]	7 x 8	18	1.25	Water-Air	1	22	Visual observations
Piteau et al. (2022), Panunzio et al. [62, 151]	20 x 5	30	1.44	Water-Air	?	?	Strain gauges Sapphire bioptical probe
Darwish et al. (2023a) [107]	9 x 9		1.64	Water-Air	1	20	-
Darwish et al. (2023b) [137]	7 x 9		1.33	Water-Air	1	20	Strain gauges

Table 12: References from literature with a two-phase flow in triangular tube bundle Part 3.

3.5 Numerical simulation review of flow-induced vibration in tube arrays

To be of interest to study single and two-phase flow-induced vibration in tube bundles, the use of numerical simulation remains a tough challenge since the problem is highly turbulent, whether single or two-phase, coupled or not with potentially many flexible tubes.

3.5.1 Numerical simulations for single phase flow configurations

Table **13** provides representative CFD computations of the flow though tube arrays with or without FSI.[3] [152] uses a Scruton equal to 10.

When a (*) is used in the columns giving L_z and H, that means that periodic boundary conditions are used in the corresponding directions. δ_{max}/D is the maximum computed displacement relative to the tube diameter. The upstream and downstream lengths used in the computations are not specified. However, the reader can refer to the corresponding reference. The references given in the column "Computational Data vs. Experiments" indicate the experiments which have been utilized to evaluate CFD outcome. They are not all detailed in the previous tables. We start here by the numerical simulation of fixed tubes then we give some outcomes of computations using FSI.

[153] and later [154] tested several turbulence models: LES, LP k-ε [155],Φ-f[156] , k-w-SST[157], SSG[158] and EB-RSM[159] on a square in-line configuration. For URANS approaches, both eddy-viscosity models and second moment closures were used. Only the computations assuming periodicity in the three directions of space by varying the number of patterns are considered here. The flow pattern taken by the fluid differs according to the treatment of turbulence and for P/D < 1.6 the mean flow is not symmetrical (this has been already observed in [160]). The interpretation for that is that the flow seeks the path of least resistance and "travels" diagonally. Almost all the URANS approaches were unable to mimic the periodic flow at P/D = 1.6. The authors concluded that in order to use the concept of wall functions, advanced ones, incorporating more physics, have to be used. They also concluded that 2D extrusion in the span-wise length is sufficient for P/D = 3.2 with LES. This latter gave pretty good results on the configuration P/D = 2.

Simonin and Barcouda experiment [40] has been widely used for CFD validation. [161] performed LES and 2D and 3D URANS computations of [40] configuration. It was shown that the LES results on a fine mesh are comparable to a DNS (this has been already stated by [162]) and experiments and reasonable agreement is still achieved with a coarse mesh. The URANS also produced satisfactory results in 3D but showed no advantage over the LES when the grid was coarsened. The 2D URANS, which produced strong vortex shedding, was found to be physically unreasonable. [163] complemented the experiments with DNS computations on restricted and wider domains for both (1.46,1.46) and (2.12,2.12) (see [164]). [165] also performed computations for this configuration with inlet/outlet conditions and much more tubes. They concluded on the ability of LES to correctly predict the staggered configuration (the spanwise length was equal to 5D for P/D = 1.46). [166] performed similar computations but compared the mean and fluctuating velocities to the experiment of [49]. [167] performed also Very Large Eddy Simulation (VLES) with TransAT code on [40] experiment and showed that even with a coarse mesh the results remain satisfactory. [168] performed Lattice Botzmann Method (LBM) and found encouraging results. [169] performed 2D URANS computations on this configuration using [170] LRN k-ε turbulence model with local refinement. They modeled 2 tubes in the transverse direction using periodic boundary conditions. The results of the computations were surprisingly good. [171] and [172] performed various 2D steady and unsteady RANS (URANS). They concluded that the steady RANS were marginal to poor. The URANS results showed that the simulations reproduce a dynamic characterized by transverse oscillatory flow structures in the near-wake region and obtained finally better agreement with the

[3]Barsamian and Hassan (1997) performed ther simulations are reported but we mention here the most important one. Schrôder and Gelbe (1999) used velocities from 1.1 to 2.2 m/s.

experimental data. The fact that 2D steady RANS do not give satisfactory results has been confirmed by [173].

[174] showed that using LES the velocity distributions obtained in the simulations were in good agreement with the experimental data. Fluctuations in the force coefficients were characterized for each arrangement and found to be directly proportional to the turbulence kinetic energy upstream of each cylinder.

Note that, for LES computations we should notice a quite low number of grid-points in the span-wise direction.

There are less references with FSI. No one-way coupling is mentioned and all the details (inner iterations) concerning the two-way coupling are not mentioned. Note that almost all the simulations found in the literature use a mass-stiffness-damping equation (called mass-spring for sake of clarity) with an ALE (Arbitrary Lagrangian Eulerian) method. [175] used a non-liner k-ε model on a normal triangular configuration at P/D = 1.25 with fairly coarse meshes. The tube bundle was flexible. The experimentally determined critical velocity by [176] seems to be higher than the computed velocity for the onset of FEI.

[177] performed 2D URANS numerical simulations combined with ALE. The predictions of the phase lag were in reasonable agreement with the experimental measurements for the range of reduced velocities U_{pc}/f_nD = 6 to 7. [178] also performed 2D URANS simulations but with a cut-ghost cell method (close to an Immersed Boundary approach). They concluded that they obtained good r.m.s. of a single tube displacement in the cross-flow direction.

[179] performed quite large computations (at that time) using LES and ALE method. The spanwise length was better resolved than in the previous works but still not enough if one considers the needed non-dimensional distance to the wall in the spanwise direction. The consistency of the calculations has been demonstrated by comparing the numerical data to the experiments found in [25] in terms of tube amplitude and frequency of motion, for various gap velocities. [180] continued the efforts and made similar computations but by moving 3 × 3 cylinders and compared to the results to [181].

[182] perfomed several 2D computation using Spalart Allmaras [183], kω [184], kω-SST [157], OES[4], k-ε and k-ω and OES-DDES(Delayed Detached Eddy Simulation.) [185], [186]. The onset of FEI is predicted for different structural parameters, mass-damping ratios and reduced velocity. The CEA-DIVA configuration [187] was used for comparisons. Both static conditions as well as vertical free motion of one of the central cylinders are considered. The turbulence motion has been captured by means of URANS and DDES modelling. The FEI of the central cylinder of the array and the phase-lag between the vertical oscillation's displacement with respect to the forces have been assessed. Similar conclusions can be found in [188] who performed 2D URANS computations on a normal triangular configuration.

[4]Organized Eddy Simulation

Author(s)	Array	CFD Code & Elem. type	CSM Tool & Elem. type	Turb. Model	FSI	δ_{max}/D	$n_x \times n_y$	Re	Upstream Turb.	D (mm)	(L/D,T/D) or (P/D,P/D)	L_z (mm)	H (mm)	$m\delta/\rho D^2$	Comp. Data vs. Exp
Barsamian & Hassan [191]	in-line	GUST (porous), Hexa, 10^5	(-)	2D WM-LES	(-)	(-)	7×3(*)	5.33×110^4	5% (random)	20	(1.95,1.95)	(-)	156	(-)	C'_L, C'_D to several exp. data
Kassera & Strohmmeier [192]	(-),	in-line & triangular 30°	mass-spring	2D kω[184]	kind of Chimera, all	up to 50%	5×6	up to 10^4 (*)	(-)	8, 12, 16	(1.2,1.2) (1.6,1.6), (2.4,2.5)	(-)	(-)	0.22 and 0.32	rms of the displacements, critical velocities [193]
Schröder and Gelbe [175]	normal triangular	STAR-CD, hexa with local refinement, 2.7×10^4	non-linear k-ε [170]	FEM subroutine	ALE?, all	5%	5×4(*)	water?	(-)	(-)	(1.25,1.25)	(-)	(-)	(-)	rms of the displacements, Cp [176]
Moulinec et al. [163]	staggered, Hexa, up to 5×10^6	staggered FV	(-)	DNS	(-)	(-)	2×2 (*)	6×10^3	(-)	20.7	(1.46,1.46) (2.12,2.12)	(-)	D	(-)	meand and fluctuation vel. [40]
Khalifa et al. [177]	parallel tri-angular	ANSYS-CFX, tri-angles prisms 2D	(-)	kω-SST[157]	ALE imposed transverse displacement	1%	2×7	2×10^3 to 1.2×10^4	(-)	(-)	(1.54,1.54)	$5.5D$	(-)	(-)	phase lag [194]
Jafari and Dehkordi [178]	normal tri-angular	in-house, hexa, 10^4	mass-spring	2D RNG k-ε [195]	Cut-Ghost cells10%	3×5 (*)	10^3 to 2.2×10^4	(-)	40	(1.32,1.32)	(-)	(-)	o	0.215	*r.m.s.* tube disp. [38]
Iacovides et al. [153]	in-line	code_saturne, Hexa, 2 to 41×10^6	(-)	(-)	several	(-)	2×2, 4×4, 7×4	4.1×10^4	(-)	(-)	(1.4,1.4) (1.6,1.6) (2,2)	2P(*), 3P(*), 9P(*)	2P(*), 4P(*), 6.4D	(-)	Cp, u, v, u' [196]
Berland & Deri [179]	in-line	code_saturne, Hexa, 24 to 140×10^6	Mass-spring in code_saturne	LES	ALE, 1	2%	7×7	1.1×10^4 to 6.6×10^4	0	22	(1.44, 1.44)	4D (*)	227	60.7	rms of tube displacements, S [25]
Slinde et al. [182]	in-line	Navier-Stokes Multi-Block solver, Hexa, 0.4 (2D) to 23×10^3 (3D)	mass-spring	several	ALE	0.5%	5×4 (*)	6×10^4	0.1%	(-)	(1.5,1.5)	D	4D (sym)	0.1 to 5	C_L, PSD of C_L (DIVA exp.)
Omar et al. [197]	in-line	STAR-CD, tets/prisms, 0.18 to 2.2×10^5	(-)	kω-SST[157]	ALE, 1	(-)	(-)	(-)	(-)	(-)	(1.33,1.33)	(-)	0.288	0.1 to 200	Cx, Cy, Fluid force phase angle [21]
[152]	in-line & square rotated 2D	Fourier pseudo-spectral scheme, up to 4×10^6	mass-spring, all	none, 2D Navier-Stokes	2	2×2 (*)	150 to 9.6×10^3 (in-line), 210 to 2.7×10^3 (rotated)	(-)	(-)	(-)	(1.5,1.5)	(-)	(-)	10	St and V_r (compilation of different exp. data)
Da Silva et al. [174]	in-line	ANSYS Fluent 14.0, Hexa, 6 to 7×10^6	(-)	LES	(-)	(-)	5×5	1.2×10^3 (*)	RFG	10	(2,1.5) (2,3) (4,1.5) (4,3)	$5.25D$	$8D$	(-)	patterns, the force coefficients, St
Zhao et al. [189]	in-line	ANSYS Fluent, Hexa, 5×10^5	ANSYS Transient Structural module	SSST-SAS[198]	ALE Ansys Coupling Module, all	10%	4×2	1.5×10^3 to 1.1×10^4 (*)	(-)	25	(1.5,1.5)	50(*)	75(*)	0.07	Vibration amplitude, spectra [20]

Table 13: CFD for tube array configurations.

[189] performed SAS simulations on an in-line tube configuration using ALE. The vibration amplitude trend and spectra of the simulation were basically consistent with that of the

experiment. Simulation accurately captured the onset of the vortex-induced resonance and the transition from the vortex-induced resonance to the FEI. However, they obtained large overestimation of vibration at the highest velocity, which corresponds to a lower critical velocity.

[190] recently performed several 3D URANS computations figuration found in [25] (same damping-mass ratio). They found a global underestimation of the critical velocity and a strong dependency on the turbulence model.

In order to conclude, Large Eddy Simulation and hybrid models seem to be a reliable option to perform FSI computations with a two-way coupling using ALE. In some configurations, even coarse LES seems to be sufficient. The feedback for hybrid RANS/LES is less important than for LES. There is a consensus about RANS; the predictions of the fluid flow seem to be poor. Finally, for the URANS approach, almost only 2D computations are reported. They seem to give somehow satisfactory results concerning the prediction of FEI but more fluid flow analysis is still required in order to assess their ability to predict such phenomenon. The 3D URANS computations are scarce but show different results when compared to the 2D ones. Note that the effect of inlet turbulence has not been apparently studied in the literature using CFD.

3.5.2 Numerical simulations for two-phase flow configurations

Due to the more recent development of two-phase flow numerical modeling, only few authors tried to address two-phase flow-induced vibration in a tube bundle.

Benguigui et al (2016,2017) [200, 199] proposed a numerical CFD model based on an Eulerian-Eulerian approach to simulate multi-regime two-phase flow in a tube bundle with a second order URANS turbulence model. They highlighted that a dispersed approach was not able to reproduce the void distribution correctly in an inclined tube, whereas the approach combining dispersed gas and continuous gas was. A comparison of behavior was done by changing the physical properties of freon/freon to air water in order to have a look at the size and void distribution (see Figure **26**). The simulated tube bundle was inclined, thus the size of gas structures, larger in air/water, was of primary interest and therefore the results were significantly different in terms of void distribution and size. A discrete forcing method [201, 202, 203] was also used to simulate the free motion of rigid or deformable tubes in a square tube bundle [204] where promising results were shown, able to reproduce phenomena observed in experiment.

Sadek et al. (2018, 2020, 2021) [205, 206, 207] proposed a different CFD based methodology to predict the unsteady fluid forces in a parallel triangular array subjected to two-phase flow with the two-phase flow modeled by the mixture model, drift-flux model, and the interfacial area concentration concept. The numerical model was used on published cases of literature and had a correct agreement in terms of force. The authors used the present model to study the influence of the pitch-to-diameter ratio on the onset of streamwise FEI and the attack angle of the flow. It is a first demonstration on how a local scale numerical model can be used to enrich our understanding of FIV phenomena.

The present review of literature in terms of numerical simulation of two-phase flow-induced vibration demonstrates the need to have a validated CFD model able to reproduce experiments to help in the understanding of two-phase FEI-phenomena. It implies to have a numerical model able to simulate all the flow pattern since it is responsible of the two-phase damping.

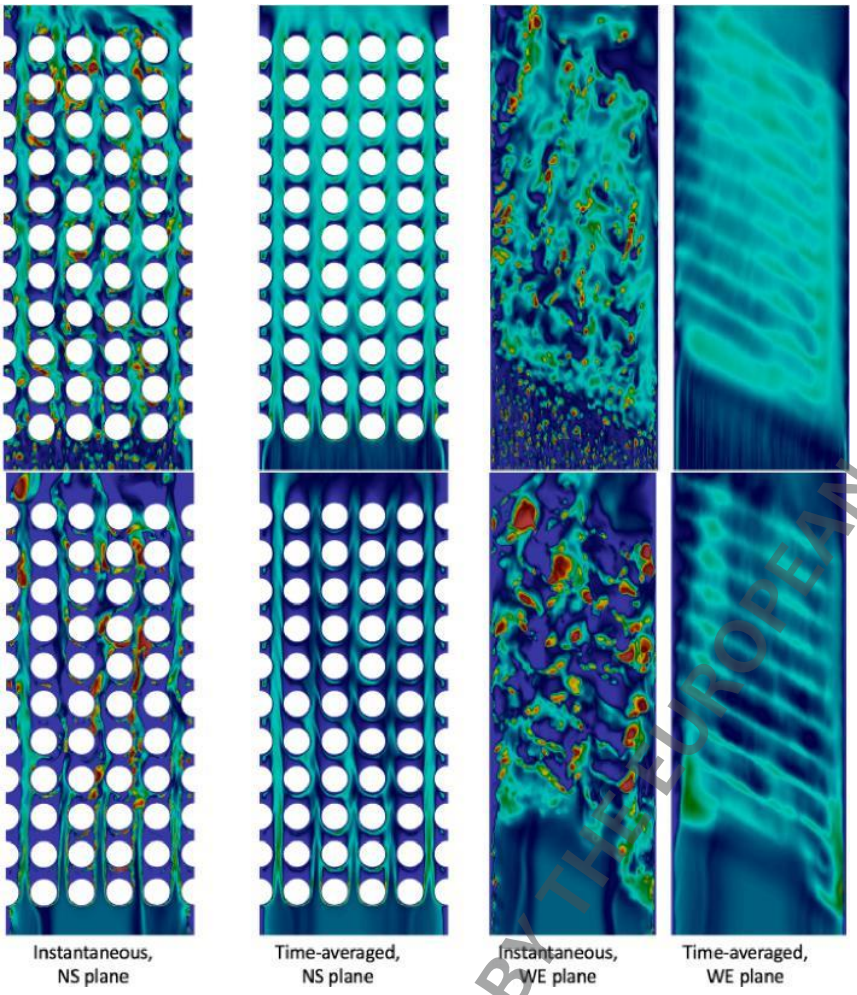

Figure 26: Numerical prediction for an inclined tube-bundle with freon/freon (top view) and air/water (bottom view). Instantaneous and time-averaged void fraction are present in the NS and WE planes [199].

3.6 Summary

In nuclear power plants, the heat from the primary loop is used to boil water in the secondary loop. Thanks to a tubular heat exchanger, known as a steam generator (SG), power is transferred from the primary to the secondary loop. The resulting steam is dried before entering the turbine through swirl separators and steam dryers. In a nuclear Pressurized Water Reactor (PWR), there are 2 to 4 SGs. Their height might be up to 20 m and weight as much as 500 tons. A typical tube bundle is composed of 3000 to 16 000 U-tubes with a diameter of approximately 20 mm for French SGs.

In a PWR recirculating SG, the primary loop flows through thousands of U-shaped tubes with a tube sheet at the bottom and U-bends at the top of the tube bundle. At the top, two-phase cross flows occurs whereas it is single-phase at the bottom. SG integrity is extremely important both for economic and safety reasons as degradation over time might occur. It might result from multiple phenomena. The present chapter is motivated by one of the main ones: flow-induced vibration of heat exchanger tubes. The authors propose a literature review on the experimental and numerical

contributions at a local scale in terms of flow and vibration; thus analytical models are not described and commented in the present work.

According to Price (1995), three main categories drive flow-induced vibration in single-phase flow: Tubulence-Induced-Vibrations (TIV); Vortex-Induced-Vibrations (VIV); and Fluid-Elastic Instability (FEI). Vibration regimes are clearly highlighted in the published experimental data with fluid-elastic instability being the most violent regime for a structure since it might cause high amplitude vibrations.

The present chapter proposed a review of the experimental and local scale numerical contributions on single and two-phase cross-flow-induced vibration in tube bundles. First, the phenomena are described based on the available literature. Then, single and two-phase experimental contributions are listed and commented. Finally, the local scale numerical contributions are described, especially in single-phase flow, since the two-phase part is still a complex and new topic in literature.

3.7 References

[1] M. Pettigrew, C. Taylor, Vibration analysis of shell-and-tube heat exchangers: an overview – part 1: vibration response, fretting wear, guidelines, Journal of Fluids and Structures 18 (2003) 485–500.

[2] S. Price, A review of theoretical models for fluidelastic instability of cylinder arrays in cross-flow, Journal of Fluids and Structures (1995).

[3] M. Païdoussis, Real-life experiences with flow-induced vibration, Journal of Fluids and Structures 22 (2006) 741–755.

[4] D. Weaver, H. Lian, X. Huang, Vortex shedding in rotated square arrays, Journal of Fluids and Structures 7 (1993) 107–121.

[5] E. D. Langre, Fluides et Solides, Ecole Polytechnique, 2002.

[6] S. Green, G. Hestroni, PWR steam generators, International Journal of Multiphase Flow 21 (1995) 1–97.

[7] G. Noghrehkar, M. Kawaji, A. Chan, Investigation of two-phase flow regimes in tube bundles under cross-flow conditions, International Journal of Multiphase Flow 25 (1999) 857–874.

[8] R. Rogers, C. Taylor, M. Pettigrew, Fluid effects on multispan heat exchanger tube vibration, Pressure Vessels and Piping, San Antonio (1984).

[9] M. Pettigrew, Vibration of a tube bundle in two-phase freon cross flow, Journal of Pressure Vessel Technology 117 (1995) 321–329.

[10] M. Pettigrew, C. Taylor, Two-phase flow induced vibration: An overview, Journal of Pressure Vessel Technology 116 (1994) 233–253.

[11] S. Ziada, Vorticity shedding and acoustic resonance in tube bundles, Journal of The Brazilian Society of Mechanical Sciences and Engineering - J BRAZ SOC MECH SCI ENG 28 (2006).

[12] B. L. da Silva, R. D. Luciano, J. Utzig, H. F. Meier, Flow patterns and turbulence effects in large cylinder arrays, International Journal of Heat and Fluid Flow 69 (2018) 136–149.

[13] S. Chen, J. Jendrzejcyk, Experiments on fluid elastic instability in tube banks subjected to liquid cross flow, Journal of Sound and Vibration 78 (1981) 355–381.

[14] M. Païdoussis, Fluidelastic vibration of cylinder arrays in axial and cross flow: State of the art, Journal of Sound and Vibration 76 (1981) 329–360.

[15] M. Païdoussis, A review of flow-induced vibrations in reactors and reactor components, Nuclear Engineering and Design 74 (1983) 31–60.

[16] R. Austermann, K. Popp, Stability behaviour of a single flexible cylinder in rigid tube arrays of different geometry subjected to cross-flow, Journal of Fluids and Structures 9 (1995) 303–322.

[17] B. W. Roberts, Low frequency, aeroelastic vibrations in a cascade of circular cylinders, I. Mech. E. Mechanical Engineering Science Mono-graph 4 (1966).

[18] H. J. Connors, Fluidelastic vibration of tube arrays excited by cross flow, in: Flow-induced Vibration in Heat Exchangers, D. D. Reiff, editor, New York: ASME, 1970, pp. 42–56.

[19] D. Weaver, H. Yeung, The effect of tube mass on the flow induced response of various tube arrays in water, Journal of Sound and Vibration 93 (1984) 409–425.

[20] D. S. Weaver, A. Abd-Rabbo, A Flow Visualization Study of a Square Array of Tubes in Water Crossflow, Journal of Fluids Engineering 107 (1985) 354–362.

[21] H. Tanaka, S. Takahara, Fluid elastic vibration of tube array in cross flow, Journal of Sound and Vibration 77 (1981) 19–37.

[22] R. D. Blevins, Fluid Elastic Whirling of a Tube Row, Journal of Pressure Vessel Technology 96 (1974) 263–267.

[23] S. Price, M. Païdoussis, The flow-induced response of a single flexible cylinder in an in-line array of rigid cylinders, Journal of Fluids and Structures 3 (1989) 61–82.

[24] A. Abd-Rabbo, D. Weaver, A flow visualization study of flow development in a staggered tube array, Journal of Sound and Vibration 106 (1986) 241–256.

[25] S. Granger, R. Campistron, J. Lebret, Motion-dependent excitation mechanisms in a square in-line tube bundle subject to water cross-flow: An experimental modal analysis, Journal of Fluids and Structures 7 (1993) 521–550.

[26] S. Ziada, A. Oengôren, E. B¨Uhlmann, On acoustical resonance in tube arrays part i: Experiments, Journal of Fluids and Structures 3 (1989) 293–314.

[27] S. Ziada, A. Oengôren, Vorticity shedding and acoustic resonance in an in-line tube bundle part i: Vorticity shedding, Journal of Fluids and Structures 6 (1992) 271–292.

[28] J. Fitzpatrick, I. Donaldson, W. McKnight, Strouhal numbers for flows in deep tube array models, Journal of Fluids and Structures 2 (1988) 145–160.

[29] L. Endres, S. Môller, On the fluctuating wall pressure field in tube banks, Nuclear Engineering and Design 203 (2001) 13–26.

[30] C. Iwaki, K. H. Cheong, H. Monji, G. Matsui, PIV measurement of the vertical cross-flow structure over tube bundles, Experiments in Fluids 37 (2004) 350–363.

[31] S. J. Price, B. Mark, M. P. Paidoussis, An Experimental Stability Analysis of a Single Flexible Cylinder Positioned in an Array of Rigid Cylinders and Subject to Cross-Flow, Journal of Pressure Vessel Technology 108 (1986) 62–72.

[32] S. Price, M. Païdoussis, R. MacDonald, B. Mark, The flow-induced vibration of a single flexible cylinder in a rotated square array of rigid cylinders with pitch-to-diameter ratio of 2➲12, Journal of Fluids and Structures 1 (1987) 359–378.

[33] J. Lever, G. Rzentkowski, Dependence of post-stable fluidelastic behavior on the degrees of freedom of a tube bundle, Journal of Fluids and Structures 7 (1993) 471–496.

[34] T. Yahiaoui, L. Adjlout, O. Imine, Experimental investigation of in-line tube bundles, MECHANIKA 85 (2010).

[35] A. Oengôren, S. Ziada, An in-depth study of vortex shedding, acoustic resonance and turbulent forces in normal triangle tube arrays, Journal of Fluids and Structures 12 (1998) 717–758.

[36] S. ZIADA, A. OENGÔREN, Flow periodicity and acoustic resonance in parallel triangle tube bundles, Journal of Fluids and Structures 14 (2000) 197–219.

[37] M. Andjel´ıc, K. Popp, Stability effects in a normal triangular cylinder array, Journal of Fluids and Structures 3 (1989) 165–185.

[38] C. Meskell, J. Fitzpatrick, Investigation of the nonlinear behaviour of damping controlled fluidelastic instability in a normal triangular tube array, Journal of Fluids and Structures 18 (2003) 573–593. Arrays of Cylinders in Cross-Flow.

[39] J. Mahon, C. Meskell, Surface pressure distribution survey in normal triangular tube arrays, Journal of Fluids and Structures 25 (2009) 1348–1368.

[40] O. Simonin, M. Barcouda, Measurements of fully developed turbulent flow across tube bundle, http://cfd.mace.manchester.ac.uk/ ercoftac/doku.php?id=cases:case078, 1986.

[41] D. Weaver, M. El-Kashlan, On the number of tube rows required to study cross-flow induced vibrations in tube banks, Journal of Sound and Vibration 75 (1981) 265–273.

[42] S. Price, S. Kuran, Fluidelastic stability of a rotated square array with multiple flexible cylinders, subject to cross-flow, Journal of Fluids and Structures 5 (1991) 551–572.

[43] M. Païdoussis, S. Price, T. Nakamura, B. Mark, W. Njuki Mureithi, Flow-induced vibrations and instabilities in a rotated-square cylinder array in cross-flow, Journal of Fluids and Structures 3 (1989) 229–254.

[44] S. Price, M. Zahn, Fluidelastic behaviour of a normal triangular array subject to cross-flow, Journal of Fluids and Structures 5 (1991) 259– 278.

[45] A. Khalifa, D. Weaver, S. Ziada, A single flexible tube in a rigid array as a model for fluidelastic instability in tube bundles, Journal of Fluids and Structures 34 (2012) 14–32.

[46] N. Mureithi, C. Zhang, M. Ruél, M. Pettigrew, Fluidelastic instability tests on an array of tubes preferentially flexible in the flow direction, Journal of Fluids and Structures 21 (2005) 75–87. Fluid-Structure and Flow-Acoustic Interactions involving Bluff Bodies.

[47] O. Romberg, K. Popp, Fluid-damping controlled instability in tube bundles subjected to air cross-flow, Flow, Turbulence and Combustion 61 (1998) 285–300. This revised version was published online in July 2006 with corrections to the Cover Date.

[48] O. ROMBERG, K. POPP, The influence of upstream turbulence on the stability boundaries of a flexible tube in a bundle, Journal of Fluids and Structures 12 (1998) 153–169.

[49] S. Balabani, M. Yianneskis, An experimental study of the mean flow and turbulence structure of cross-flow over tube bundles, Proceedings of the Institution of Mechanical Engineers, Part C: Journal of Mechanical Engineering Science 210 (1996) 317–331.

[50] L. K. Grover, D. S. Weaver, Cross-flow induced vibrations in a tube bank—Vortex shedding, Journal of Sound Vibration 59 (1978) 263– 276.

[51] D. S. Weaver, L. K. Grover, Cross-flow induced vibrations in a tube bank—Turbulent buffeting and fluid elastic instability, Journal of Sound Vibration 59 (1978) 277–294.

[52] N. W. Mureithi, S. J. Price, M. P. Païdoussis, The Post-Hopf-Bifurcation Response of a Loosely Supported Cylinder in an Array Subjected to Cross-Flow. Part I: Experimental Results, Journal of Fluids and Structures 8 (1994) 833–852.

[53] D. Polak, D. Weaver, Vortex shedding in normal triangular tube arrays, Journal of Fluids and Structures 9 (1995) 1–17.

[54] J. Mahon, C. Meskell, Surface pressure survey in a parallel triangular tube array, Journal of Fluids and Structures 34 (2012) 123–137.

[55] G. Xu, C. Tso, K. Tou, Hydrodynamics of two-phase flow in vertical up and down-flow across a horizontal tube bundle, International journal of multiphase flow 24 (1998) 1317–1342.

[56] R. Ulbrich, D. Mewes, Vertical, upward gas-liquid two-phase flow across a tube bundle, International Journal of Multiphase Flow 20 (1994) 249.

[57] H. Murakawa, M. Baba, T. Miyazaki, K. Sugimoto, H. Asano, D. Ito, Local void fraction and heat transfer characteristics around tubes in two-phase flows across horizontal in-line and staggered tube bundles, Nuclear Engineering and Design 334 (2018) 66–74.

[58] V. Fichet, B. Mallat, A. Mourgues, J. Moulin, Q. Andrzejewski, Two-phase flow induced vibration in a tube bundle of steam generators, in: FIV2022 Conference, 2022.

[59] G. Noghrehkar, M. Kawaji, A. Chan, Investigation of two-phase flow regimes in tube bundles under cross-flow conditions, International Journal of Multiphase Flow 25 (1999) 857–874.

[60] W. P. Hong, Y. Liu, Investigation of gas-liquid two-phase flow patterns based on high-speed imaging methods, in: 2010 3rd International Congress on Image and Signal Processing, volume 1, IEEE, 2010, pp. 154–156.

[61] H. Murakawa, Y. Miyoshi, K. Araki, K. Sugimoto, H. Asano, S. Maki-moto, Effect of bubble motion on local heat transfer around a tube across horizontal in-line and staggered tube bundles in bubbly and intermittent flows, Mechanical Engineering Journal 9 (2022) 22–00069.

[62] P. Piteau, X. Delaune, D. Panunzio, R. Lagrange, J. Antunes, Experi-mental investigation of in-flow fluidelastic instability for rotated trian-gular tube bundles subjected to single-phase and two-phase transverse flows, in: FIV2022 Conference, 2022.

[63] F. Axisa, B. Villard, R. Gibert, G. Hetsroni, P. Sundheimer, Vibration of tube bundles subjected to air-water and steam-water cross flow: Preliminary results on fluidelastic instability, Technical Report, CEA Centre d'Etudes Nucleaires de Saclay, 1984.

[64] F. Axisa, B. Villard, R. Gibert, M. Boheas, Vibration of tube bundles subjected to steam-water cross flow: a comparative study of square and triangular pitch arrays (1985).

[65] F. Axisa, M. Wullschleger, B. Villard, C. Taylor, Two-phase cross flow damping in tube arrays (1988).

[66] T. Nakamura, K. Fujita, K. Kawanishi, N. Yamaguchi, A. Tsuge, Study on the vibrational characteristics of a tube array caused by two-phase flow. part i: Random vibration, Journal of Fluids and Structures 9 (1995) 519–538.

[67] T. Nakamura, K. Fujita, K. Kawanishi, N. Yamaguchi, A. Tsuge, Study on the vibrational characteristics of a tube array caused by two-phase flow. part II: Fluidelastic vibration, Journal of Fluids and Structures 9 (1995) 539–562.

[68] T. Nakamura, K. Hirota, Y. Watanabe, N. Mureithi, T. Kusakabe, H. Takamatsu, Dynamics of an in-line tube array subjected to steam– water cross-flow. part i: two-phase damping and added mass, Journal of fluids and structures 16 (2002) 123–136.

[69] K. Hirota, T. Nakamura, J. Kasahara, N. Mureithi, T. Kusakabe, H. Takamatsu, Dynamics of an in-line tube array subjected to steam– water cross-flow. part III: fluidelastic instability tests and comparison with theory, Journal of fluids and structures 16 (2002) 153–173.

[70] N. Mureithi, T. Nakamura, K. Hirota, M. Murata, S. Utsumi, T. Kusakabe, H. Takamatsu, Dynamics of an in-line tube array subjected to steam–water cross-flow. part ii: Unsteady fluid forces, Journal of fluids and structures 16 (2002) 137–152.

[71] J. Boivin, B. Bussy, G. Pierotti, PWR steam generators: a set of experimental programs for three dimensional code validation, Technical Report, American Society of Mechanical Engineers, New York, NY, 1987.

[72] J. Campan, J. Bouchter, Steam generetor experiment for advanced computer code qualification: Clotaire international program, 3rd int, in: Topical Meeting on nuclear power plant thermohydraulics and op-erations, Seoul, South Corea, 1988.

[73] B. Jatzlau, F. Mayinger, Vibrations in Heat Exchangers Under Two-Phase Flow and Boiling Conditions, Technical Report, Lehrstuhl A fur Thermodynamik der Technischen Universitat Munchen, 1989.

[74] K. Cornwell, The influence of bubbly flow on boiling from a tube in a bundle, International Journal of Heat and Mass Transfer 33 (1990) 2579–2584.

[75] W. Mann, F. Mayinger, Flow induced vibration of tube bundles subjected to single-and two-phase cross-flow, in: Multiphase Flow 1995, Elsevier, 1995, pp. 603–612.

[76] J. Haquet, J. Gouirand, Local two-phase flow measurements in a cross-flow steam-generator tube bundle geometry: the minnie II xf program, in: Multiphase Flow 1995, Elsevier, 1995, pp. 613–618.

[77] R. Dowlati, M. Kawaji, A. Chan, Two-phase crossflow and boiling heat transfer in horizontal tube bundles (1996).

[78] D. Soussan, V. Saldo, A. Gontier, Local two phase flow measurements in a oblique tube bundle geometry, 4th ICMF, May 2001 New Orleans, LA, USA (????).

[79] P. Feenstra, D. Weaver, T. Nakamura, Vortex shedding and fluidelastic instability in a normal square tube array excited by two-phase cross-flow, Journal of Fluids and Structures 17 (2003) 793–811.

[80] G. Pierotti, B. Bussy, Experimental studies of two-phase flow across tube banks, in: European Two Phase Flow Meeting, Trondheim, Nor-way, 1987.

[81] B. Delenne, N. Gay, R. Campistron, D. Banner, Experimental determination of motion-dependent fluid forces in two-phase water-freon cross flow, in: ASME International Mechanical Engineering Congress and Exposition, volume 26768, American Society of Mechanical Engineers, 1997, pp. 349–356.

[82] A. Gosse, A. Adobes, C. Baratte, Qualification of motion dependent fluid force coefficients for simulation of flow-induced vibrations, in: PRESSURE VESSELS AND PIPING CONFERENCE, 2001.

[83] W. Heilker, R. Vincent, Vibration in nuclear heat exchangers due to liquid and two-phase flow (1981).

[84] R. Remy, Flow-induced vibration of tube bundles in two-phase cross-flow, in: Proceedings of 3rd International Conference on Vibration in Nuclear Plants, volume 1, Keswick, U.K., 1982, pp. 135–160.

[85] M. Pettigrew, D. Gorman, Experimental studies on flow-induced vibration to support steam generator design, part iii, in: Proceedings of the International Symposium on Vib. Prob. in Industry, AECL-5804, 1973.

[86] M. Pettigrew, J. Tromp, C. Taylor, B. Kim, Vibration of tube bundles in two-phase cross-flow: part 2—fluid-elastic instability (1989).

[87] A. Serizawa, K. Huda, I. Kataoka, Z. Kawara, K. Kawanishi, T. Ueno, Phase distribution in inclined tube bundle geometries, in: Proceedings of the German-Japanese Symposium on Multi-Phase Flow, Karlsruhe, Germany, 1994, pp. 23–25.

[88] A. Serizawa, K. Huda, I. Kataoka, O. Takahashi, Z. Kawara, K. Kawanishi, T. Ueno, Phase distribution across an inclined tube bundle, in: Proceedings of the Second International Conference on Multi-Phase Flow, Kyoto, Japan, 1995, pp. 3–7.

[89] A. Serizawa, K. Huda, Y. Yamada, I. Kataoka, Experiment and numerical simulation of bubbly two-phase flow across horizontal and inclined rod bundles, Nuclear engineering and design 175 (1997) 131–146.

[90] S. Caillaud, E. de Langre, P. Piteau, Measurement of critical velocities for fluidelastic instability using vibration control, J. Vib. Acoust. 122 (2000) 341–345.

[91] S. b. Caillaud, E. de Langre, F. Baj, Active vibration control for the measurement of fluidelastic effects, J. Pressure Vessel Technol. 125 (2003) 165–170.

[92] C. Iwaki, K. Cheong, H. Monji, G. Matsui, Vertical, bubbly, cross-flow characteristics over tube bundles, Experiments in fluids 39 (2005) 1024–1039.

[93] T. Sasakawa, A. Serizawa, Z. Kawara, Fluid-elastic vibration in two¬phase cross flow, Experimental thermal and fluid science 29 (2005) 403–413.

[94] X. Delaune, P. Piteau, L. Borsoi, J. Antunes, Experimental investigation of in-flow fluidelastic instability for square tube bundles subjected to single-phase and two-phase transverse flows, in: FIV2018 Conference, 2018.

[95] C. Taylor, M. Pettigrew, F. Axisa, B. Villard, Experimental determination of single and two-phase cross flow-induced forces on tube rows, Technical Report, CEA Centre d'Etudes Nucleaires de Saclay, 1986.

[96] F. Hara, Vibration of a single row of circular cylinders subjected to two-phase bubble cross-flow, in: Int. Conf. on Flow Induced Vibrations, 1987, 1987.

[97] D. Schrage, J.-T. Hsu, M. Jensen, Two-phase pressure drop in vertical crossflow across a horizontal tube bundle, AIChE journal 34 (1988) 107–115.

[98] M. Pettigrew, C. Taylor, B. Kim, Vibration of tube bundles in two-phase cross-flow: part 1—hydrodynamic mass and damping (1989).

[99] R. Dowlati, M. Kawaji, A. M. Chan, Pitch-to-diameter effect on two-phase flow across an in-line tube bundle, AIChE journal 36 (1990) 765–772.

[100] D. Mitra, V. K. Dhir, I. Catton, New experimental data and analysis for two-phase flow-induced vibration of tube bundles: Preliminary results, in: ASME Pressure Vessels and Piping Conference, volume 41561, 2003, pp. 23–30.

[101] H. J. Chung, I.-C. Chu, Fluid-elastic instability of rotated square tube array in an air-water two-phase crossflow, Nuclear Engineering and Technology 38 (2006) 69–80.

[102] K. Bamardouf, D. A. McNeil, Experimental and numerical investigation of two-phase pressure drop in vertical cross-flow over a horizontal tube bundle, Applied Thermal Engineering 29 (2009) 1356–1365.

[103] A. Sadikin, D. A. McNeil, K. H. Barmadouf, Two-phase flow on the shell side of a shell and tube heat exchanger, in: International Heat Transfer Conference, volume 49392, 2010, pp. 599–608.

[104] J. A. X Delaune, P. Piteau, L. Borsoi, Experiments and computations of a loosely supported tube under two-phase buffeting and fluid-elastic coupling forces (2011).

[105] G. Spina, D. Vivaldi, G. Brillant, C. Colin, W. Benguigui, R. Denéfle, M. Lelong, A new experimental facility for two-phase flow characterization in a tube bundle and vibration study, in: FIV2022 Conference, 2022.

[106] F. T. Kanizawa, G. Ribatski, Two-phase flow patterns across triangular tube bundles for air–water upward flow, International Journal of Multiphase Flow 80 (2016) 43–56.

[107] S. Darwish, N. Mureithi, A. Hadji, M. Cho, Experimental investigation of fluidelastic instability of a rotated square array subjected to two-phase and air cross-flow, Nuclear Engineering and Design 404 (2023) 112155.

[108] L. Aprin, P. Mercier, L. Tadrist, Experimental analysis of local void fractions measurements for boiling hydrocarbons in complex geometry, International journal of multiphase flow 33 (2007) 371–393.

[109] I. Grant, D. Chisholm, Two-phase on shell-side of a segmentally baffled shell-and-tube heat exchanger, ASME Winter Annual Meeting, Atlanta (1977).

[110] F. De Kerret, C. Béguin, S. Etienne, Two-phase flow pattern identification in a tube bundle based on void fraction and pressure measurements, with emphasis on churn flow, International Journal of Multi-phase Flow 94 (2017) 94–106.

[111] M. Kondo, K.-i. Nakajima, Experimental investigation of air-water two phase upflow across horizontal tube bundles: Part 1, flow pattern and void fraction, Bulletin of JSME 23 (1980) 385–393.

[112] I. Grant, D. Chisholm, Two-phase flow on the shell-side of a segmentally baffled shell-and-tube heat exchanger (1979).

[113] C. E. Taylor, M. J. Pettigrew, I. G. Currie, Random Excitation Forces in Tube Bundles Subjected to Two-Phase Cross-Flow, Journal of Pressure Vessel Technology 118 (1996) 265–277. URL:

https://doi.org/10.1115/1.2842189. doi:10.1115/1.2842189.

arXiv:https://asmedigitalcollection.asme.org/pressurevesseltech/article-pdf/

[114] S. Pascal-Ribot, Y. Blanchet, Buffeting lift forces and local air-water flow aspects around a rigid cylinder, International Journal of Multiphase Flow 33 (2007) 1237–1254.

[115] W. Benguigui, C. Pinto, O. Ries, Experimental investigation on two-phase cross-flow-induced vibration of a cylinder in a confined channel,Journal of Fluids and Structures 120 (2023) 103909. URL: https://www.sciencedirect.com/science/article/pii/S0889974623000774. doi:10.1016/j.jfluidstructs. 2023.103909.

[116] P. Feenstra, R. Judd, D. Weaver, Fluidelastic instability in a tube array subjected to two-phase r-11 cross-flow, Journal of Fluids and Structures 9 (1995) 747–771.

[117] Two-Phase Flow Induced Vibrations of Tube Bundles With Tube Surface Boiling, volume 4th International Symposium on Fluid-Structure Interactions, Aeroelasticity, Flow-Induced Vibration and Noise: Volume II of ASME International Mechanical Engineering

Congress and Exposition, 1997. URL: https://doiorg/10.1115/IMECE1997-0133.doi:10.1115/IMECE1997-0133.
arXiv:https://asmedigitalcollection.asme.org/IMECE/proceedings-pdf/IMECE97/2

[118] C. Taylor, M. Pettigrew, Effect of flow regime and void fraction on tube bundle vibration, J. Pressure Vessel Technol. 123 (2001) 407–413.

[119] M. J. Pettigrew, C. Zhang, N. Mureithi, D. Pamfil, Detailed flow and force measurements in a rotated triangular tube bundle subjected to two-phase cross-flow, Journal of Fluids and structures 20 (2005) 567– 575.

[120] C. Zhang, N. Mureithi, M. Pettigrew, Development of models correlating vibration excitation forces to dynamic characteristics of two-phase flow in a tube bundle, International journal of multiphase flow 34 (2008) 1048–1057.

[121] R. Violette, M. Pettigrew, N. Mureithi, Fluidelastic instability of an array of tubes preferentially flexible in the flow direction subjected to two-phase cross flow (2006).

[122] G. Ricciardi, M. Pettigrew, N. Mureithi, Fluidelastic instability in a normal triangular tube bundle subjected to air-water cross-flow, Journal of pressure vessel technology 133 (2011).

[123] T. Sawadogo, N. Mureithi, Fluidelastic instability study in a rotated triangular tube array subject to two-phase cross-flow. part i: Fluid force measurements and time delay extraction, Journal of Fluids and Structures 49 (2014) 1–15.

[124] T. Sawadogo, N. Mureithi, Fluidelastic instability study on a rotated triangular tube array subject to two-phase cross-flow. part ii: Experimental tests and comparison with theoretical results, Journal of Fluids and Structures 49 (2014) 16–28.

[125] S. Olala, N. W. Mureithi, Prediction of streamwise fluidelastic instability of a tube array in two-phase flow and effect of frequency detuning, Journal of Pressure Vessel Technology 139 (2017).

[126] E. Deri, J. Nibas, A. Adobes, A new test-bench for studying vibrations of tubes in parallel triangular bundles under two-phase cross-flow, in: ASME 2014 Pressure Vessels and Piping Conference, ASME, 2014.

[127] E. Deri,Operational modal analysis of a triangular-pitch tube bundle subjected to two-phase cross-flow, Journal of Pressure Vessel Technology 140 (2018) 031301. URL: https://doi.org/10.1115/1.4038725. doi:10.1115/1.4038725.
arXiv:https://asmedigitalcollection.asme.org/pressurevesseltech/article-pdf/

[128] R. ´Alvarez Brice˜no, F. T. Kanizawa, G. Ribatski, L. P. de Oliveira, Updated results on hydrodynamic mass and damping estimations in tube bundles under two-phase crossflow, International Journal of Multiphase Flow 89 (2017) 150–162. URL: https://www.sciencedirect.com/science/article/pii/S0301932216300386.

doi:https://doi. org/10.1016/j.ijmultiphaseflow.2016.09.022.

[129] R. ´Alvarez Brice˜no, F. T. Kanizawa, G. Ribatski, L. P. de Oliveira, Validation of turbulence induced vibration de sign guidelines in a normal triangular tube bundle during two-phase crossflow, Journal of Fluids and Structures 76 (2018) 301–318. URL: https://www.sciencedirect.com/science/article/pii/S0889974616304959. doi:https://doi.org/10.1016/ j.jfluidstructs.2017.10.013.

[130] R. ´Alvarez Brice˜no, F. T. Kanizawa, G. Ribatski, L. P. R. de Oliveira, Experimental estimation of equivalent loads on upward two-phase crossflow in tube bundles via kalman filtering, Journal of Fluids and Structures 120 (2023) 103900. URL: https://www.sciencedirect.com/science/article/pii/S0889974623000683. doi:https://doi.org/10.1016/j.jfluidstructs.2023.103900.

[131] J. Lai, L. Sun, L. Gao, P. Li, Mechanism analysis on fluidelastic instability of tube bundles in considering of cross-flow effects, Nuclear Engineering and Technology 51 (2019) 310–316.

[132] J. Lai, L. Sun, P. Li, T. Tan, L. Gao, Z. Xi, C. He, H. Liu, Eigen-value analysis on fluidelastic instability of a rotated triangular tube array considering the effects of two-phase flow, Journal of Sound and Vibration 439 (2019) 194–207.

[133] J. Lai, L. Sun, L. Gao, T. Tan, Z. Xi, P. Li, Study on fluidelastic instability of a tube array subjected to two-phase cross-flow, Annals of Nuclear Energy 126 (2019) 303–311.

[134] J. Lai, L. Sun, P. Li, Flow-induced instability and nonlinear dynamics of a tube array considering the effect of a clearance gap, Nuclear Engineering and Technology 51 (2019) 1650–1657.

[135] J. Lai, L. Sun, L. Gao, T. Tan, P. Li, Numerical study on fluidelastic instability of tube bundles in two-phase flow considering the effect of tube boundary constraint, Annals of Nuclear Energy 144 (2020) 107532.

[136] J. Lai, T. Tan, S. Yang, L. Sun, Experimental and theoretical study on fluidelastic instability of tube bundles subjected to cross-flow in the parallel direction, Annals of Nuclear Energy 169 (2022) 108927.

[137] S. Darwish, N. Mureithi, M. Cho, In-plane fluidelastic instability study of a tube bundle with a rotated triangular layout and small pitch ratio, Nuclear Engineering and Design 405 (2023) 112202.

[138] L. Sutherland, I. Murray, Pressure-drop and Heat-transfer on the Shell-side of a Model Heat Exchanger with Two-phase Flow, National Engineering Laboratory, 1969.

[139] I. D. R. Grant, I. Murray, Pressure drop on the shell-side of a seg-mentally baffled shell-and-tube heat exchanger with vertical two-phase flow, National Engineering Laboratory, 1972.

[140] N. Gay, P. Decembre, J. Launay, Comparison of air-water to water-freon two-phase cross flow effects on the vibratory behaviour of a tube bundle, in: Proceedings of the International Symposium on Flow-Induced Vibration and Noise: Flow-Induced Vibration and Noise in Cylinder Arrays, Chicago, IL, 1988, pp. 139–158.

[141] C. Taylor, K. Boucher, M. Yetisir, Vibration and impact forces due to two-phase cross-flow in u-bend region of nuclear steam generators, in: Proceedings of the 6th International Conference on Flow-Induced Vibration, volume 1, 1995, pp. 401–412.

[142] V. Janzen, E. Hagberg, M. Pettigrew, C. Taylor, Fluidelastic instability and work-rate measurements of steam-generator u-tubes in air–water cross-flow, J. Pressure Vessel Technol. 127 (2005) 84–91.

[143] Y. Joo, V. Dhir, On the mechanism of fluidelastic instability of a tube placed in an array subjected to two-phase crossflow (1995).

[144] M. Pettigrew, C. Taylor, V. Janzen, T. Whan, Vibration behavior of rotated triangular tube bundles in two-phase cross flows, J. Pressure Vessel Technol. 124 (2002) 144–153.

[145] R. Violette, N. Mureithi, M. Pettigrew, Two-phase flow induced vibration of an array of tubes preferentially flexible in the flow direction, in: ASME Pressure Vessels and Piping Conference, volume 41898, 2005, pp. 331–338.

[146] M. Pettigrew, C. Taylor, Vibration of a normal triangular tube bundle subjected to two-phase freon cross flow, Journal of pressure vessel technology 131 (2009).

[147] H. Senez, N. Mureithi, M. Pettigrew, Vibration excitation forces in a rotated triangular tube bundle subjected to two-phase cross flow, in: Fluids Engineering Division Summer Meeting, volume 54518, 2010, pp. 565–573.

[148] A. Sadikin, D. McNeil, Two-phase flow through a staggered tube bundle of a shell and tube heat exchanger, International Conference on Heat Transfer, Fluid Mechanics and Thermodynamics, 2014.

[149] S. Azuma, Investigation of critical flow velocity of a triangular u-tube bundle subjected to two-phase flow, in: FIV2018 Conference, 2018.

[150] T. Tan, Experimental study on fluidelastic instability of rotated tri¬angular tube bundles subjected to two-phase cross flow, in: FIV2018 Conference, 2018.

[151] D. Panunzio, R. Lagrange, P. Piteau, X. Delaune, Experimental investigation of cross-flow fluidelastic instability for rotated triangular tube bundles subjected to single-phase and two-phase transverse flows, in: FIV2022 Conference, 2022.

[152] A. Ghasemi, N.-R. Kevlahan, The role of reynolds number in the fluid-elastic instability of tube arrays, Journal of Fluids and Structures 73 (2017) 16–36.

[153] H. Iacovides, B. Launder, A. West, A comparison and assessment of approaches for modelling flow over in-line tube banks, International Journal of Heat and Fluid Flow 49 (2014) 69–79. 8th Symposium on Turbulence & Shear Flow Phenomena (TSFP8).

[154] J. L. Blackall, H. Iacovides, J. C. Uribe, Modeling of in-line tube banks inside advanced gas-cooled reactor boilers, Heat Transfer Engineering 41 (2020) 1731–1749. URL: https://doi.org/10.1080/01457632. 2019.1640486.

[155] V. Guimet, D. Laurence, A linearised turbulent production in the k −ε model for engineering applications, in: W. RODI, N. FUEYO (Eds.), Engineering Turbulence Modelling and Experiments 5, Elsevier Science Ltd, Oxford, 2002, pp. 157–166.

[156] D. R. Laurence, J. C. Uribe, S. V. Utyuzhnikov, A robust formulation of the v2–f model, Flow Turbul. Combust. 73 (2005) 169–185.

[157] F. R. Menter, Two-equation eddy-viscosity turbulence models for engineering applications, AIAA Journal 32 (1994) 1598–1605.

[158] C. G. Speziale, S. Sarkar, T. B. Gatski, Modeling the pressure-strain correlation of turbulence: an invariant dynamical system approach, J. Fluid Mech. 227 (1991) 245–272.

[159] R. Manceau, Recent progress in the development of the elliptic blending reynolds-stress model, Int. J. Heat Fluid Fl. 51 (2015) 195–220.

[160] S. Benhamadouche, D. Laurence, N. Jarrin, I. Afgan, Large eddy simulation of flow across in-line tube bundles, in: The 11th International Topical Meeting on Nuclear Reactor Thermalhydraulics, NURETH-11, October 2-6, Avignon, France, 2005.

[161] S. Benhamadouche, D. Laurence, Les, coarse les, and transient rans comparisons on the flow across a tube bundle, International Journal of Heat and Fluid Flow 24 (2003) 470–479. Selected Papers from the Fifth International Conference on Engineering Turbulence Modelling and Measurements.

[162] P. Rollet-Miet, D. Laurence, J. Ferziger, Les and rans of turbulent flow in tube bundles, International Journal of Heat and Fluid Flow 20 (1999) 241–254.

[163] C. Moulinec, M. Pourqui'e, B. Boersma, T. Buchal, F. Nieuwstadt, Direct numerical simulation on a cartesian mesh of the flow through a tube bundle, International Journal of Computational Fluid Dynamics 18 (2004) 1–14.

[164] C. Moulinec, J. Hunt, F. Nieuwstadt, Disappearing wakes and dispersion in numerically simulated flows through tube bundles, C 73 (2004) 95–116.

[165] Y. Hassan, H. Barsamian, Tube bundle flows with the large eddy simulation technique in curvilinear coordinates, International Journal of Heat and Mass Transfer 47 (2004) 3057–3071.

[166] C. Liang, G. Papadakis, Large eddy simulation of cross-flow through a staggered tube bundle at subcritical reynolds number, Journal of Fluids and Structures 23 (2007) 1215–1230.

[167] M. Labois, D. Lakehal, Very-large eddy simulation (v-les) of the flow across a tube bundle, Nuclear Engineering and Design 241 (2011) 2075–2085. (W3MDM) University of Leeds International Symposium: What Where When? Multi-dimensional Advances for Industrial Process Monitoring.

[168] A. Tiftikçi, C. Kocar, Lattice boltzmann simulation of flow across a staggered tube bundle array, Nuclear Engineering and Design 300 (2016) 135–148.

[169] J. Watterson, W. Dawes, A. Savill, A. White, Predicting turbulent flow in a staggered tube bundle, International Journal of Heat and Fluid Flow 20 (1999) 581–591.

[170] T. Shih, Z. J., J. Lumley, A realizable Reynolds stress algebraic equation model, Technical Report, NASA TM-105993, 1993.

[171] A. RIDLUAN, A. TOKUHIRO, Benchmark simulation of turbulent flow through a staggered tube bundle to support cfd as a reactor design tool. part i: SRANS CFD simulation, Journal of Nuclear Science and Technology 45 (2008) 1293–1304.

[172] A. Ridluan, A. Tokuhiro, Benchmark simulation of turbulent flow through a staggered tube bundle to support CFD as a reactor design tool. part ii: URANS CFD simulation 45 (2008) 1305–1315.

[173] K. Narasingamurthi, B. Prasad, Performance of 2-d turbulence rans models for prediction of flow past a staggered tube bank array, Engineering Applications of Computational Fluid Mechanics 3 (2009) 386– 407.

[174] B. L. da Silva, R. D. Luciano, J. Utzig, H. F. Meier, Analysis of flow behavior and fluid forces in large cylinder bundles by numerical simulations, International Journal of Heat and Fluid Flow 75 (2019) 209–226.

[175] K. Schrôder, H. Gelbe, Two- and three-dimensional CFD-simulation of flow-induced vibration excitation in tube bundles, Chemical Engineering and Processing: Process Intensification 38 (1999) 621–629.

[176] W. Gog, ntersuchungen der Erregermechanismen am Einzelrohr und am querangestrômten Rohrb¨undel, Ph.D. thesis, Dissertation D 83, Technische Universit¨at Berlin, 1982.

[177] A. Khalifa, D. Weaver, S. Ziada, Modeling of the phase lag causing fluidelastic instability in a parallel triangular tube array, Journal of Fluids and Structures 43 (2013) 371–384.

[178] H. Houri Jafari, B. Ghadiri Dehkordi, Numerical Prediction of Fluid-Elastic Instability in Normal Triangular Tube Bundles With Multiple Flexible Circular Cylinders, Journal of Fluids Engineering 135 (2013) 031102.

[179] Large-Eddy Simulation of Cross-Flow Induced Vibrations of a Single Flexible Tube in a Normal Square Tube Array, volume Volume 4: Fluid-Structure Interaction of Pressure Vessels and Piping Conference, 2014.

[180] A Numerical Investigation of the Fluidelastic Coupling for a Cell of Flexible Tubes in a Square-in-Line Bundle Subject to Water Cross-Flow, volume Volume 4: Fluid-Structure Interaction of Pressure Vessels and Piping Conference, 2015.

[181] Qualifications of motion dependent fluid force coefficients for simulation of flow induced vibrations, volume 420 of Pressure Vessels and Piping Conference, 2001.

[182] V. Shinde, T. Marcel, Y. Hoarau, T. Deloze, G. Harran, F. Baj, J. Cardolaccia, J. Magnaud, E. Longatte, M. Braza, Numerical simulation of the fluid-structure interaction in a tube array under cross flow at moderate and high Reynolds number, Journal of Fluids and Structures 47 (2014) 99–113. Special Issue on Unsteady Separation in Fluid-Structure Interaction-I.

[183] P. Spalart, S. Allmaras, A one-equation turbulence model for aerodynamic flows (1992).

[184] D. C. Wilcox, Reassessment of the scale-determining equation for advanced turbulence models, AIAA Journal 26 (1988) 1299–1310.

[185] R. Bourguet, M. Braza, G. Harran, R. El Akoury, Anisotropic organised eddy simulation for the prediction of non-equilibrium turbulent flows around bodies, Journal of Fluids and Structures 24 (2008) 1240– 1251. Unsteady Separated Flows and their Control.

[186] P. Spalart, S. Deck, M. Shur, K. Squires, M. Strelets, A. Travin, A New Version of Detached-eddy Simulation, Resistant to Ambiguous Grid Densities, Theoretical and Computational Fluid Dynamics 20 (2006) 181–195.

[187] S. Caillaud, E. de Langre, P. Piteau, Measurement of Critical Velocities for Fluidelastic Instability Using Vibration Control, Journal of Vibration and Acoustics 122 (2000) 341–345.

[188] B. de Pedro, J. Parrondo, C. Meskell, J. F. Oro, Cfd modelling of the cross-flow through normal triangular tube arrays with one tube under-going forced vibrations or fluidelastic instability, Journal of Fluids and Structures 64 (2016) 67–86.

[189] H. Zhao, P. Gao, R. Tian, X. Li, A three-dimensional refined numerical simulation of cross-flow induced vibration mechanism in the tube bundle, Nuclear Engineering and Design 405 (2023) 112223.

[190] S. Benhamadouche, W. Benguigui, Wall-resolved les and low-Reynolds number URANS combined to an arbitrary Lagrangian Eulerian approach for predicting water cross-flow induced vibration of a single flexible tube in a normal square tube array, in: The 11th International Topical Meeting on Nuclear Reactor Thermalhydraulics, NURETH-20, August 20–25, 2023, Washington, D.C, 2023.

[191] H. Barsamian, Y. Hassan, Large eddy simulation of turbulent crossflow in tube bundles, Nuclear Engineering and Design 172 (1997) 103–122.

[192] V. KASSERA, K. STROHMEIER, Simulation of tube bundle vibrations induced by cross-flow, Journal of Fluids and Structures 11 (1997) 909–928.

[193] Experimental determination of tube bundle vibrations induced by cross-flow, volume PVP-Vol. 273 of Pressure Vessels and Piping Conference, ASME, 1994.

[194] A. Khalifa, D. Weaver, S. Ziada, An experimental study of flow-induced vibration and the associated flow perturbations in a parallel triangular tube array, Journal of Pressure Vessel Technology, Transactions of the ASME 135 (2013). Cited by: 14.

[195] V. Yakhot, S. A. Orszag, S. Thangam, T. B. Gatski, C. G. Speziale, Development of turbulence models for shear flows by a double expansion technique, Physics of Fluids A: Fluid Dynamics 4 (1992) 1510–1520.

[196] S. Aiba, H. Tsuchida, T. Ota, Heat transfer around tubes in in-line tube banks, Jsme International Journal Series B-fluids and Thermal Engineering 25 (1982) 919–926.

[197] H. Omar, M. Hassan, A. Gerber, Numerical simulations of unsteady fluid forces in heat exchanger tube bundles, in: J. Zhu (Ed.), Computational Simulations and Applications, IntechOpen, Rijeka, 2011.

[198] F. R. Menter, Y. Egorov, The scale-adaptive simulation method for unsteady turbulent flow predictions. part 1: Theory and model description, Flow, turbulence and combustion 85 (2010) 113–138.

[199] W. Benguigui, E. Deri, J. Lavieville, S. Mimouni, E. Longatte, Numerical experiment on two-phase flow behaviors in tube-bundle geometry for different mixtures, Pressure Vessel and Piping, Hawai, USA (2017).

[200] W. Benguigui, J. Lavieville, S. Mimouni, L. Elisabeth, First step in the development of an eulerian fixed grid postulation for two-phase flow-induced vibration numerical modeling, in: FIV2018 Conference, 2018.

[201] W. Benguigui, A. Doradoux, J. Lavieville, S. Mimouni, E. Longatte, A discrete forcing method dedicated to moving bodies in two-phase flows, International Journal of Numerical Methods in Fluids (2018).

[202] W. Benguigui, J. Laviéville, N. Merigoux, Fluid-structure interaction in two-phase flow using a discrete forcing method, International Journal for Numerical Methods in Fluids 91 (2019) 247–261. URL: https://onlinelibrary.wiley.com/doi/abs/10.1002/fld.4753.

[203] F. Baraglia, W. Benguigui, R. Denèfle, A corotational finite element approach coupled to a discrete forcing method to solve hyperelastic deformation induced by two-phase flow, Journal of Fluids and Structures 107 (2021) 103403. URL: https://www.sciencedirect.com/

science/article/pii/S0889974621001869. doi:https://doi.org/10.1016/j.jfluidstructs.2021.103403.

[204] W. Benguigui, Numerical simulation of two-phase flow-induced vibration in tube-bundle, PhD Thesis, Université Paris-Saclay (2018).

[205] O. Sadek, A. Mohany, M. Hassan, Numerical investigation of the cross flow fluidelastic forces of two-phase flow in tube bundle, Journal of Fluids and Structures 79 (2018) 171–186. URL: https://www. sciencedirect.com/science/article/pii/S0889974617301597. doi:https://doi.org/10.1016/j.jfluidstructs.2017.11.009.

[206] O. Sadek, A. Mohany, M. Hassan, Numerical simulation of streamwise fluidelastic instability of tube bundles subjected to two-phase cross flow, Journal of Fluids and Structures 92 (2020) 102816. URL: https://www.sciencedirect.com/science/article/pii/S0889974618310132. doi:https://doi.org/10.1016/ j.jfluidstructs.2019.102816.

[207] O. Sadek, A. Mohany, M. Hassan, The prediction of fluidelastic forces in triangular tube bundles subjected to a two-phase flow: The effect of the flow approach angle, Journal of Fluids and Structures 106 (2021) 103386. URL: https://www.sciencedirect.com/science/article/pii/S0889974621001699. doi:https://doi.org/10.1016/j.jfluidstructs.2021.103386.